CONSEJO SUPERIOR DE INVESTIGACIONES CIENTÍFICAS

INSTITUTO DE CIENCIAS DE MATERIALES DE MADRID

LEAD FREE FERROIC MULTILAYER COMPOSITE FILMS BASED ON $(Bi_{0.5}Na_{0.5})TiO_3$-$BaTiO_3$ AND $BiFeO_3$.

PH.D THESIS

ARMANDO JANIER PEREZ RIVERO

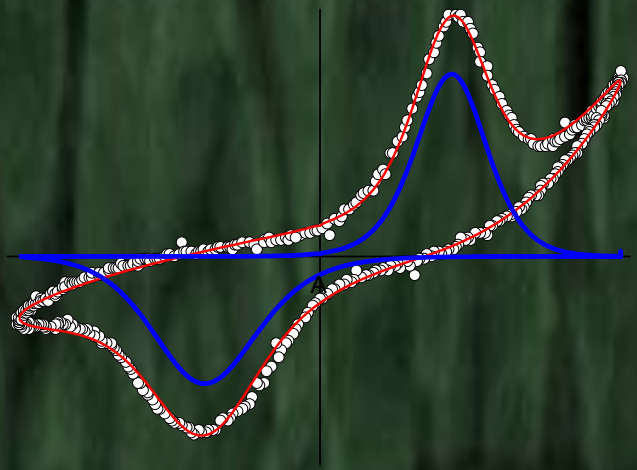

UNIVERSIDAD AUTÓNOMA DE MADRID

MADRID 2015

CONSEJO SUPERIOR DE INVESTIGACIONES CIENTÍFICAS

INSTITUTO DE CIENCIAS DE MATERIALES DE MADRID

DEPARTAMENTO DE MATERIALES PARA LAS TECNOLOGÍAS DE LA INFORMACIÓN

Doctoral Thesis

LEAD FREE FERROIC MULTILAYER COMPOSITE FILMS BASED ON $(Bi_{0.5}Na_{0.5})TiO_3$-$BaTiO_3$ AND $BiFeO_3$.

Author

Armando Janier Perez Rivero

Supervisors:

Dr. Ricardo Jiménez Rioboó

Dr. Jesús Ricote Santamaría

UNIVERSIDAD AUTÓNOMA DE MADRID

Departamento de Física Aplicada

Madrid 2015

A la memoria de mi madre "SORI"

y mis abuelos "NINI" y "PEPIN"

A mi familia, GRACIAS POR TODO.

Agradecimientos.

La presente Tesis Doctoral se ha realizado en el Departamento de Materiales para las Tecnologías de la Información, en particular en el grupo de Electrocerámicas para las Tecnologías de la Información del Instituto de Ciencia de Materiales de Madrid (ICMM-CSIC) bajo la dirección del Dr. Ricardo Jiménez Rioboó y el Dr. Jesús Ricote Santamaría, gracias a la concesión de una beca del Programa de Formación de Personal Investigador (FPI, BES-2011-047263) del Ministerio de Economía y Competitividad, asociada al proyecto de investigación "Capas y multicapas delgadas ferroeléctricas para dispositivos integrados. Composiciones y métodos de depósito químico de disoluciones de bajo impacto ambiental (MAT2010-15365)".

Es inevitable llegado al final de este trabajo agradecer a varias personas las cuales me han brindado su apoyo incondicional en lo profesional y en lo personal durante estos largos e interesantes últimos 4 años de mi vida. Para todos ellos van dedicadas los siguientes párrafos como señal de mis más sinceros agradecimientos por haber contribuido cada uno a su manera a poner punto final a esta aventura que le llaman "Tesis".

En primer lugar, tengo que agradecer mis dos directores, elDr. Ricardo Jiménez Rioboó y el Dr. Jesús Ricote Santamaría, sus sorprendentes ganas de enseñarme a ser mejor científico, su dedicación infatigable me han hecho mejorar tanto en el trabajo experimental como en la comprensión de los resultados obtenidos en esta tesis. Gracias además por la confianza demostrada desde el momento cero que aterricé en este gran país, por demostrarme que podía contar con ustedes. Además por haberme brindado la posibilidad de crecer profesionalmente y como persona permitiéndome participar en varios congresos y estancias de investigación durante esta tesis.

Mi agradecimiento al Dr. Miguel Manso Silván del Departamento de Física Aplicada de la Universidad Autónoma de Madrid (UAM), por aceptar ser mi tutor y por su ayuda con todos los trámites requeridos para presentar esta Tesis.

A la Prof. Maria Lourdes Calzada, por su gran ayuda con la preparación y caracterización estructural de las láminas delgadas. Además de su apoyo y dedicación para ayudarme a mejorar mis presentaciones de resultados tanto en congresos como en reuniones de grupo.

Al Dr. Iñigo Bretos, por su ayuda desde mi primer día en los laboratorios de química, por enseñarme los trucos y manías de ellos, desde cómo usar una pipeta y pinzas hasta preparar una SUPER disolución de bismuto hierro.

A la Prof. Mar García Hernández, por su ayuda en la caracterización magnética de las láminas y la interpretación de los resultados obtenidos.

Al Dr. Harvey Amorín González, por todo los buenos deseos y consejos aportados en esta etapa desde que llegue con mi cara de cubano asustado hasta estos últimos momentos, donde que me trasmitieras tus experiencias me ha servido para encontrar la tranquilidad y fuerza necesaria para terminar esta tesis. También agradecer nuestras múltiples discusiones sobre los materiales multiferroicos que de tanta ayuda me han servido para entender muchas cosas de esta tesis.

Al Dr. Pablo Ramos, por su ayuda en la simulación de las propiedades físicas en los materiales en forma de multicapas ferroeléctricas, gracias por tu colaboración y tus aportes en la programación. Además agradecer su continua preocupación por la marcha de este trabajo.

Al Dr. Miguel Algueró, por su colaboración a la hora de preparar mis resultados para algunas de mis presentaciones en congresos, por ayudarme a contextualizar y ver en ocasiones detalles de mi trabajo que resaltaban su interés y yo no era capaz de ver.

Quiero agradecer también al resto de los miembros del Departamento de Electro-cerámicas para las Tecnologías de la Información, ya que todos en algún momento de esta etapa me han brindado su apoyo para hacerme más fácil este trabajo. Resaltando a mis compañeras de Tesis y congresos, Dulce Pérez y Carmen Fernández, porque en algún momento de esta aventura les toco "cargar" con este cubano "despistado" por algún rincón de España o Europa.

I thank Monika Tomczyk and Paula M. Vilarinho from the Department of Ceramics and Glass Engineering, CICECO, University of Aveiro, Portugal, for their assistance in the preparation and structural and microstructural characterization of the single phase $BiFeO_3$ films.

I would like to thankfully acknowledge Javier Pérez de la Cruz and Jose R.A. Fernandez for accepting me in their group in the INESC TEC, Instituto de Engenharia de Sistemas e Computadores do Porto, Portugal, to perform the first piezoelectric characterization in my lead-free thin films.

I am also grateful to Prof. Dr Guus Rijnders and Dr. Ruud Steenwelle for giving me the opportunity of using their laboratory facilities and help me to orient my work in the right direction during my stay in the Inorganic Materials Science Group, MESA+ Institute for Nanotechnology of the University of Twente, Netherlands (1^{st} September to 29^{th} November 2014) , financed by the "Ministerio de Economía y Competitividad" with reference EEBB-I-14-08445. Thanks for their unconditional support that allowed me learning different microfabrication methods. I am also grateful to the members of the group because without your help my stay would have been harder. I would like to specially thank Dr. Nirupam Banerjee for his support during the wet-etching and the use of the clean-room, and Dr. Minh Duc Nguyen for his patience in helping me during the piezoelectric characterization of my composite films.

Llegado a este punto se hace prácticamente imposible no mirar hacia atrás, no agradecer también a muchas personas que han tenido menos que ver en la colaboración y ayuda científica, pero que sin ellos llegar aquí hubiese sido imposible porque me han transmitido las fuerzas y tranquilidad necesaria para superar esta etapa, ya sea estando a mi lado en ella, o a la distancia que obligó mi decisión de venirme a hacer la tesis a este maravilloso país.

Comenzaré agradeciendo a las personas que en estos últimos años han estado más cerca de mí en esta etapa de tanto aprendizaje continuo no solo de ciencias, sino de culturas diferentes, formas de actuar y de comportarme tan distintas a las que traía arraigada durante 26 años en ese país hermoso donde nací y me crie, "Cuba". Sé que será difícil mencionar a todas las personas que me han apoyado, pero también sé que todos ellos saben lo agradecido que estoy, porque he intentado siempre más que escribirlo en este momento, demostrárselo. Gracias a todos mis "socitos", gracias por estar, gracias por aguantar mis bromas en ocasiones, mejor dicho, casi siempre muy "pesadas" y cubanas. Repetiré algunos pero es inevitable, gracias HARVEY, antes de montarme por primera vez en un avión en la Habana sabía que podría contar con tu apoyo en la nueva etapa que comenzaba, pero me has demostrado en estos años que podía contar más de lo que yo esperaba, gracias por estar ahí siempre pendiente de lo bueno y lo malo que me podría pasar. Por intentar siempre que tomara el camino correcto en mis decisiones y que amoldara siempre éstas al lugar donde me encontraba y a la cultura distinta a la que me estaba enfrentado, gracias "CHAMA", y junto a tí agradezco también a EVA, por adoptarme como un "cuñadito" desde que llegué también. Aún recuerdo por qué la sequía de Madrid no me destrozó los labios en mi primer "otoño", y tú siempre pendiente de que no pagara la novatada de estar en un nuevo país, GRACIAS. A "MERCETON", gracias niña, me has enseñado mucho estos

últimos años que hemos compartido el café de las 11 casi a diario, aunque no lo creas he aprendido mucho de ti, casi siempre sin hablarme, con solo la mirada, ya sabía que estaba actuando mal y eso lo captaba muy rápido, además he conocido pocas personas con tan buenos sentimientos y deseos hacías los demás, GRACIAS por aguantarme. A "Alvarito" gracias chamaquito, por compartir casi desde el minuto 1 tantos buenos ratos juntos, tantas BIRRAS compartidas e inculcarme el arte de la cerveza "alemana" y las "rusas", estas últimas no las cervezas. Por haber hecho tantos esfuerzos por entender mi idioma y en ocasiones hacer mis frases "cubanas" tuyas, además de compartir conmigo tantas filosofías de vida y lo mejor, tantas botellas de "caney" y "Santiago", que vengas muchas más. A "Karmen", gracias por enseñarme que es una "gallega" de pura cepa. Nuestra relación de amistad ha pasado muchos momentos que yo llamo "interesantes", que iban desde una hostia bien dada hasta un bote de yogur encima mía, "SABES QUE NO OLVIDO", pero de esas cosas, de tu carácter he aprendido mucho también, me has enseñado que pueden existir personas muy diferentes en el mundo, pero que siempre con el respeto por delante se puede pasar ratos muy buenos de risas y alegrías juntos, y además ratos también tensos. Papa "BRETÓS", gracias máquina, figura, crack, si no fuera por tus controvertidos gustos por algunos equipos de futbol y preferencias en barrios para vivir, tendría otra opinión de los "VASCOS", en verdad no son lo que me pintaban, pero agradezco tu presencia en esta etapa de la vida y espero seguir encontrando gente en mi vida que desborde esa alegría que llevas dentro y que sabes como nadie transmitir a los demás, ha sido más fácil contigo en el grupo de los "ferroeléctricos". A MIRIAM, eres la mejor, gracias por poner en muchos momentos la parte de respeto y cordura que necesitaba el "piquete", por los buenos ratos de birras y picnics rodeados de peques, que son un amor, que nos hemos pasado, además de tantas charlas futboleras y basquetboleras y partidos

compartidos aunque fuera, en ocasiones, por el wassap "HALA MADRID!!". "ELE", a ti, igual que a todos los anteriores, espero poder agradecerte personalmente por mucho tiempo en el futuro. Has sido la última adopción del piquete de "MUNUERA", pero eso no quita que seas de lo mejooooooorrrrrrr, GRACIAS por compartir conmigo estos últimos y más difíciles momentos de esta tesis, por dejarme entrar prácticamente en tu familia que es preciosa. También indirectamente agradezco a Jesus, Elia y Eire, por hacerme reír tanto y pasar buenos ratos, además de en ocasiones hacerme sentir en familia, que es la cosa que más se extraña cuando se está tan lejos de "casa", gracias por tu sinceridad. A "COVITA", me dolió mucho que te fueras tan lejos y además a un país tan frío en todos los sentidos, sin ti esto no es lo mismo, gracias por ser como eres, por enseñarme que podía encontrar también españolas con mucho desparpajo, incluso más que muchos cubaniches, y que además de todo ese desparpajo, en algunos momentos, tenía que sobresalir la cordura, para no liarla.

Por desgracia en estos últimos tiempos de mi tesis ha aparecido otra personita a la cual me es inevitable agradecer, aunque sé que ella como yo es mas de palabras que de cosas que queden reflejadas en papel, para nosotros las cosas verdaderas son las que quedan marcadas en el corazón. Y digo por desgracia, porque si te hubiera conocido antes hubiera disfrutado más de este tiempo. Aunque nunca es tarde si la dicha es buena, GRACIAS "MARITZITA". Ojala todas las personas del mundo tuvieran tus valores y corazón, me queda mucho por aprender aún de ti.

Agradezco también a todos los demás "chamaquitos" con los que en algún momentos me he echado unas risas, bailes, o hemos compartido tiempo y espacio juntos en el transcurso de la tesis en el ICMM.

A mis compañeros de master, con ustedes mis primero días fuera de casa fueron más fáciles: a Mery, Rogger, Norberto, Leo, Ruben, Jose, Jose A, Cristian, Luis, gracias chavales, siempre los recordaré con alegría.

Se me está haciendo largo, pero son muchas las personas que me he encontrado a lo largo de este camino a mi lado y de todas he aprendido algo y tengo algo que agradecer. Esta etapa la cierro además de con muchas nuevas personas en mi corazón, pero con el convencimiento de que en mucho momentos las personas de mi pasado me han dado ánimo para sacar fuerzas de donde no las tenías para salir adelante, por eso no puedo dejar de mencionarlos. A mis "hermanos", "EL RAYMON", "EL JUACO", "EL TIO", "EL BOLO", no nos une la sangre pero nos unen cosas casi tan fuertes como eso, y siempre ustedes irán conmigo donde yo este. "ROBER-TA" tú también eres uno de esos que yo llamo "hermanos", de los que muchas veces pasan más trabajos contigo que personas de tu misma familia, pero a ti además te he tenido mucho más cerca estos años, GRACIAS mamita por todo lo que has hecho por mí. Gracias a todos los demás chavales de "UO", los que he tenido la suerte de ver a menudo por aquí por Europa, y los que no, a "YONNI", "EL POLLO", "YUNIOR", a "ANITA" la chica más guapa de mi aula, y además por soportar a tantos y tan pesados a tu lado, en fin a todos, chavales que sino no termino la tesis y tengo que "Imprimir".

Gracias a mi "PURO", YURI y el "VIEJO", FGUERRE. Por transmitirme todo lo que sabían, de todo, sobre todo de la vida.

Ahora viene la parte más difícil, para mí, pero que puedo resumir en pocas palabras, agradecer a personas que han ido amoldando mi forma de ser, actuar, mi carácter y mi YO, todo esto después de cada uno de los golpes duro que nos puede ir dando la vida. GRACIAS A TODA MI FAMILIA, sin su excesivo amor, dedicación y sin todo lo que han hecho por mí, esta tesis, estos últimos años lejos de ustedes y sobre todo Yo, no

tendríamos motivos de ser. Gracias a mi Hermana Querida "YUDE" y mi sobrina bella "SAMI", han sido mi inspiración en los últimos años. A mi PAPÁ ,MARTI y mis hermanos "MICHE" y "HEN", por enseñarme tantas cosas, sobre todo, el amor a la familia y millones de valores más que me han servido en esta vida, y por estar siempre a mi lado. A mis tíos, PEPINSITO, ISABEL, EVA, ILIANA, JORGE, que me tuvieran siempre como uno más de sus hijos ha sido muy importante para mí. A mis quinicientos primos, a los que también puedo considerar hermanos, a todos, a todos, a todos, MUCHAS GRACIAS.

Y como lo mejor se deja para el final, le toca el turno a una de las personas que más me ha aportado en esta vida. Una persona sin la cual no sé si podría haber llegado al final de esta historia, no sé si hubiese podido estar escribiendo estos agradecimientos ahora. A veces, los grandes filósofos dicen que las personas llegan a tu vida cuando más lo necesitas, tu "NIÑITA", no has hecho eso, ha sido mucho más grande, eres esa personita que has aparecido porque era inevitable para que, cuando llegué a este país no me descarrilara por completo y cogiera otro de eso tantos y tan diversos caminos por los cuales me hubiese sido sencillo descarrilar. Gracias por ser lo que eres, por estar a mi lado estos últimos 4 años en los momentos buenos y sobre todo en los malos, en esos que de verdad donde se miden las verdaderas amistades, gracias por no dejarme solo nunca. Y gracias por existir, "nuestro amistad será leyenda".

RESUMEN

Tradicionalmente, una de las maneras de conseguir mejorar las propiedades de un material, es la combinación con otros en composites. En la presente tesis se explora la fabricación de composites multicapa (MLC, del inglés multilayer composite) en forma de lámina delgada, combinando capas de $(Bi_{0.5}Na_{0.5})_{1-x}Ba_xTiO_3$ *(BNBT) y* $BiFeO_3$ *(BF). Una de las hipótesis de partida es mantener un valor mayor de la polarización en las capas de BNBT a través de un campo eléctrico interno inducido por capas polarizadas de BF. Al retirar el campo eléctrico externo las capas de BF mantienen su polarización y el campo interno inducido en la capa de BF impide que la capa de BNBT se despolarice completamente, y por tanto mejore su remanencia. Además, las capas de BNBT pueden actuar como capas barrera de las corrientes de fuga de las capas de BF.*

Para comprobar estas hipótesis se han fabricado y estudiado composites multicapa en forma de lámina delgada con diferentes configuraciones hasta encontrar aquellas que solucionan de forma eficiente los problemas de pérdida de remanencia de BNBT y de los altos valores de conductividad de BF.

Con este objetivo, primero se han estudiado en detalle las propiedades de láminas de BNBT y de BF por separado. En el caso de las láminas de la solución solida de BNBT se han estudiado diferentes composiciones próximas a la frontera de fase morfotrópica MPB (del inglés, Morphotropic phase boundary) con el fin de identificar la composición que poseía las mejores propiedades ferroeléctricas. Se han estudiado los efectos que la adición de excesos de Bi y Na en las disoluciones precursoras tiene en las propiedades de estas láminas. Además se ha investigado cómo evolucionan las

propiedades de estas láminas con la temperatura, para proponer un diagrama de fases para las láminas delgadas de BNBT preparadas a partir de disoluciones con y sin excesos de Bi y Na. Se ha demostrado que la lámina más próxima a la MPB, y por tanto con las mejores propiedades ferroeléctricas, era la que poseía un contenido de $BaTiO_3$ de x=0.055, similar a lo reportado para cerámicas. Esta lámina presenta una polarización de P_s=26.5 $\mu C \cdot cm^{-2}$ y P_r= 12.3 $\mu C \cdot cm^{-2}$. De la falta de remanencia (P_r/P_s =0.5) se concluye que es consecuencia del pequeño tamaño de grano de esta láminas.

En el caso de las láminas delgadas de BF se han preparado láminas con diferentes condiciones de fabricación, variando la temperatura de cristalización. Además se han preparado láminas a partir de disoluciones precursoras con y sin excesos de Bi. Se ha estudiado la dependencia de la polarización con estos parámetros. Además se ha realizado un análisis de las corrientes de fuga y la presencia de ruptura dieléctrica en función de la temperatura de cristalización. En estas láminas de BF se ha observado los efectos que el dopaje con Ca^{2+} tienen en las propiedades ferroeléctricas. Se determinaron láminas de BF puro con mejores propiedades ferroelectricas, altos valores de remanencia y pocas contribuciones no-ferroeléctricas con polarización de saturación es P_s=70.2 $\mu C \cdot cm^{-2}$ y la de remanencia, P_r= 66.0 $\mu C \cdot cm^{-2}$(P_r/P_s =0.9). Sin embargo, en estas láminas seguía existiendo el problema de ruptura dieléctrica a bajas temperaturas. Los dopajes con Ca mejoran este problema de ruptura dieléctrica y disminuyen las corrientes de fugas no-lineales por lo que son las más adecuadas para su uso en composite multicapas.

Como parte final de la tesis se han estudiado diferentes configuraciones de láminas MLC combinando capas de BNBT y BF. Se ha demostrado que para láminas MLC donde el BNBT no está en el medio de dos capas de BF, las propiedades de las

multicapas se corresponden con aquellas que se obtienen del efecto suma de las propiedades ferroeléctricas de las capas constituyentes. Cuando el BNBT está en el centro de la MLC, con dos capas de BF rodeándola, se estabiliza la polarización de BNBT lo que produce una mejora en la polarización remanente. La lámina MLC con los mejores valores (P_s = 43.6 $\mu C \cdot cm^{-2}$ y P_r = 32.4 $\mu C \cdot cm^{-2}$, P_r/P_s = 0.7) representa una mejora considerable con respecto a la láminas de BNBT. Usando un modelo de continuidad de corriente entre las diferentes capas de la MLC, se ha podido concluir que, cuando se combinan capas de polarización de saturación muy diferentes, es difícil conmutar esta polarización en la capa con mayores valores (BF). Para solventar esto, se han estudiado láminas MLC usando capas de BF dopadas con Ca (BCF) en lugar de las de BF puro. Este dopado disminuye la polarización de saturación de las capas de BCF, respecto a las capas sin dopar, y los aproximan a los valores del BNBT. Esto debería permitir polarizar totalmente esta capas e inducir una mejora en la polarización remanente, haciéndola más estable en el tiempo. Esto se ha podido demostrar, obteniendo P_s=24.5 $\mu C \cdot cm^{-2}$ y P_r=17.9 $\mu C \cdot cm^{-2}$, (P_r/P_s = 0.7), lo que significa una remanencia similar a la obtenida cuando se usaban capas de BF puro, pero con una mayor retención en el tiempo.

Las mejoras en los valores de conductividad relacionados con las capas de BF cuando se fabrican las láminas MLC también se han demostrado en esta tesis. Además se ha obtenido un ferromagnetismo latente mejorado con respecto a las láminas de BF, cuando se preparan como láminas MLC y se cambian sus condiciones de espesor de las capas, tensiones y tamaño de grano.

Finalmente, las mejoras en las propiedades de los composite multicapa respecto a las láminas delgadas de sus componentes por separado, tales como valores mayores de

polarización remanente, la disminución de las corrientes de fuga pertenecientesy la mejora en las propiedades magnéticas, hacen que estos materiales sean muy prometedores para su posible integración en microdispositivos multifuncionales.

TABLE OF CONTENTS

LIST OF FIGURES

CHAPTER-I.

CHAPTER-II.

CHAPTER-III.

CHAPTER-IV.

CHAPTER-V.

CHAPTER-VI.

LIST OF TABLES

CHAPTER-I

INTRODUCTION

1.1 Motivation and purpose of the work

The solid solution $(Bi_{0.5}Na_{0.5})_{1-x}BaxTiO3$ (BNBT) is nowadays one of the most studied lead-free materials, since it has emerged as an alternative to replace the toxic Pb-based materials used in most ferroelectics-based devices[1].This fact has been motivated by the environmental regulation of the European Union that restricts the use of lead in electronic devices due to its toxicity [2]. The main reason behind the interest in BNBT is the high piezoeletric coefficient values found in the morphotropic phase boundary (MPB). Currently, the integration of any material in electronic devices is normally performed in thin film configuration, to keep pace with the trend in miniaturization. When BNBT is fabricated in this configuration, the investigation of the ferroelectric properties has shown the reduction of the remnant polarization in thin films, related with the decrease in grain size [3].

Another Pb-free material that has generated considerable interest due to its potential integration in microelectronics devices is the bismuth ferrite perovskite $BiFeO_3$ (BF). This interest is based on the coexistence, at room temperature, of ferroelectric and antiferromagnetic orders. Nonetheless, despite the high polarization values found in BF, this system has high conductivity values, which restricts the access to the full functional ferroelectrics properties for microdevice application [4].

If we understand the mechanisms that affect the changes in the functional properties when going from bulk to thin films in lead-free materials, we could propose multilayer composite films with tailored properties. Similar to what has been proposed in previous work of our research group, where it is possible to obtain enhanced ferroelectric

properties of thin films of (1-x)Pb($Mg_{1/3}Nb_{2/3}$)O_3x $PbTiO_3$ (PMNT) sandwiched between two poled layers [5].

The aim of this thesis is:

- *Propose lead-free ferroic alternative materials for application in microdevices.*

To fulfill this principal objective it is necessary to achieve other secondary objectives as:

- *Understand the mechanisms that determine the changes in the functional properties for the case of the most promising lead-free thin films with ferroelectric and multiferroic properties, BNBT and BF respectively.*
- *Propose, fabricate and study multilayer composite films (MLC) with improved performance for their possible integration in magnetoelectric microdevices.*

1.2 Ferroelectric polycrystalline materials.

The ferroelectricity in single-crystals was discovered in 1921 by J. Valasek in Rochelle Salt and some years later in polycrystalline ceramics (barium titanate, $BaTiO_3$). Since then, it has been a continuous succession of research studies aimed at their integration in devices. Ferroelectrics possess a spontaneous polarization that can be switched by an applied electric field. However, in the pioneering investigations on polycrystalline ceramics, the prevailing opinion was that they could not be piezoelectrically active, i.e., that, when subjected to mechanical stress, they generate an electric charge or, conversely, they generate mechanical strain in response to an applied electric field [6]. This was based on the idea that, on the sintered ceramics, the polarization within the grains would be randomly oriented, yielding no net spontaneous polarization, and thus

no net piezoelectricity. This idea changed when it was proved that an external electric field could reorient the polarization within the grains (poling). In fact, poling affects the ferroelectric domains. Ferroelectric domains are the regions of the crystal with uniformly oriented spontaneous polarization, separated by the so-called domain walls. The movement of these domains walls during the poling process produces materials with net polarization, possessing both ferroelectric and piezoelectric properties, similarly to single crystals, but with simpler fabrication processes. The discovery of poling was the key to turning an inert ceramic into an electromechanically active material with a multitude of industrial applications. In this thesis we will focus in the ferroelectric properties of polycrystalline materials in thin film form.

1.2.1 Ferroelectric hysteresis loops.

The switchable spontaneous polarization that presents the ferroelectric materials under the application of an electric field, exhibits a characteristic hysteresis loop as shown in Figure 1.1. The parameters that define the ferroelectric loop and determine the suitability of this type of material for electronic applications are: the remnant polarization, P_r, the saturation polarizations, P_s, and the coercive field, E_c. These parameters are related with the behavior of the ferroelectric domains under the action of the electric field. In this type of polycrystalline material, with increasing electric field intensity, the ferroelectric domain whose polarization is parallel to the electric field grows at the expense of those with polarizations in other directions, producing a net polarization. When all the possible domains have their polarization aligned in the direction of the electric field, a saturation state is reached and the net polarization of the material is P_s. With the decrease of the electric field intensity, the polarization decreases, but does not go back to zero. Not all ferroelectric domains go back to their

starting state and the materials exhibit a remnant polarization P_r when the electric field is zero. This remnant polarization cannot be removed until the applied electric field in the opposite direction reaches a certain value. The value of the electric field in the opposite sense required to reduce the polarization to zero is called the coercive field E_c. Therefore, in order to change the sign of the polarization (switching) of a material, the minimum electric field that we need to apply is the coercive field. The saturation values are attained for electric fields higher that E_c. Generally with the application of a field three times higher, saturation is reached, and a saturated P-E hysteresis loop is obtained.

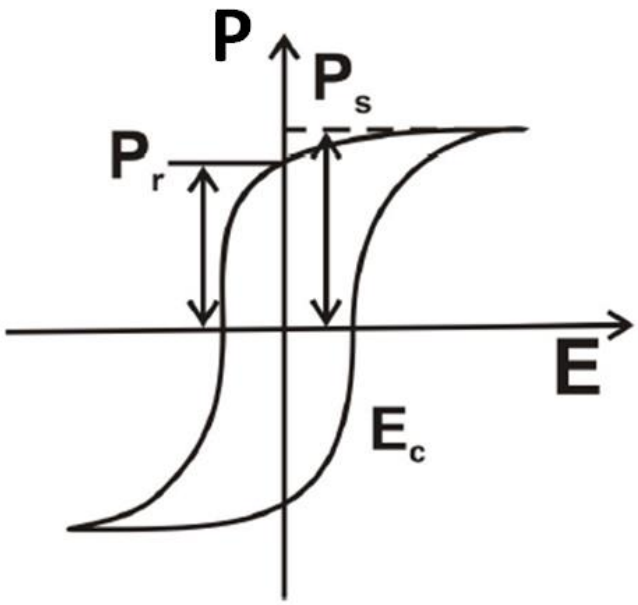

Figure1.1: *Typical P-E hysteresis loop of a ferroelectric material.*

1.2.2 Phase transitions and relaxor-ferroelectrics.

One important aspect that is necessary to take into account in ferroelectrics is that they typically present a structural phase transition from a high-temperature paraelectric phase into a low-temperature ferroelectric phase. This phase transitions from this non-

polar phase to the ferroelectric state takes place at the so-called Curie temperature T_C, and it is accompanied by the appearance of a dielectric anomaly (Figure 1.2). This anomaly, depending on the form of the peak, has been separated into two groups: normal ferroelectrics (Figure 1.2 a,b), that show a sharp phase transition of first or second order and, therefore, a well-defined Curie temperature (T_C), and relaxor ferroelectrics, that present a diffuse phase transition with a strong frequency dispersion (Figure 1.2c). Another important characteristic of ferroelectric materials is that the spontaneous polarization vanishes with the temperature, which is called thermal depolarization. The depolarization curves are different for the different types of ferroelectric materials. In the case of normal ferroelectrics, the spontaneous polarization disappears at T_C, sometimes sharply (Figure 1.2 a, normal ferroelectric with a first order transition) and in other cases, gradually (Figure 1.2 b, normal ferroelectric with a second order transition). In the case of relaxor ferroelectrics, with increasing temperatures the spontaneous polarization decreases but does not disappear for temperatures above the dielectric anomaly (Figure 1.2 c) [7].

The reason that these relaxor ferroelectrics are not completely depolarized above the dielectric anomaly is related with the fact that, upon cooling from high temperatures, polar nanometric regions (PNRs) appear, whose dipole moments are randomly distributed. The temperature at which these polar nanometric regions appear is called Burns Temperature (T_B), which is higher than T_C. These PNRs affect the behavior of the crystal dramatically, giving rise to unique physical properties. For this reason, the state of a crystal at lower temperatures than T_B is considered a new phase, different from the paraelectric one.

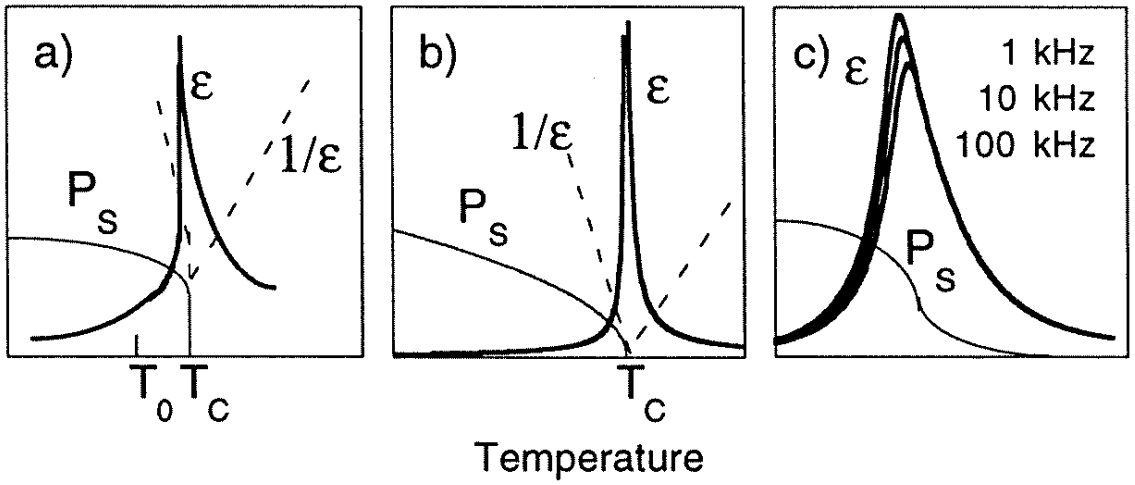

Figure1.2: *Dependence of the dielectric permittivity and spontaneous polarization P_S with the temperature for (a) a first- and (b) a second-order phase transitions of normal ferroelectrics and (c) relaxor ferroelectric[7].*

The formation of these PNRs cannot be considered a phase transition because it is not accompanied by any crystallographic structural change, either on the macroscopic or mesoscopic scale. But it is known that the presence of these PNRs with randomly distributed dipole moments up to temperatures just below T_B, makes the relaxor ferroelectrics to transform from a paraelectric phase into an ergodic relaxor (ER) state. In this ergodic state the polar nanoregions are characterized by their high fluctuation and vibrations. On cooling, their dynamics slows down enormously and, at a low enough temperature, called freezing temperature, T_f, the polar nanoregions become immobile, i.e. frozen, in a non-ergodic state (NR). The slowing down of the PNR dynamics produces a large and wide peak in the temperature dependence of the dielectric permittivity (ε), with the characteristic dispersion shown in the example of figure 1.3 [7].This peak is characterized by a temperature T_m, which depends on the frequency, f. This is the behavior of a so-called canonical relaxor ferroelectrics (Figure 1.4a).

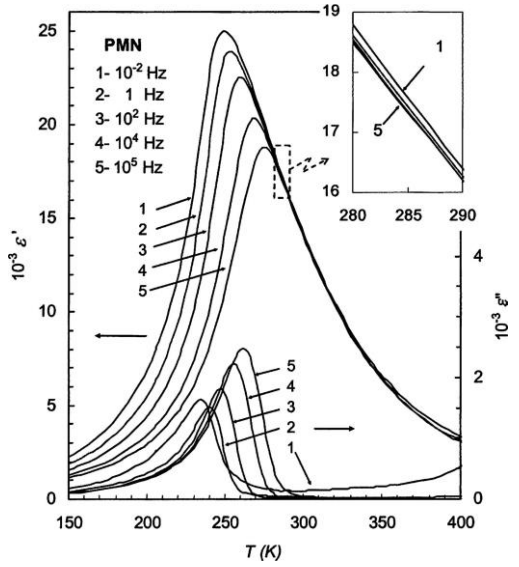

Figure1.3: *Real and imaginary part of the permittivity with temperature for relaxor ferroelectric* $Pb(Mg_{1/3}Nb_{2/3})O_3$ *reported by A.A. Bokov et al. [7].*

In canonical relaxor ferroelectrics, the application of a large enough electric field can transform the non-ergodic relaxor phase into a long range polarization ferroelectric phase. Upon heating, this ferroelectric phase is transformed again into an ergodic relaxor at the Curie temperature T_C*, which is very close to the freezing temperature* (T_f)*. In the so-called non-canonical relaxor ferroelectric materials there is a transition from the ergodic relaxor phase to a low-temperature ferroelectric phase (Figure 1.4b).*

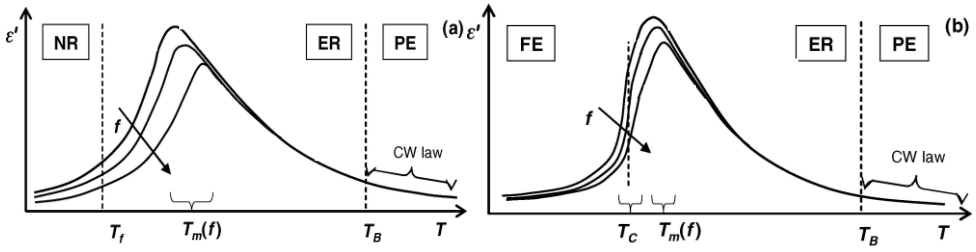

Figure1.4: *Behaviour of the permittivity vs. temperature in relaxor ferroelectric materials: a) canonical and b) non-canonical relaxors with ferroelectric stable state without need of apply high electric fields for temperature below of the* T_m *and* T_f *[7].*

The analysis of the observed frequency dispersion of T_m in these relaxor ferroelectric materials can be done using the Vogel-Fulcher (VF) law [8] (equation 1.1) for the real and imaginary parts of the permittivity (ε′(T) and ε′′(T)):

$$f = (2\pi\tau_0)^{-1} exp[{}^{-E_a}/_{T_m - T_f}] \qquad (1.1)$$

where f is the measurement frequency, τ_0 the relaxation time, E_a activation energy and T_f freezing temperature.

1.2.3 Multiferroics.

The ferroelectric order can coexist with other ferroic orders. The multiferroic materials are those that present the coexistence of at least two primary ferroic orders, ferroelectric (spontaneous polarization that can be switched by the application of an electric field), ferromagnetic (spontaneous magnetization that is stable and can be switched by the application of a magnetic field), or ferroelastic (spontaneous deformation that is stable and can be switched by the application of an electric field) [9]. Figure 1.5a, shows a schematic diagram where the relationships between the different primary ferroic orders in multiferroics are indicated. In addition, in this multiferroic material the coexistence of at least two of the three ferroic orders enables the existence of additional interactions [10]. In the magnenoelectric coupling the magnetic field H controls the polarization and the application of an electric field E produces variation of the magnetization M (Figure 1.5b).

a)

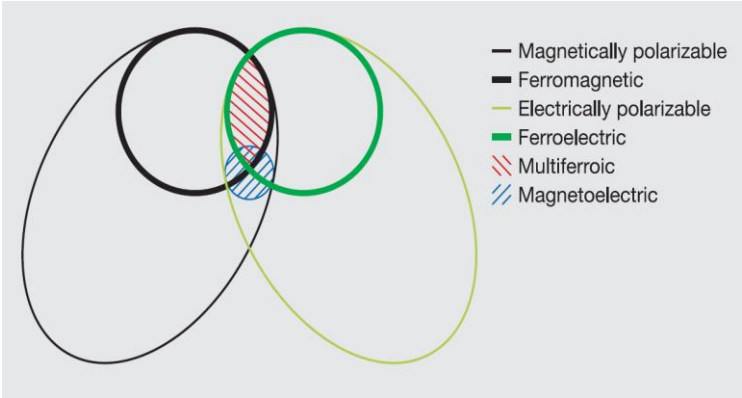

b)

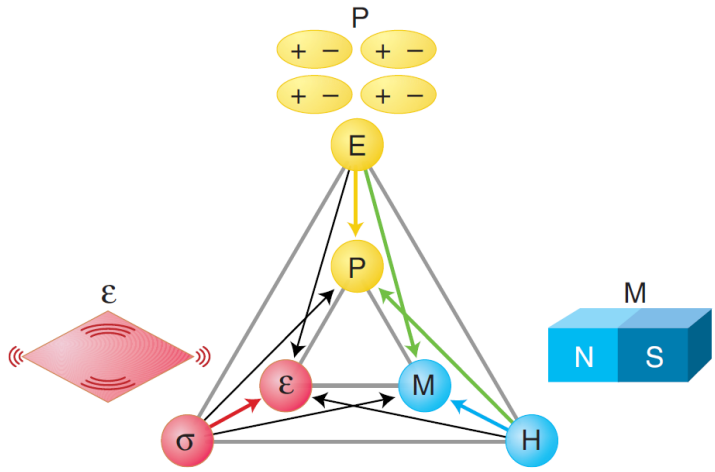

Figure1.5: *a) The relationship between multiferroic and magnetoelectric [9], b) Schematic illustrating different types of coupling present in multiferrioc materials [10].*

In the direct magnetoelectric response, the relationship between the electric polarization, P, obtained upon applying a magnetic field, H or the voltage output, produced by application of the magnetic field, which is the so-called magnetoelectric effect, is given by:

$$\Delta P = \alpha \Delta H \quad or \quad \Delta E = \alpha_E \Delta H \qquad (1.2)$$

where E is the electric field, α is the magnetoelectric coefficient and α_E is the magnetoelectric voltage. Similarly, the converse magnetoelectric effect, describing the change in the magnetization, M, with an applied electric field, E, is given by:

$$\Delta M = \alpha \Delta E \qquad (1.3)$$

This means that it is possible to modulate the magnetism with the application of an electric field.

In a multiferroic material with coexisting ferroelectric and ferromagnetic orders and with a strong magnetoelectric coupling, the electric polarization would show a hysteretic response as a function of the applied magnetic field and similar to the response of the magnetization with the application of an electric field, as is shown in Figure 1.6 [11]. These hysteresis loops are somewhat similar to the well-known ferroelectric hysteresis loops and it is this possibility of switching polarization with a magnetic field and magnetization with an electric field in magnetoelectric materials, which makes them promising for applications such as sensors, transducer, filters, oscillators, phase shifters, memory devices, and so on.

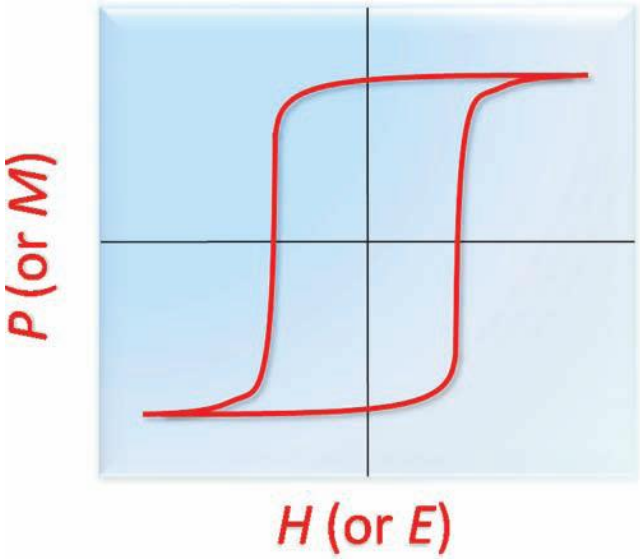

***Figure1.6**: Schematic illustration of an ideal case of the magnetoelectric coupling: magnetic response to an electric field (M–E hysteresis response), and, vice versa, the modification of polarization by magnetic field (P–H behavior) [11].*

From the point of view of material constituents, magnetoelectric materials can be divided into two types: single-phase and composite materials. The magnetolectric effect

has been observed as an intrinsic effect in some single phase materials as for example the hexagonal manganites ($YMnO_3$, $BiMnO_3$) and the perovskite of bismuth ferrite $BiFeO_3$ (BF), that are the most promising for magnetoelectric applications and have been under intensive study in the last years [9-15]. In most of them it is not possible to obtain the magnetoelectric coupling at room temperature because only the ferroelectricity o ferromagnetism appears only at low temperature. In addition, a high inherent magnetoelectric coupling has not yet been found. In the case of the manganites, the main drawback for applications is that the magnetic properties appear at very low temperatures (low Neel temperature). On the contrary, the perovskite of bismuth ferrite BF is the unique that has simultaneously, ferroelectric and antiferromagnetic properties at room temperature, which makes it more attractive for multiferroic applications.

1.3 Lead-free compositions.

About ten years ago, stimulated by one publication of Saito et al [16], the research in order to find lead-free functional materials increased considerably. This has been motivated by environmental regulations that require the removal of toxic elements such as Pb from any electronic device. This means that a replacement for the widely used lead-based compositions, as PZT, must be found. In the last decade the number of research works on lead-free piezoceramics has increased from 60 in 2004 to 400 in 2011 [1].

The term lead-free materials is a generic term that includes two general groups: one competes for the substitution of PZT in the same applications and another offers better or new properties that are outside the range where PZT can be used. To the first group

belong mostly solid solutions with polymorphic or morphotropic phase boundary compositions [1] (see Figure 1.7):

- *(Ba,Ca)(Zr,Ti)O_3 (BCZT): limited due to the low Curie temperature (Tc < 120^{0}C)*
- *$K_{0.5}Na_{0.5}NbO_3$ (KNN) based solid solutions that have giant piezoelectric at the transition between orthorhombic and tetragonal structure and limited due to the transition temperature that can be tuned down to near room temperature.*
- *$(Bi_{0.5}Na_{0.5})_{1-x}Ba_xTiO_3$ (BNBT) based solid solutions have good piezoelectric coefficients and high maximum dielectric permittivity. However, depolarization occurs at around 100^{0}C [1].*

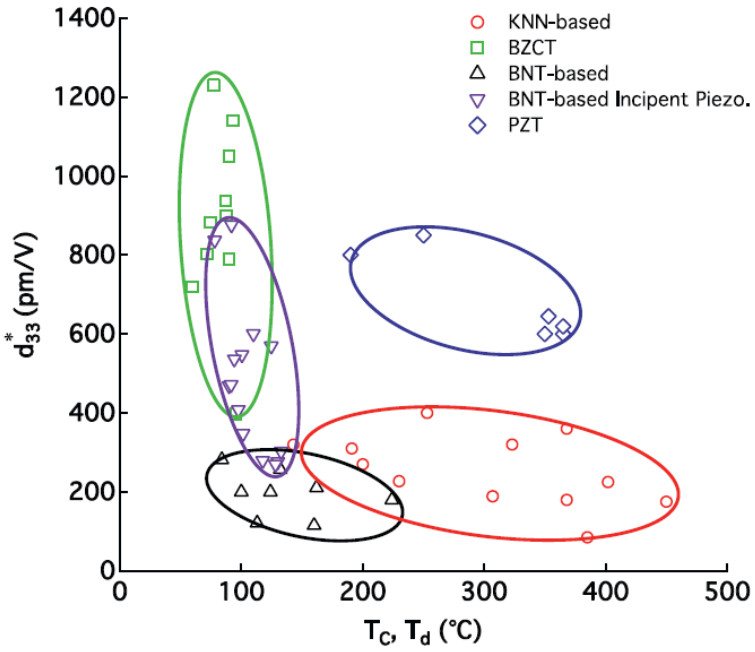

***Figure1.7**: The large signal piezoelectric coefficient (at room temperature) as a function of depolarization temperature for KNN-based, BCZT, BNT-based, BNT-based incipient piezoelectrics [1].*

The second group includes materials with properties with which PZT cannot compete. Among them we can mention $LiNbO_3$ single crystals, Aurivillius structures (Bi-based

layered structure) or multiferroic $BiFeO_3$. This latter material stands out due to the coexistence of ferroelectric and antiferromagnetic states at room temperature [4]. In addition, it has been reported its preparation as thin film for their integration in microdevices [17].

Here we describe the main known characteristics for the two lead-free compositions analysed in the present thesis.

1.3.1 Solid solution $(Bi_{0.5}Na_{0.5})_{1-x}Ba_xTiO_3$.

In 1991, Takenaka et al.[18] studied the phase diagram of the solid solution of the relaxor ferroelectric $(Bi_{0.5}Na_{0.5})TiO_3$ and the normal ferroelectric $BaTiO_3$ (figure 1.8). They reported Curie temperatures close to 300^0C for all compositions and depolarization temperatures between 160 and 250 ^0C for compositions below 10 mol % of $BaTiO_3$, which appear in the diagram as a transition to an antiferroelectric (AF) phase.

In addition, it is known that in solid solutions formed with perovskites of different crystalline structures, a structural phase transition induced by a compositional change occurs. This phase boundary is known as the morphotropic phase boundary (MPB) and plays a special role in obtaining excellent piezoelectric properties [6]. This morphotropic transformation occurs due to free energy differences between two crystallographic structures. In a solid solution, as one ion replaces another, the energies of the different structures change, and the crystal assumes the structure having the minimum free energy. For the compositions in this MPB the elastic constant tend to minimize, while the electrical properties tend to increase, reaching their highest values in parameters such as the dielectric constant, the polarization and the piezoelectric coefficient.

In the case of the solid solution of BNBT, several studies have reported some discrepancies on the existence of other intermediate phases at room temperature in this region of the phase diagram [19-22] and still some controversy persists. For example , based on the variation in the electrical properties and in situ synchrotron diffraction analysis, the MPB region for BNBT bulk ceramics has been positioned for x between 0.055 and 0.110, where the transition from the rhombohedral R3c/R3m space group to tetragonal P4mm occurs [23]. Recently in other works also indicate the existence in BNBT bulk ceramics of a tetragonal P4bm relaxor phase for compositions between x = 0.055 and 0.080 and a P4mm ferroelectric phase for x = 0.100–0.110 [24]. The results obtained by Takenaka et al. indicated the occurrence of an antiferroelectric phase, which has been identified later, with new evidence collected, as a relaxor phase [23,25]. This is attributed to A-site cation disorder. In this type of material the piezoelectric coefficient and the polarization have a drop at relatively low temperature (T_d -see Figure 1.8), which are the currently known drawbacks for possible piezoelectric applications. A large amount of attempts using conventional methods based on solid solution or chemical doping have been explored, but failed to suppress or eliminate the depolarization of BNT-based solid solutions. Such methods generally lead to decreased T_d towards root temperature to enhance piezoelectric properties at room temperature, while the increase on T_d is at the expense of reduced piezoelectric properties[26-29]. Up to now, it is still a challenge to increase T_d and enhance piezoelectric properties simultaneously. However, in recent investigations it has been reported improvements in this depolarization temperature through the integration in a BNBT matrix of Wurtzite ZnO that is a polar semiconductor with piezoelectricity. This material has been prepared with 0–3 type composites, in which the BNBT grains form a three-dimensional network, while the ZnO particles are isolated [30].The idea of this work is based in that

the depolarization field in the BNBT ceramics is partially compensated by the charges stemming from ZnO and it is possible to improve or remove the depolarization in the BNBT bulk ceramics.

The integration of this material in thin film for its possible applications in microelectronic devices with optimum electrostrictive and piezoelectric actuation receives actually large interest. Therefore, several publications have been devoted to BNBT thin films [31-34], although most of them focused on processing issues. Although there are few studies that make a full description of the behavior in the ferroelectric properties and their evolution with the temperature, it is possible to find in the literature some research which shows that the BNBT films has problems in the retention of the properties [35, 36], which is typically foundin thin films due to size grain effect [3].

Therefore, the novelty of this thesis is that in this works we present for the first time a rigorous analysis of the ferroelectric properties in thin films of BNBT with composition closed to the MPB, the evolution of these properties with the temperature and the macroscopic piezoelectric responses.

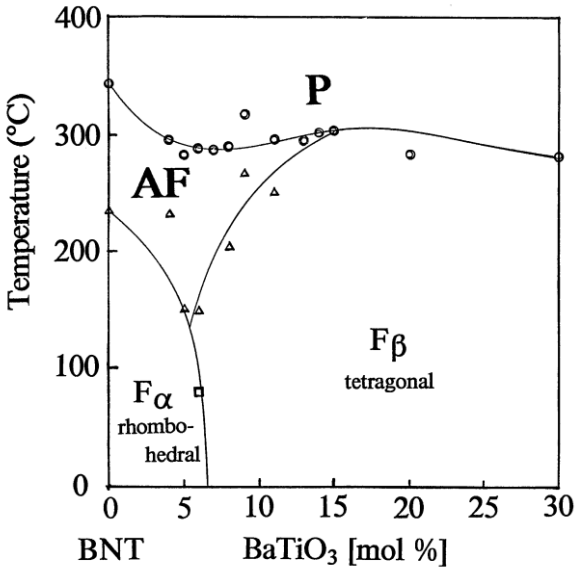

Figure1.8: *Phase diagram of solid solution $(Bi_{0.5}Na_{0.5})_{1-x}Ba_xTiO_3$, reported by Takenaka et al. [18].*

1.3.2 $BiFeO_3$ perovskite.

Bismuth ferrite $BiFeO_3$ (BF) is a multiferroic composition that exhibits simultaneously ferroelectric and antiferromagnetic ordering at room temperature [4]. Smolensky's group is pioneering in the study of this composition [37-39]. They found that it was very difficult to grow single crystals of this composition without the formation of secondary phase, and when prepared as bulk ceramic, the conductivity is very high, mainly due to the presence of oxygen vacancies and mixed Fe valences [40]. In these first studies, the experimental values of the remnant polarization obtained in ceramic were very low, but different reported simulations proved that the remnant polarization of $BiFeO_3$ could be 15 times higher than that obtained experimentally [17]. It was observed that the theoretically predicted high remnant polarization values can be reached in thin film form ($Pr \sim 60\ \mu C/cm^2$) thanks to the strain produced by the substrate that deforms the unit cell [17]. Later, when improvements in the fabrication methods allowed obtaining high quality single crystals, the occurrence of these high remnant polarization values was confirmed [41]. More recently, in bulk ceramics, it has also been reported high values of the remnant polarization, after optimizing the processing methods [42]. Despite these great efforts made by different authors in understanding the structure and the properties of the BF, there are still problems that hinder its integration in microelectronic devices, as can be the high values of conductivity [4,17,43].

Regarding the magnetic properties of $BiFeO_3$, it shows local short-range magnetic ordering of G-type antiferromagnet, which means that every Fe^{3+} spin is surrounded by six antiparallel spins of the nearest Fe neighbors [4]. The spins are in fact not perfectly antiparallel, but a weak canting moment appears, caused by local magnetoelectric coupling with the polarization vector [4]. Superimposed on this canting, however, is

also a long-range superstructure consisting of an incommensurate spin cycloid of the antiferromagnetically ordered sublattices. The cycloid shows a periodicity of about 62-64 nm, and a propagation vector in the (10-1) direction [44,45]. The magnetic plane in which the spin rotates is defined by the propagation (10-1) and the polarization (111) vectors, and it is used to represent the spin cycloid (figure 1.9).

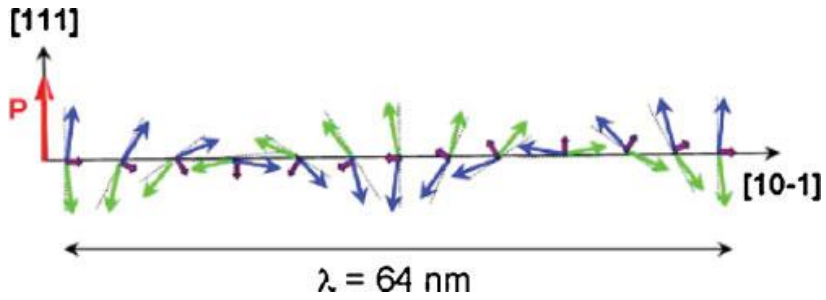

Figure 1.9: *Representation of the spin cycloid in the magnetic plane [44], blue and green vectors correspond to the non-parallel ferromagnetic spin (canted antiferromagnetic- purple arrows).*

Several improvements have been obtained in the ferroelectric and magnetic properties when the BF is prepared as thin film, which would benefit its possible integration in microelectronic devices. Despite this, there is still work needed to properly integrate this material in functional devices, as the improvement of the high leakage current and dielectric breakdown that prevents the switching of the polarization at room temperature.

In the last few years, attention has also been given to studying doped BF thin films (both A-site and B-site doping) in an attempt to reduce the leakage currents and alter the magnetic properties. In addition, the divalent ion doping generates imbalance of valence states, changing the dielectric properties of the material and allowing the change in the ferroelectric properties. This change can be achieved for example in Ca doped BF films. The doping of BF thin films can improve the microstructure, reducing

the vacancies number and preventing the formation of secondary phases. Another work shows that the decrease of the leakage currents can be attributed to an increase of percent of crystalline phase (crystallinity) rather than doping [46].This indicates that there are different forms of improving the functional properties of the BF thin films with the aim to integrate them in microelectronic devices, but much work is still needed to solve the shortcomings of BF films.

In the case of the magnetic properties in BF thin films, they continue to be a contentious subject to this date. In several investigations it has been reported an enhanced thickness-dependent magnetism compared to polycrystalline bulk materials [17,47-51], which is attributed to an in-plane epitaxial constraint in the [111] direction that can break the cycloidal spin order, resulting in the release of the latent magnetization locked within the cycloid. In addition doping with divalent alkali metal ions, such as Ca^{2+}, Ba^{2+}, Sr^{2+}, Pb^{2+} La^{3+}, Nd^{3+}, etc., at the Bi site (A-site) also would increase the magnetization of BF films [52-56]. Besides, the introduction of A-site impurities results in the variation of the magnetic anisotropy constant, and, thus, provokes the transition from a spatially modulated spin structure to a homogeneously canted one. Magnetization measurements showed that the magnetic state of the films is determined by the ionic radius of the substituting elements, and dopants with the largest ionic radius effectively suppress the spiral spin structure of BiFeO3 [52].

1.4 From ferroic bulk ceramics to thin films.

The miniaturization trend of the microelectronics industry has produced a gradual reduction of the device size, which has forced the transition from bulk to thin film materials. As a consequence, ferroics must be prepared in thin film form to be integrated in smaller devices, but developing the same functions with similar reliability.

This is a challenge, as the reduction of the material dimensions and the fact that now they are attached to a substrate, produce significant variations of their properties.

In the case of ferroelectric materials, the clamping of the film to the substrate affects directly the piezoelectric properties. Using the converse or direct effect, and taking into account the stresses imposed on the film by the substrate, it has been reported that the measured coefficient in films is always smaller than in unclamped bulk materials [57]. This is one of the effects that it is necessary to take into account for their integration, for example, in microelectromechanical systems (MEMS). Nevertheless, the residual stress that are created by the clamping of the sample with the substrate also have a positive impact on the properties as in the case of the perovskite of bismuth ferrite, which create a latent remnant magnetization[4].

One of the main aspects to be considered when dealing with polycrystalline thin films is their reduced grain size, due to the lower crystallization temperatures used, and the reduced thickness. For both, ferroelectric and ferromagnetic materials, the size effect is an important parameter to take into account in the resultant properties of the films.

In ferromagnetic materials, the nature of the problem is quite well defined: when the size of ferromagnetic nanoparticles decreases, the magnetic anisotropy energy decreases at the same time. When this energy becomes smaller than the thermal energy k_BT of the grains, thermal fluctuations will flip the magnetic moment of the nanoparticles and cause the loss of the macroscopic magnetic moment. This size effect for ferromagnetic nanoparticles usually appears in particles smaller than 50 nm [58].

In ferroelectric materials, the size effects have been studied, mostly related to the disappearance of ferroelectricity below a critical size [59].The electrical properties of these polycrystalline materials present a distinctive variation with grain size that is

associated with the evolution of the ferroelectric domain configuration, and their mobility [3, 60-63]. For example in the most employed ferroelectric for piezoelectric technologies, PZT, a strong decreasing of the piezoelectric coefficient with the decrease of the grain size has been reported, as a result of the decrease of the domain wall mobility [64]. In addition, due to the same effect, it has been reported that in complex perovskites with an end member showing relaxor ferroelectric characteristics, like the PMN-PT, grain size reduction leads to the stabilization of phases in which the ferroelectric long range order is destroyed [65]. The main size effect identified in these relaxor-based solid solutions is a slowing down of the kinetics of the ferroelectric to relaxor transition [66], until the high temperature relaxor state stabilizes for the smallest, nanometric grains [67,68] In this type of material changes in the kinetics of the transition can be understood within the two-stage model for the development of ferroelectric long range order in relaxor systems, proposed by Ye et al [69]. The model proposes that the kinetics of the transition is controlled by the volume of polar nanoregions (PNRs) at the onset of the ferroelectric fluctuations, and that there is a temperature at which the volume of PNRs reaches a threshold that hinders the ferroelectric fluctuations triggered by the transition, and slows down its kinetics.

Ferroelectric properties in thin films are also affected by the formation of "dead layers". These layers can be formed in the surface by bombardment of the sputtering ions during the deposition of a top electrode or by changes in stoichiometry due to the loss of volatile elements. The "dead layer" can reduce the ferroelectric properties due to the pinning of domain walls or the screening of the internal field by a depletion layer [59]. In fact, the "dead layer" can gives rise to worse properties or directly suppress ferroelectricity. Nowadays the advances in the fabrication methods and experimental

techniques allow studying the influence of all these defects created by the processing in different thin films and separate the intrinsic and extrinsic size effect.

1.5 Multilayer composite films.

The fabrication of composites by combining different materials has received much attention, because it allows combining the properties of different materials. The properties of composites can be classified as sum properties (averaging of similar properties in the component phases following a mixing rule, e.g. dielectric permittivity, piezoelectric coefficient), combination properties (properties involving two or more different coefficients with often different mixing rules, e.g. acoustic wave velocity that depends on material stiffness and density) and product properties (properties of the constituent phases yield a new property in the composite, e.g. magnetostriction and piezoelectricity of constituent phases yield magnetoelectricity in the composite) [70]. The models applied to define the mixing rules are determined, especially for composite electroceramics, by the self-connection of the phases [71]. The application of series or parallel models is connected to the connectivity pattern of the composite. Connectivity is expressed by two or more numbers, one for each constituent phase. Each phase in a composite may be self-connected in zero, one, two or three dimensions. Therefore, for a diphasic composite there are ten possibilities: 0-0, 1-0, 2-0, 3-0, 1-1, 2-1, 3-1, 2-2, 2-3 and 3-3.

Regarding composites with ferroelectric phases, the saturation polarization, P_s, is obtained from the P_s of the constituent phases, taking the volume fractions, V_i, for a weighted sum:

$$P_s^n = V_1 P_{s1}^n + V_2 P_{s2}^n + \ldots \qquad (1.6)$$

The mixing rule in this case introduces an exponent n, which depends on the geometric arrangement of the phases.

The 2-2 connectivity achieved in multilayer capacitors with alternating layer of two phases, where both phases are self-connected in the lateral directions but not perpendicularly to them, proves to be very effective for producing high electric fields with the application of relatively small voltages. The use of multilayer composites (MLC) produces improvements in the piezoelectric properties respect to the single-phase material [71]. The combination of hard PZT (large coercive field) and soft PZT (small coercive field) in a multilayer composite takes advantage of the large piezoelectric response of the soft PZT , while keeping it in a poled state with the electric field induced by the poled hard PZT layers. This was first proposed for bulk multilayer composites, with thick ceramic , but the idea can be successfully translated to thin films of PMN-PT, when prepared as multilayer composites of films [5]. In this type of multilayer composites, the longitudinal piezoelectric coefficient, d^{MLC}_{33}, can be calculated from the following equation, which considers the sum of the piezoelectric properties of two layers in series connection:

$$d_{33}^{MLC} = d_{33}^{1} \cdot \varepsilon_{33}^{2} \cdot V^{1} + d_{33}^{2} \cdot \varepsilon_{33}^{1} \cdot V^{2} \Big/ \varepsilon_{33}^{2} \cdot V^{1} + \varepsilon_{33}^{1} \cdot V^{2} \qquad (1.7)$$

where 1 and 2 denotes the two phases of the composite, V^1 and V^2 are the volume fractions, and ε_{33}^{1} and ε_{33}^{2} are the dielectric permittivities of each phase.

Based on the principles traditionally used in bulk composites, the packing of layers of different ferroelectric compositions in a multilayer composite configuration in thin film form has proved to be successful for the improvement of the dielectric, ferroelectric, piezoelectric and pyroelectric properties compared to single phase films, as recent

reviews show [72,73]. In addition, several multilayer ferroelectric films and superlattices have been designed searching the inducement of stress or strain effects in the films, not only through epitaxial relations in superlattices [74,75], with the enhancement of the polarization by strain, but also in polycrystalline films, where the enhancement of the dielectric and pyroelectric properties are attributed to the lower residual stress found in the heterostructures [76].

In recent years, composites and multilayers ferroelectric oxides in thin film form have been intensively studied [77-85] ,motivated by the possibility of expected enhancement in the resultant property, which can be used for the development of microelectronic devices. The major problem for the integration of the ferroelectric films in devices is the decrease in switchable polarization after many cycles of field reversals (fatigue) when a pure metal such as Pt is used as the electrode. The fabrication of the multilayer ferroelectric films is a possibility to resolve this problem. Some authors have studied how is the change in the properties for the most used ferroelectrics when integrated in electromechanical devices. Barrow et al [78] studied the dielectric properties of films composite of PZT with different compositions, deposited on Pt-coated Si. In these composites it was observed an improvement in the remnant polarization and the piezoelectric coefficients, and values of these properties comparable with the bulk materials were obtained. Another problem of the ferroelectric materials that can be improved with the fabrication of composites is the leakage current. Jia et al [86] constructed a multilayer capacitor structure of $BaTi0_3$ with layers of polycrystalline, and amorphous $BaTiO_3$ by sputter deposition technique on RuO_2-coated SiO_2/Si substrates. The authors observed a considerable reduction in leakage current density as the number of the amorphous phase increased. They related this effect with the charges accumulation at the interfaces between amorphous and crystalline phases in

the MLC .These charges may create a local electric field when an external electric field is applied, which may act as a potential barrier in order to reduce the leakage current. Many other studies have been performed that demonstrate the possibility to improve the functionality of the ferroelectrics films when they are prepared as composites, given rise to different reviews as the reported by Jayadevan et al. [87] where several ferroelectric composites, properties and fabrication methods are discussed.

1.6 References.

[1] J. Rödel, K. G. Webber, R. Dittmer, W. Jo, M. Kimura, D. Damjanovic, J. Eur. Ceram. Soc. 35 ,1659–1681, (2015).

[2] EU-Directive 2002/95/EC, Offi. J. Europ Union, 46[L37] 19-23,(2003).

[3] M. Algueró, J. Ricote, R. Jiménez, P. Ramos, J. Carreaud, B. Dkhil, J. M. Kiat, J. Holc, M. Kosec, Appl. Phys. Lett. 91, 112905, (2007).

[4] G. Catalan, J. F. Scott, Adv. Mater, 21, 2463–2485, (2009).

[5] H. El Hosiny Ali, R. Jiménez, J. Ricote, J. Pérez de la Cruz, J.R.A. Fernandes, M.L. Calzada, Thin Solid Films 520, 7205-7211, (2012).

[6] Jaffe B, Cook W, Jaffe H. Piezoelectric Ceramics. New York: Academic. (1971).

[7] A. A. Bokov, Z.-G. Ye, J. Mater. Sci. 41, 31–52, (2006).

[8] D. Viehland, S. J. Jang, L. E. Cross and M. Wuttig, J. Appl. Phys. 68, 2916, (1990).

[9] W. Eerenstein, N. D. Mathur, J. F. Scott , Nature 442, 759-765, (2006)

[10] N. A. Spaldin, M. Fiebig, Science 309, 391-392, (2005)

[11] J. Ma , J. Hu , Z. Li , C. W. Nan, Adv. Mater., 23, 1062–1087, (2011).

[12] W. Prellier , M. P. Singh , P. Murugavel , J. Phys.-Condens. Mat. , 17 , R803, (2005).

[13] S. W. Cheong , M. Mostovoy , Nat. Mater, 6 , 13, (2007) .

[14] D. Khomskii , Physics , 2 , 20, (2009) .

[15] K. F. Wang , J. M. Liu , Z. F. Ren , Adv. Phys , 58 , 321, (2009) .

[16] Y. Saito, H. Takao, T. Tani, T. Nonoyama, K. Takatori, T. Homma, T. Nagaya, M. Nakamura, Nature;432:84–7.2, (2004).

[17] J. Wang, J. B. Neaton, H. Zheng,V. Nagarajan, S. B. Ogale, B. Liu, D. Viehland, V. Vaithyanathan, D. G. Schlom,U. V. Waghmare, N. A. Spaldin, K. M. Rabe,M. Wuttig, R. Ramesh, Sci. Vol 299, (2003).

[18] Takenaka, K. Maruyama, K. Sakata, Jpn. J. Appl. Phys. [30], 2236–2239p, (1991).

[19] B. Wylie-Van Eerd, D. Damjanovic, N. Klein, N. Setter, and J. Trodahl, Phys. Rev. B, 82, 104112, (2010).

[20] Y. Hiruma, Y. Watanabe, H. Nagata, and T. Takenaka, Key Eng. Mater., 350, 93–96, (2007).

[21] F. Cordero, F. Craciun, F. Trequattrini, E. Mercadelli, and C. Glassi, Phys. Rev. B, 81, 144124, (2010).

[22] J. Yao, L. Yan, W. Ge, L. Luo, J. Li, and D. Viehland, Phys. Rev. B, 83, 054107, (2011).

[23] W. Jo, S. Silke, E. Sapper, L. A. Schmitt, H. J. Kleebe, A. J. Bell, and J. Rödel, J. Appl. Phys., 110, 074106, (2011).

[24] M. Cheng, G. Hanzheng, P. B. Scott, T. Xiaoli, Phys. Rev. Lett. 109, 107602, (2012).

[25] C. Xu, D. Lin, and K. W. Kwok, Sol. Sta. Sci , 10 [7] 934-40, (2008).

[26] T. Takenaka, , H. Nagata, Y. Hiruma, IEEE Trans. Ultrason. Ferroelectr. Freq. Control 56, 1595–1612, (2009).

[27] S. T. Zhang, , A. B. Kounga, , E. Aulbach, H. Ehrenberg, J. Rödel, Appl. Phys. Lett. 91, 112906, (2007).

[28] Y. Hiruma, H. Nagata, T. Takenaka, Appl. Phys. Lett. 95, 052903, (2009).

[29] A. B. Kounga, , S. T. Zhang, , W. Jo, T. Granzow, J. Rödel, . Appl. Phys. Lett. 92, 222902, (2008).

[30] J. Zhang , Z. Pan, F.F.Guo, W.C. Liu, H. Ning, Y.B. Chen, M.H. Lu, B. Yang, J. Chen, S.T. Zhang, X. Xing, J. Rödel, W. Cao, Y.F. Chen, Nat. Comm, 6, 6615 ,(2015).

[31] H. W. Cheng, X.J. Zhang, S.T. Zhang, Y. Feng, Y.F. Chen, Z.G. Liu. Appl Phys Lett; 85: 2319–21, (2004).

[32] N. Scarisoreanu, F. Craciun, V. Ion, S. Birjega, M. Dinescu. Appl Surf Sci; 254: 1292–7, (2007).

[33] Y. Guo, D. Akai, K. Sawada, M. Ishida. Solid State Sci; 10:928–33, (2008).

[34] D. Alonso-San José, R. Jiménez, I. Bretos, M.L. Calzada. J Am Ceram Soc; 92, 2218–25, (2009).

[35] I. Bretos, D. Alonso-San José, R. Jiménez, J. Ricote, M. L. Calzada, Materials Letters 65, 2714–2716, (2011).

[36] D. Y. Wang, N. Y. Chan, S. Li, S. H. Choy, H. Y. Tian, and H. L. W Chan, Appl. Phys. Lett. 97, 212901, (2010).

[37] G. A. Smolensky, V. A. Isupov, A. I. Agronovskaya, Sov. Phys. Solid State, 1, 150, (1959).

[38] G. A. Smolenskii, A. I. Agranovskaya, S. N. Popov, V. A. Isupov, Zh. Tekh. Fiz., 28, 2152, (1958).

[39] A. Smolenskii, A. I. Agranovskaya, S. N. Popov, V. A. Isupov, Sov. Phys. Tech. Phys. Tech. Phys. 1958, 3, (1981).

[40] G. A. Smolenskii, I. E. Chupis, Usp. Fiz. Nauk, 137, 415, (1982).

[41] D. Lebeugle, D. Colson, A. Forget, M. Viret, P. Bonville, J. F. Marucco, S. Fusil, Phys. Rev. B, 76, 024 116, (2007).

[42] V. V. Shvartsman, W. Kleemann, R. Haumont, J. Kreisel, Appl. Phys. Lett., 90, 172115, (2007).

[43] A. K. Mikael, P. C. Tim, J. B. Andrew, Appl. Phys. Lett. 92, 072908, (2008).

[44] D. Lebeugle, D. Colson, A. Forget, M. Viret, A. M. Bataille, A. Gukasov, Phys. Rev. Lett., 100, 227602, (2008).

[45] I. Sosnovska, T. Peterlin-Neumaier, E. Steichele, J. Phys. C, 15, 4835, (1982).

[46] Lee Y-H, Wu J-M and Lai C-H, Appl. Phys. Lett. 88 042903, (2006).

[47] Jiagang Wu, John Wang, Dingquan Xiao, Jianguo Zhu, Appl. Mater. Interfaces, 3 (9), 3261–3263, (2011).

[48] C. Ederer, N. A. Spaldin, Phys. Rev. B 71, 224103, (2005)

[49] C.-C. Lee, J.-M. Wu, Appl. Sur. Scien. 253, 7069–7073, (2007).

[50] H. Béa, M. Bibes, S. Fusil, K. Bouzehouane, E. Jacquet, K. Rode, P. Bencok and A. Barthélemy, Phys. Rev. B 74 020101, (2006).

[51] F. Gao, X. Chen, K. Yin, S. Dong, Z. Ren, F. Yuan, T. Yu, Z. Zou and J. M. Liu Adv. Mater. 19, 2889, (2007).

[52] V. A. Khomchenko, D. A. Kiselev, J. M. Vieira, L. Jian, A. L. Kholkin, A. M. L. Lopes, Y. G. Pogorelov, J. P. Araujo, M. Maglione, J. Appl. Phys. 103, 024105, (2008).

[53] S. R. Das, P. Bhattacharya, R. N. P. Choudhary and R. S. Katiyar, J. Appl. Phys. 99, 066107, (2006).

[54] V. A. Khomchenko, D. A. Kiselev, J. M. Vieira, A. L. Kholkin, M. A. Sa, Y. G. Pogorelov, Appl. Phys. Lett. 90, 242901, (2007).

[55] H. Uchida, R. Ueno, H. Nakaki, H. Funakubo, and S. Koda, Jpn. J. Appl.Phys., Part 2 44, L561, (2005).

[56] Y. Sheng, W. Rui, X. Qiu, J. Du, S. Zhou, and Q. Xu, J. Appl. Phys. 115, 17D902, (2014).

[57] K.Lefki, G.J.M.Dormans, J. Appl. Phys. 76 1764, (1994).

[58] V. Skumryev, S. Stoyanov, Y. Zhang, G. Hadjipanayis, D. Givord, J. Nogues, Nature 423, 850–853, (2003).

[59] C. Lichtensteiger, M. Dawber, J. M. Triscone, Topics Appl. Phys 105, 305-338, (2007).

[60] G. Arlt, D. Hennings, and G. Dewith, J. Appl. Phys. 58, 1619 (1985).

[61] G. Arlt, Ferroelectrics 104, 217 , (1990).

[62] T. Hungría, M. Algueró, A. B. Hungría, A. Castro, Chem. Mater. 17, 6205, (2005).

[63] G. Arlt, J. Mater. Sci. 25, 2655 (1990).

[64] C. A. Randall, N. Kim, J. P. Kucera, W. Cao, and T. R. Shrout, J. Am. Ceram. Soc. 81, 677, (1998).

[65] J. Carreaud, J. M. Kiat, B. Dkhil, M. Algueró, J. Ricote, R. Jimenez, J. Holc, M. Kosec, Appl. Phys. Lett. 89, 252906 (2006)

[66] R. Jiménez, H. Amorín, J. Ricote, J. Carreaud, J. M. Kiat, B. Dkhil, J. Holc, M. Kosec, M. Algueró, Phys. Rev. B 78, 094103 (2008)

[67] M. Algueró, T. Hungría, H. Amorín, J. Ricote, J. Galy, A. Castro, Small 3, 1906 (2007)

[68] H. Amorín, R. Jimenez, T. Hungria, A. Castro, M. Algueró, Appl. Phys. Lett. 94, 152902 (2009)

[69] Z. G. Ye, Y. Bing, J. Gao, and A. A. Bokov, Phys. Rev. B 67, 104104, (2003).

[70] R. E. Newnham. Ann. Rev. Mater. Sci. 16 :47-8, (1986).

[71] R.E. Newnham, D. P. Skinner, L. E. Cross, Mater. Res. Bull. 13, 525, (1978).

[72] K. P. Jayadevan, T.Y. Tseng, J. Mater. Sci. Mater. Electron. 13, 439, (2002).

[73] D. Bao, Curr. Opin. Solid State Mater. Sci. 12, 55, (2008).

[74] H.N. Lee, H.M. Christen, M.F. Chisholm, C.M. Rouleau, D.H. Lowndes, Nature 433, 395, (2005).

[75] T. Shimuta, O. Nakagawara, T. Makino, S. Arai, H. Tabata, T. Kawai, J. Appl. Phys. 91, 2290, (2002).

[76] R. Poyato, M. L. Calzada, L. Pardo, Appl. Phys. Lett. 84, 4161, (2004).

[77] Y. Ohya , T. Ito, Y. Takahashi , Jpn. J. Appl. Phys. 33 5272, (1994).

[78] D. A. Barrow, T. E. Petroff, R. P. Tandon, M. Saye , J. Appl. Phys. 81 876, (1997).

[79] J. H. Park , D. H. Kang and K. H. Yoon , J. Am. Ceram. Soc. 82, 2116, (1999).

[80] T. Yu , Y.-F. Chen , Y.-Y. Zhu , Z.-G. Liu , N.-B. Ming and X.-S. Wu , Appl. Surf. Sci. 138-139 609, (1999).

[81] T. Tsurumi , T. Miyasou , Y. Ishibashi, N. Ohashi , Jpn. J. Appl. Phys. 37 , 5104, (1998).

[82] O. Nakagawara , T. Shimuta , T. Makino, S. Arai , Appl. Phys. Lett. 77, 3257, (2000).

83 V. Bornand and S. T. Mckinstry, J. Appl Phys. 87, 3958, (2000).

[84] V. Bornand , S. T. Mckinstry, K. Takemura, C. A. Randall , ibid. 87, 3965, (2000).

[85] Z. Wang , S. Oda , J. Electrochem. Soc. 147, 4615, (2000).

[86] Q. X. Jia, L. H. Chang, W. A. Anderson , Thin Solid Films 259, 264, (1995).

[87] K. P. Jayadevan, T. Y. Tseng, J. Mat. Scie: Mat. in Elec 13, 439-459, (2002).

CHAPTER-II

EXPERIMENTAL PROCEDURE

In this chapter, details of the preparation process by chemical solutions deposition (CSD) of the single phase $(Bi_{0.5}Na_{0.5})_{1-x}Ba_xTiO_3$ (BNBT) ceramics and thin films are described, as well as those of pure and Ca^{2+} doped $BiFeO_3$ (BF) thin films and the multilayer composite films (MLC). The methods used for the characterization of their properties are also presented.

2.1. Materials processing

2.1.1. Preparation of $(Bi_{0.5}Na_{0.5})_{1-x}Ba_xTiO_3$ thin films and ceramics.

2.1.1.1 Precursor solutions.

Two precursor sols of $(Bi_{0.5}Na_{0.5})TiO_3$, with and without 10 % mol of Bi^{3+} and Na^+ excess , denoted as BNTxs and BNT, respectively, were synthesized by refluxing for 8 h in air sodium acetate tri-hydrated ($Na(OCOCH_3)\ 3H_2O$; Aldrich, 99%), bismuth acetate ($Bi(OCOCH_3)_3$; Aldrich, 99.99%), and titanium di-isopropoxide bis-acetylacetonate ($Ti(OC_3H_7)_2(CH_3COCHCOCH_3)_2$; Aldrich, 75%) in a mixture of 1,3-propanediol, acetic acid and water [1]. The molar ratio of Ti^{4+} to any of the solvents was 1.0: 10.0 and the Ti^{4+}: Na^+: Bi^{3+} molar ratio of the metal reagents was 2.0: 1.0: 1.0 for the BNT sol and 2.0: 1.1: 1.1 for the BNTxs sol. Distilling off the byproducts in a volume of 80% of the equivalent 2-propanol contained in the sols with an equivalent concentration of $(Bi_{0.5}Na_{0.5})TiO_3$ of ≈0.60 mol/L (Figure 2.1).

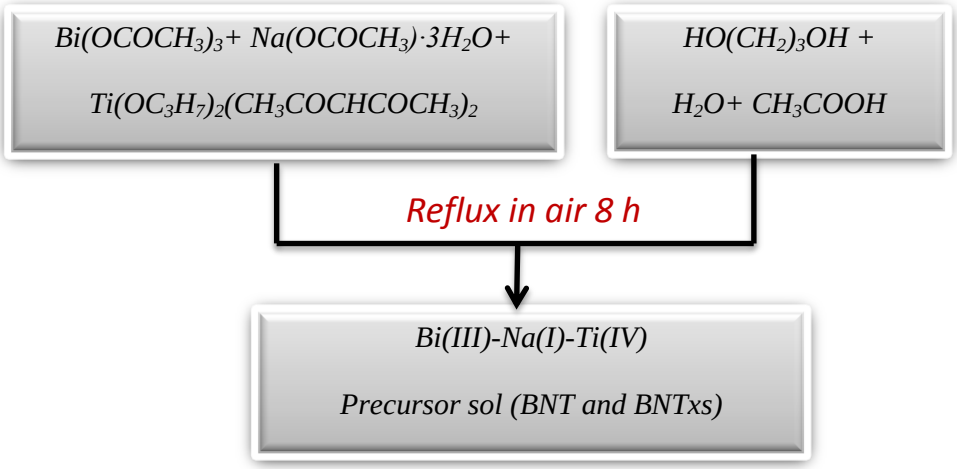

Figure 2.1: *Scheme of the synthesis route of BNT and BNTxs sols.*

To prepare the BaTiO3 (BT) precursor solution, barium carbonate ($BaCO_3$; Alfa Aesar, 99.997%) was dissolved in propionic acid and propionic anhydride at 140°C for 2 h. Then, titanium tetra-butoxide ($Ti(O(CH_2)_3CH_3)_4$; Aldrich, 99%) and 2,4-pentadione ($C_5H_8O_2$; Aldrich, 99%) were added. Finally, the mixture was diluted with 1-butanol ($C_4H_{10}O$; Sigma-Aldrich, 99.4%) to obtain a solution with an equivalent concentration of $BaTiO_3$ of 0.30 mol/L [2] (See scheme Figure 2.2).

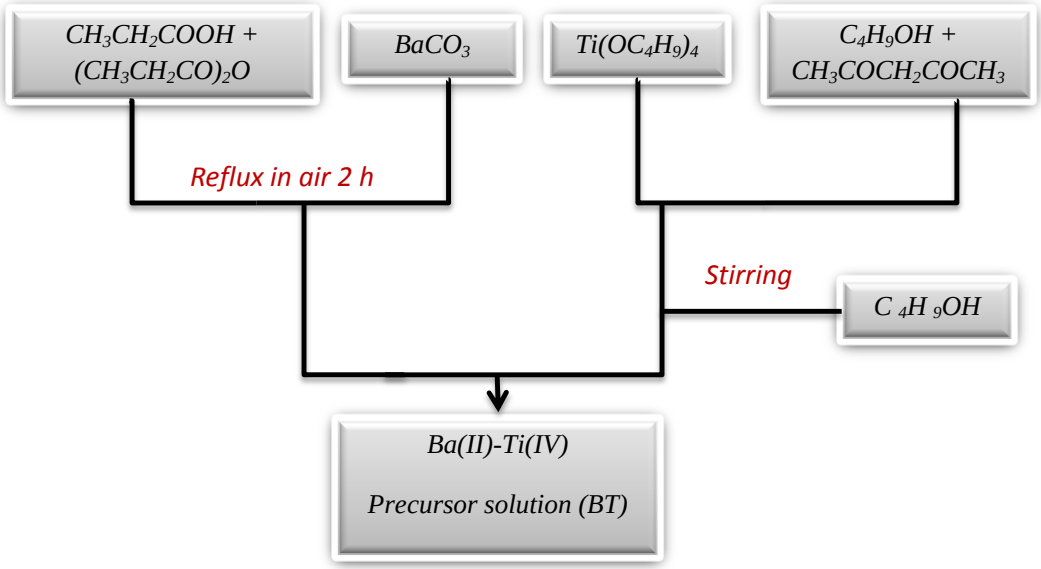

Figure 2.2: *Scheme of the synthesis route of BT sols.*

BNT sols and BT solutions were mixed to obtain $(Bi_{0.50}Na_{0.50})_{1-x}Ba_xTiO_3$ precursor solutions with the stoichiometric nominal compositions and with different Ba^{2+} contents (x = 0.035, 0.055, 0.080, 0.100). The resulting precursor solutions will be denoted as BNBT3.5, BNBT5.5, BNBT8.0, and BNBT10.0. The BNTxs sols and BT solutions were mixed to obtain $(Bi_{0.55}Na_{0.55})_{1-x}Ba_xTiO_{3.30}$ precursor solutions containing a 10 % mol of Bi^{3+} and Na^{+} with different Ba^{2+} contents (x = 0.055 (BNBT5.5xs), 0.100 (BNBT10.0xs), 0.150 (BNBT15.0xs)).

2.1.1.2 Thin films.

Diluted solutions with dried ethanol (0.2 mol/L) were deposited onto $Pt/TiO_2/SiO_2/(100)Si$ substrates (Radiant Technologies) by spin coating at 2000 rpm for 45 s and dried at 350°C for 60 s, in a hot plate. The substrates were preannealed at 700°C for 5 min (~30°C/s, O_2). The as-deposited amorphous films were crystallized by rapid thermal processing (RTP; JetStar 100T JIPELEC) in an oxygen atmosphere at 650°C for 60s and a heating rate of ~30°C/s. Deposition, drying and crystallization were repeated six times to obtain crystalline films with thickness between 350 and 550 nm. Films were labeled with the same names as the corresponding precursor solutions.

2.1.1.3 Ceramics.

Regarding the bulk ceramics processing, the mixture of the BNTxs and BT precursor solutions were dried at 120^0C for 12 h in air. The resulting gels were then heated at 350^0C for 12 h in air and subsequently calcined at 800^0C for 2 h (heating rate 2 $^0C \cdot min^{-1}$). The powder obtained was mixed with 2-propanol ($(CH_3)_2CHOH$, Aldrich, 99.5%), which will act as a binder, and then pressed uniaxialy into pellets. After calcination, the

green ceramics were sintered at 1150^{0}C for 2 h (heating rate 2^0 C·min^{-1}). The relative densities of the resulting ceramics were ≈97% as determined by the Archimedes method. Ceramics with different Ba^{2+} contents were prepared: x=0.035(BNBTc3.5) , x=0.055 (BNBTc5.5) and x= 0.100 (BNBTc10.0).

2.1.2 Preparation of $BiFeO_3$ thin films.

The preparation of the precursor solutions of the $BiFeO_3$ (BF) was performed using bismuth nitrate, [$Bi(NO_3)_3·5H_2O$, 99.99%; Sigma-Aldrich] and iron 2,4-pentanedionate [$(C_5H_8O_3)_3Fe$, 99.9%; Sigma-Aldrich] as the Bi(III) and Fe(III) reagents, respectively. Glacial acetic acid (CH_3CO_2H, 100%; Merck) and 1,3-propanediol [$OH(CH_2)_3OH$] were used as solvent (Figure 2.3) [3]. In addition, similar solutions were prepared with 3 and 5% mol of Ca^{2+} in substitution of Bi, using the precursor sol with excess of Bi.

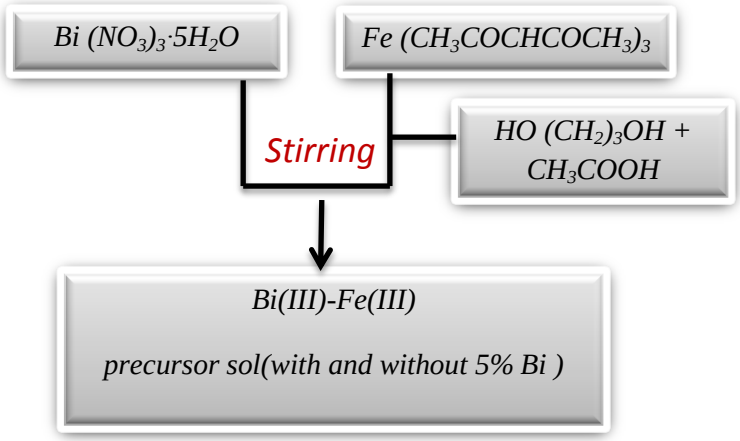

Figure 2.3: *Scheme of the synthesis route of $BiFeO_3$ sols.*

These solutions were spin-coated at 3000 rpm for 45s onto $Pt/TiO_2/SiO_2/(100)Si$ substrates. Wet layers were dried on a hot plate at 350ºC/60s. The crystallization was performed by rapid thermal treatments (RTP, JetStar 100T JIPELEC) in static air (1 bar), at temperatures of 400ºC, 450ºC and 500ºC for the films prepared from solutions

with and without Bi excess. When a precursor solution without excess is used, the films are denominated: BF400, BF450 and BF500. For the films prepared from solutions with a 5% mol excess of Bi, BF400xs, BF450xs and BF500xs. For the films obtained from Ca^{2+} doped solutions, the chosen crystallization temperature is 500^0C and the films obtained are referred as BCF3 when a 3% mol of Ca^{2+} is used and BCF5 for 5% mol Ca^{2+}. Deposition, drying and RTP treatment were repeated up to a maximum of 9 times to fabricate crystalline films with thickness between 300 and 350 nm.

2.1.3 Preparation of multilayer composite films.

Multilayer composite films (MLC) were fabricated by the deposition, drying and crystallization of alternating layers of BNBT and BF, following the same processing conditions as the ones described in the previous sections. Regarding the preparation of a bilayer, two configurations are possible: BNBT/BF, with the BF in contact with the substrate, and BF/BNBT with the BNBT layer deposited on the substrate. The MLC films with three layers were prepared also with different order of the layers: with a BF layer sandwiched between two BNBT layers (MLC-BF) or with a BNBT layer between two BF layers (MLC-BNBT).

In the bilayer was deposited 6 successive coating of BNBT and 3 of BF and was changed the order of the deposit of the compositions for obtain two different bilayers. Regarding of the MLC films the BNBT layers were obtained by 3 successive coatings, while BF single phase layers were the result of 6 coatings. The layer thickness obtained for both compositions are the lowest to obtain optimum properties from them. In order to induce a remnant polarization in the BNBT layer, this was deposited between two BF layers, producing the multilayer composite film MLC-BNBT. For the sake of

comparison, another configuration was checked, with the BF layer sandwiched between two BNBT layers, resulting in the multilayer composite film MLC-BF. This same configuration was used for bismuth ferrite pure and doped with Ca^{2+}.

2.2 Structural and microstructural characterization.

2.2.1 Thickness measurements

The thickness of the single phase and multilayer composite films has been first determined by profilometry, and the results obtained corroborated by the direct observation of cross sections by Scanning Electron Microscopy (SEM) as it is mentioned in section 2.2.3.

Profilometry refers to the measurement of the surface roughness from the measurement of the deflection of a tip scanning a surface with which is kept in contact. The contact force between the tip and the film is maintained through a low elastic constant spring. The tip deflection induced by the surface irregularities is measured through an inductive transducer. A Taylor-Hobson profilometer, Form Talysurf 50 model, was used. A carbon fiber calliper of 60 mm length, with a 60º cone-shaped diamond tip with a radius of 2 μm, allows thickness measurements with a resolution of 20 nm.

To obtain film thickness, the profilometer is used to measure the step between the substrate and the film surface. Therefore, a small region of the film was first peeled-off dipping it in HF (fluoride acid), in order to reveal the substrate. It must be noted that the height profile obtained, not only shows the step, but the curvature resulting from the stress between film and substrate produced during film processing. The curvature is

then fitted to the most appropriate form (parabola, circumference) with home-made software, and subtracted from the profile to obtain the film thickness.

2.2.2 Crystalline phases characterization.

The crystalline phases present in the films have been studied by X-ray Diffraction, with Bragg-Brentano (XRD) geometries. The experimental diffraction patterns were compared with powder diffraction files, when available, of the expected crystalline phases of the film, in order to identify all the peaks of the X ray patterns. For $(Bi_{0.55}Na_{0.55})_{1-x}Ba_xTiO_3$ *we use the diagram of a ceramic powder and for* $BiFeO_3$ *the powder diffraction file from the database of the Joint Committee on Powder Diffraction Standards of the International Centre for Diffraction Data (JCPDS-ICDD) number 86-1518. Deconvolution and separation of reflections in the experimental patterns were carried out by using pseudo-Voigt functions.*

The XRD measurements were carried out using a D500 powder diffractometer equipped with Cu anode ($\lambda_{CuK\alpha}$ *= 1.5418 Å). Diffracted beams were collected by a scintillation detector. Two slits of 1º for the incident beam and other two of 1º and 0.15º for the diffracted beam were used. Diffraction patterns were collected in the 2θ interval between 20 and 50º, with a step of 0.05º/3s,with the configuration that is show in the figure 2.4.*

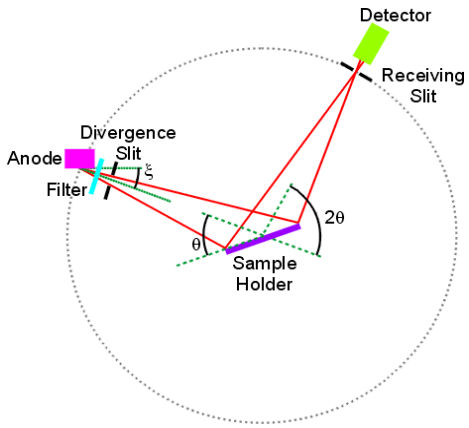

Figure 2.4: *Schematic illustration of Bragg-Brentano geometry X-ray diffraction experimental set-up.*

2.2.3. Microstructural study.

The microstructure of the films has been studied by Scanning Electron Microscopies (SEM). A study of the surfaces with higher magnification with a SEM revealed the grain size of the films. As mentioned before, the preparation and observation of cross section of the films allows thickness determination. But not only that, information on the columnar nature of the grains or the distribution of the layers in the MLC films is obtained. An ISI-DS-130 field emission gun microscope (FEG-SEM) has been used for this purpose.

2.3 Electrical characterization.

In order to perform the electrical characterization of the films, top and bottom electrodes (capacitor configuration) are required. The top Pt layer of the Si-based substrates serves as bottom electrode. Top Pt electrodes of different sizes, between 0.03 and 1.0 mm^2, were deposited on the film surfaces by cold D.C. sputtering (BAL-TEC SCD 050) using shadow masks. In order to minimize the damage of the film surface

during sputtering, firstly a deposition in mild conditions (40mA for 200s) is carried out. Then, once this first Pt protecting layer is deposited, more aggressive conditions are used for further Pt deposition (80mA for 100s) until the top electrode is ready. To improve the quality of the final capacitor, a post-annealing treatment was performed at 350^{o}C for 6 min. For the measurements, a contact with the Pt of the substrate is also necessary. Wet-etching of one edge of the film with an acidic solution, which dissolves the film but not the Pt bottom electrode, is carried out. This solution was prepared by mixing fluorhidric acid (HF 48%, Panreac), clorhidric acid (HCL 37%, Panreac) and deionized water in a volume ratio of HF: HCl: H_2O equal to 1:1:15.

2.3.1. Conventional ferroelectric hysteresis loops.

The measurement of the P-E hysteresis loops defines the ferroelectric behavior of the material (Figure 2.5a). From this measurement, the remnant and saturation polarization ($P_r = (|+P_r| + |-P_r|)/2$), ($P_s = (|+P_s| + |-P_s|)/2$) and the coercive field ($E_c = (|+E_c| + |-E_c|)/2$) values are obtained. The asymmetry of hysteresis loops with respect to the electric field axis is due to the existence of internal electric fields or electrical bias ($E_{bias} = (|+E_c| - |-E_c|)/2$) in the sample.

Another equivalent representation of the inversion of the polarization with electric field of a ferroelectric material is the current density ($\delta P/\delta t$) versus electric field (J-E) hysteresis loops (Figure 2.5b). The current maxima peaks correspond to the polarization inversion phenomena, and, thus, the electric field value where the current is maximum is the coercive field E_c. The remnant polarization can be calculated from the areas enclosed by those peaks by integration with time. The J vs. E presentation of the hysteresis loop has the advantage of clearly demonstrating the presence of

ferroelectric switching in the sample even if the contributions to the current related to conductivity and leakage are large.

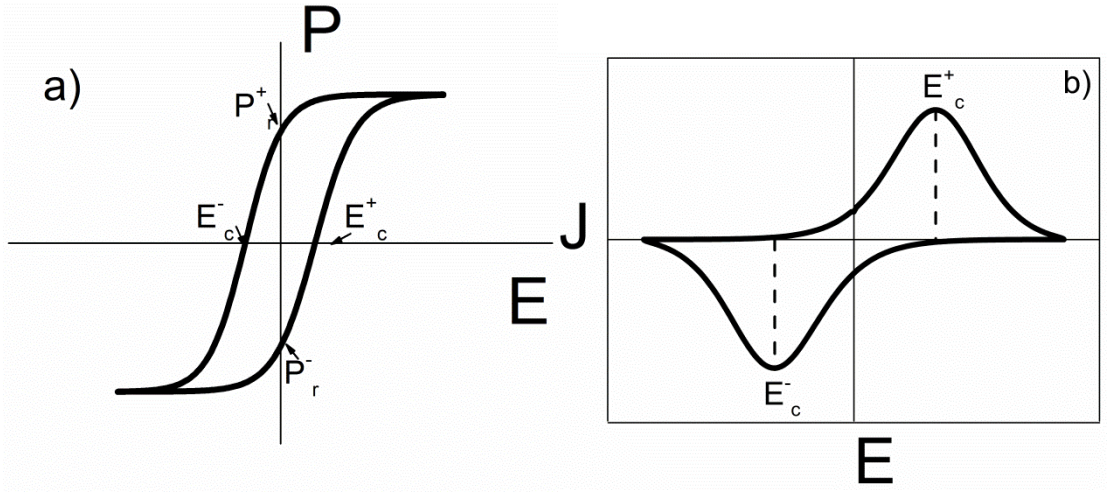

Figure 2.5: *P-E (a) and J-E (b) hysteresis loops typical of a ferroelectric where P_r is the remnant polarization and E_c coercive field.*

Measurements of current density hysteresis loops have been carried out using a virtual ground circuit [4,5] shown in Figure 2.6. Experimental setup consisted of a HP 8116A pulse generator that allows the application of sinusoidal waves with electrical amplitude signals between 0.01-16 V and frequencies of 1-50 MHz. Current intensity generated values, after amplification with a Keithley 428 current amplifier, together with the voltage applied were collected with a Tektronix TDS 520 oscilloscope. Data acquisition and further processing of the data was carried out by homemade software. The integration of the current density loops obtained led to the P-E hysteresis loops. The non-ferroelectric contributions from the loops were calculated by a fitting of the experimental J-E curves to a phenomenological model that simulates the linear part of these contributions, by introducing the capacitance and resistance of the films [6,7].

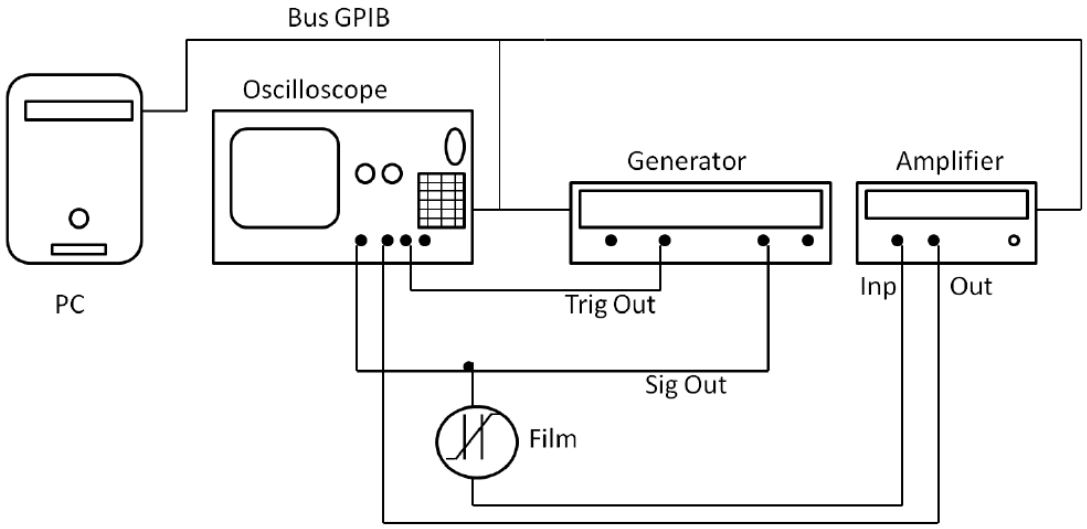

Figure 2.6: *Scheme of the experimental system for measuring current density ferroelectric loops.*

Due to the presence of non-ferroelectric switching contributions, the remnant polarization obtained from the experimental loop can be much larger than the real one. These contributions come from the non-relaxed and non-switching accumulated electrical charge associated with finite capacity and resistance of the film studied. In order to eliminate these contributions, the method used is based on that proposed by R. Jimenez et al. [6]. The possible asymmetry of the positive and negative switching parts of the ferroelectric hysteresis loops can also be introduced in the model [6]. This difference between the accumulated charges of different sign is attributed to an internal bias field induced by the different interfaces of both electrodes (top and bottom) with the ferroelectric film. Note that the film is deposited on the bottom electrode, and, therefore, subjected to the thermal crystallization process, while the upper electrode was deposited on the film after that. The equation used for the polarization switching, P^+*, for positive voltage ramp is:*

$$P^+ = P_s \tanh[(V - V_c^+)/2\delta^+] \qquad (2.1)$$

where P_s is the spontaneous polarization, V_c^+ is the coercive voltage, V is the voltage applied and δ^+ defines the shape of the curve of hysteresis from the following equation:

$$\delta^+ = V_c^+[\log[(1 + P_r^-/P_s)/(1 - P_r^-/P_s)]] \qquad (2.2)$$

where P_r^- is the remnant polarization for negative voltage ramp.

The same equations are valid for the negative part of the loop, by changing the superscripts + and -. The non-switching contribution to the total charge Q from the finite capacitance and resistance of the sample was evaluated separately using the equation:

$$Q_{non-switching} = C_{sample} \cdot V(t) + \int_0^{1/f} \left(V(t)/R_{sample}\right) dt \qquad (2.3)$$

where f is the frequency of the applied voltage signal and C_{sample} and R_{sample} are the capacitance and resistance of the sample. It is possible that C_{sample} and R_{sample} at high fields are slightly different for the positive and negative voltages parts of the loops, which can also be considered [8].

There is another effect that must be also taken into account. This effect is the leakage current, which becomes more important as the thickness of the film decreases. The effect of these currents is important, since they produce a significant increase of the apparent polarization and coercive field to the point of hiding completely the switching phenomena in the deformed charge loops. It should be noted that leakage currents are not electrical displacement currents but real electric currents. They are associated with a continuous current phenomenon that is electronic in nature, while the contributions to the conductivity of the loops are related to ionic conductivity, electronic conductivity or mixed conductivity. Thin films may present for large electric fields strong contributions

from leakage currents, which can be represented by a non-linear, almost parabolic behavior with the electric field, usually proportional to V^2. In the case of the tunneling currents of Space Charge Conduction Limited (SCLC) the exponent varies between 2 and 3.5 before entering in the degradation region [9]. According to the models proposed by Juan et al. [10] and Rose et al. [11] these non-linear contributions to J can be expressed as:

$$J\alpha V^n/d^3 \qquad (2.4)$$

where d is the thickness of the film.

We introduce a threshold voltage V_0, above which the leakage currents starts being a significant contribution to the current response. Below it, linear conductivity contributions are only considered. Taking into account this, the non-linear J coming from leakage current (J_l) can be expressed as follows [7]:

$$J_l = B \cdot (V(t) - V_0)^n \quad (2.5)$$

where B is a proportionality coefficient. In the proposed model a simple approximation is made, fixing the value of the exponent n to 2.3. It was found that the best fittings are obtained for this value in the thin films analyzed.

It should be noted that the objective of this study is to be able to observe the lineal and non-lineal current behavior in thin films when it is impossible to measure it directly, due to the high leakage current. In addition, non-ferroelectric contribution of the J-E loops can be removed. Once this is done, we can correct the experimental loops with a function that produces approximately the experimental leakage currents, so that we can obtain ferroelectric loops with only switching contributions, which allows comparison between the single and MLC films measured in the same experimental conditions.

Figure 2.7 shows an example of the good agreement between the experimental data and the model used in all thin films studied in this thesis. The current loop is an example of the worst possible case: a film with high leakage currents. The different parameters obtained from this fitting reveal relevant information about the electrical behavior of the films.

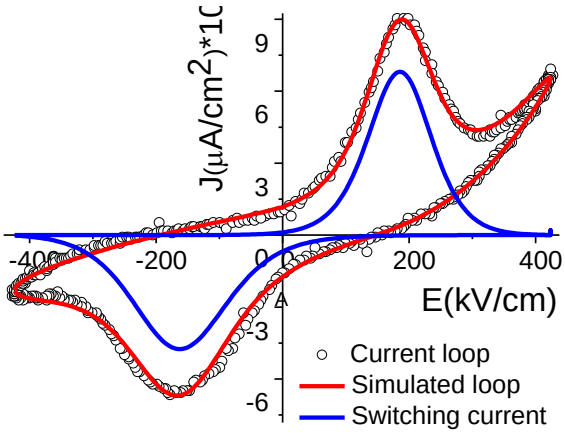

Figure 2.7: *Example of the good agreement between the experimental data and the phenomenological model.*

2.3.2. Remnant ferroelectric hysteresis loops.

The P-E hysteresis loops described above show the polarization behavior when a sinusoidal electric field is applied. Non-ferroelectric contributions are present and must be corrected by a fitting procedure. These contributions switch with the ferroelectric polarization, but once the electric field is removed, this part of the polarization does not maintain its switched state, but discharge. Therefore, the measurement of the actual values of the remnant polarization obtained after the application of the electric field will produce pure remnant ferroelectric hysteresis loops. Based on this idea, a

procedure has been designed and implemented in the Precision Premier II (Precision Material Analyzer) system.

The strategy followed is to obtain two hysteresis loops. One in which no ferroelectric switching takes place, and therefore we have only information from the non-ferroelectric components of the polarization. And a second one in which both ferroelectric and non-ferroelectric components switch. Subtracting the first from the second we construct the only ferroelectric-switching, remnant hysteresis loop.

Both hysteresis loops are the combination of two actual measurements. As shown in Figure 2.8, a normal hysteresis measurement (with a triangular wave) is preceded by a conditioning pulse that sets the sample to a polarization polarity. Note that, although unmarked, there is a one second delay between the end of the conditioning pulse and the beginning of the hysteresis measurement. For the first hysteresis loop, this polarity is in the same of the first half of the measuring waves (Figure 2.8a). This ensures that no ferroelectric switching takes place. We take the polarization values measured for the two first halves of the measuring waves (note that one starts "positive" and the other "negative"), and we build from them a full hysteresis loop with only switching information from the non-ferroelectric components of the polarization. Similarly, but with conditioning pulses that set the sample polarization opposite to the first half of the measuring wave (Figure 2.8b), we obtain the hysteresis loop in which both ferroelectric and non-ferroelectric components switch. After that we subtract the first hysteresis loop from the second, and we build the desired remnant hysteresis loop.

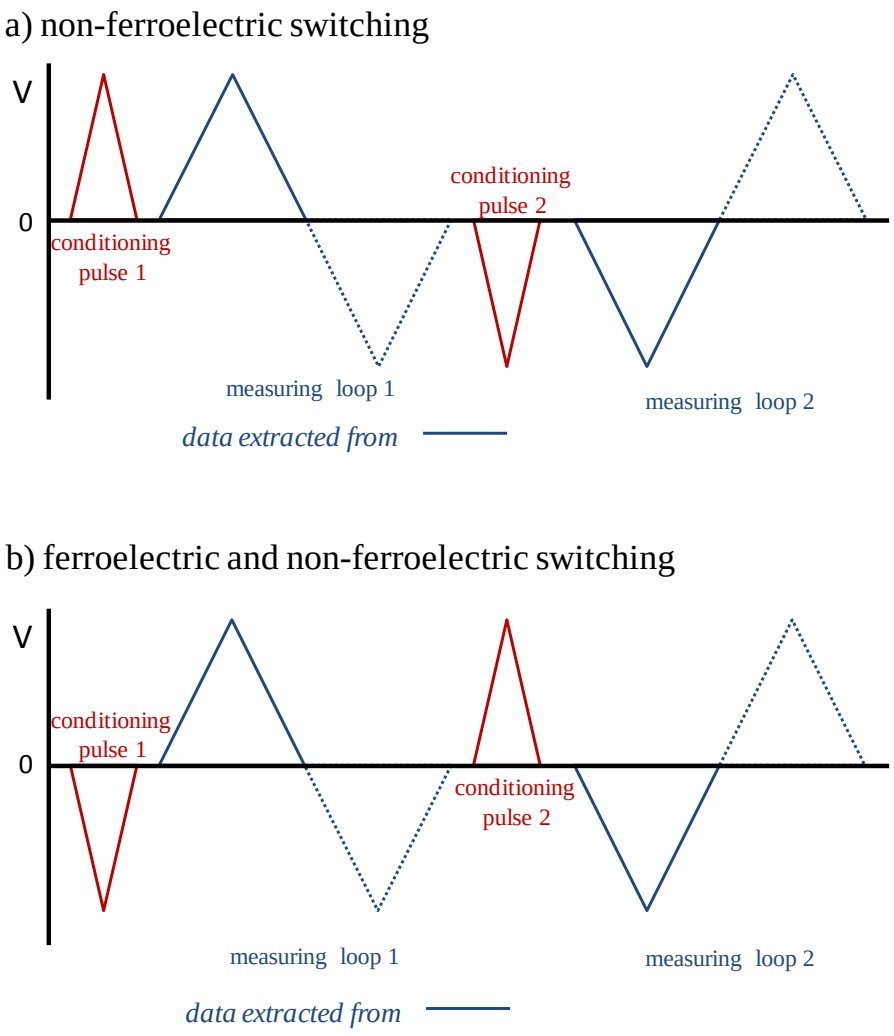

Figure 2.8: *Voltage trains used for the measurement of remnant loops. a) for hysteresis loops where no ferroelectric switching takes place, and b) for those where both ferroelectric and non-ferroelectric contributions contribute to the polarization switching (1s delay between the measurement and the conditioning pulse).*

Voltage amplitude can vary between 0.01- 100V. A delay time of 1 s between the conditioning and the measuring triangular voltage waves was applied. As the values of the polarization after conditioning determine the initial values in the hysteresis loop, if during this time there is a significant relaxation of the non-ferroelectric contributions, we will observe a difference between the initial and final values of the polarization in the hysteresis loop. Therefore, the measured decrease of P_r in the loop, in the case of

full retention of the polarization, should be quite similar to the corrected P_r value of the home-made hysteresis loops measurements with sinusoidal E fields. In case that some of the ferroelectric polarization relaxes during the 1 second delay, the relaxed P_r value obtained with the Precision Premier II system will be lower than the one obtained from the home-made measurements, and the difference should be the relaxed ferroelectric polarization. The figure 2.9 shows how the Precision Premier II system calculated the remnant loops of the relaxed polarization (brown loop of the figure 2.9). With the pulses of the figure 2.8a, the non-switching contribution is obtained, and with the pulses of the figure 2.8b the switching and non-switching response. By subtracting these two loops, it is possible to obtain the relaxed remnant polarization.

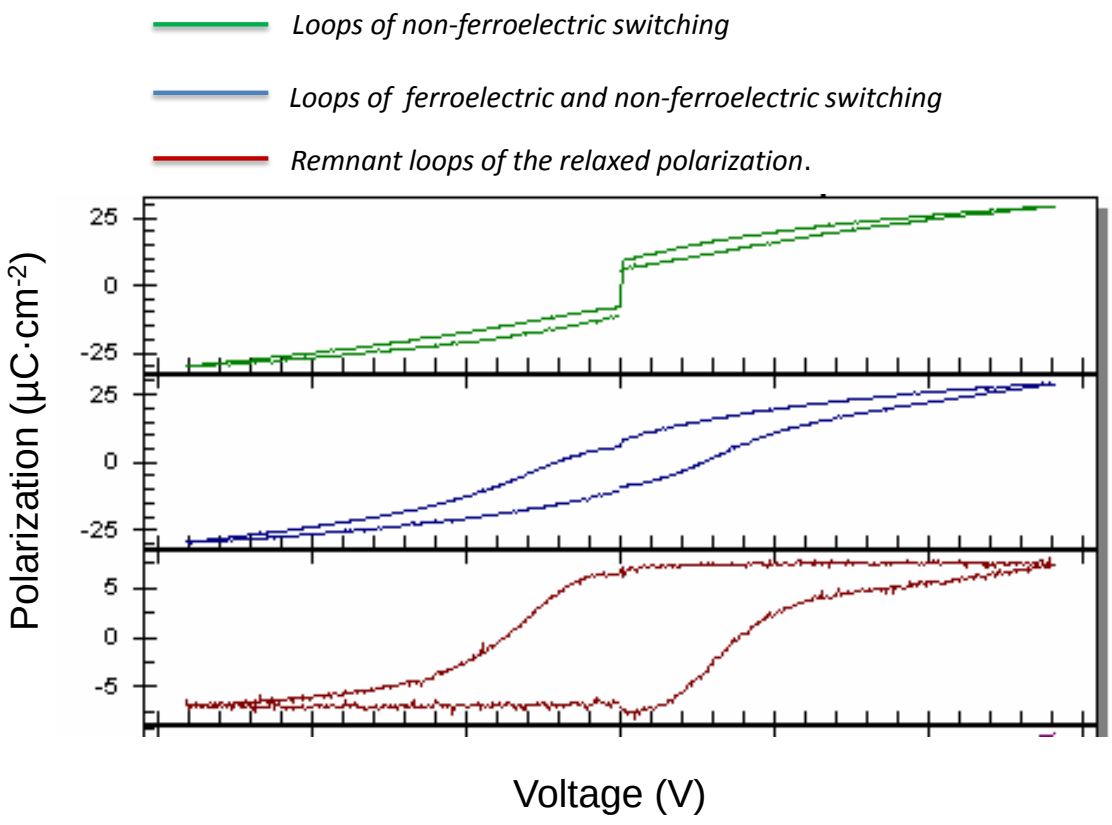

Figure 2.9: *Different loops measured by the Precision Premier II for obtained the relaxed remnant polarization.*

2.3.3 Measurement of the polarization retention

The retention of the polarization in the films has also been studied in this work, after long time periods (up to 6h), using the Precision Premier II system. The measurement experiment consists on the application of three square pulses to the sample. The first one is a pre-polarization pulse (preset pulse), which sets the sample to a particular polarization state, and, therefore an initial polarization value. After a fixed delay time, two measurement pulses (Read Pulses) are used to measure the loss of retention in the sample [12] (Figure 2.10).

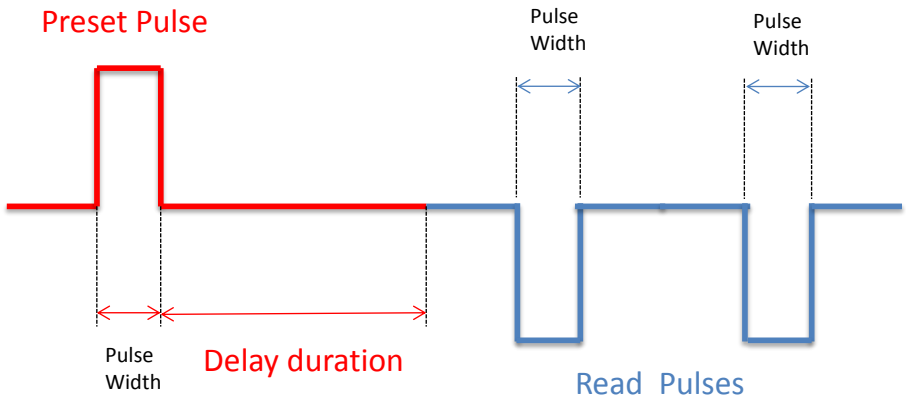

Figure 2.10: *Schematic diagram of the train of pulses used for measurements of the polarization retention.*

We measured the integrated charge from the beginning of the first reading pulse until it reaches the maximum voltage. The polarization obtained includes the ferroelectric switching contribution, but also other non-ferroelectric contributions. After 1 second, the measurement was repeated with the second identical reading pulse. This time, the polarization obtained from the measured integrated charge does not include any ferroelectric switching contribution. The difference between the polarizations obtained

in both pulses gives us the remaining ferroelectric switchable polarization after the fixed delay time, which is a measurement of the retention of the polarization. After 1 s, a new poling of the sample is carried out and the experiment is repeated successively for increasing delay times, until a polarization retention curve is obtained.

2.3.4. Current vs. voltage curves.

The occurrence of leakage currents at high electric fields, and the subsequent electrical breakdown at a specific applied electric field, must be studied to define the operating conditions of the ferroelectric films. The study of the current vs. voltage (I–V) characteristics provides information on charge transport mechanisms in thin films. In this work, I-V curves were measured with the Precision Premier II system in some films, while in those with higher values of leakage currents and the presence of the electrical breakdown at low electric fields, this study was performed from the experimental J-E curves.

The I/V test profile of the Precision Premier II system consists on the application of a series of voltage steps where the associated current is measured. Figure 2.11 shows a single DC voltage step used. The "soak time" represents the time necessary for the induced current to stabilize, i.e., reach the steady-state current state. This prevents any contributions from currents induced by the polarization switching. Voltage always returns to zero after finishing the established "measure time", so that each new step measurement starts at a common reference point. The "Step Delay" is necessary, so that the sample can again reach steady-state current before a new measurement is made. For our experiments, a soak time and step delay of 100ms is used, because it is sufficient time for the current to stabilize, to measure only the leakage current. The

measure time is fixed to 150 ms. These times cannot be very long because it could cause the dielectric breakdown.

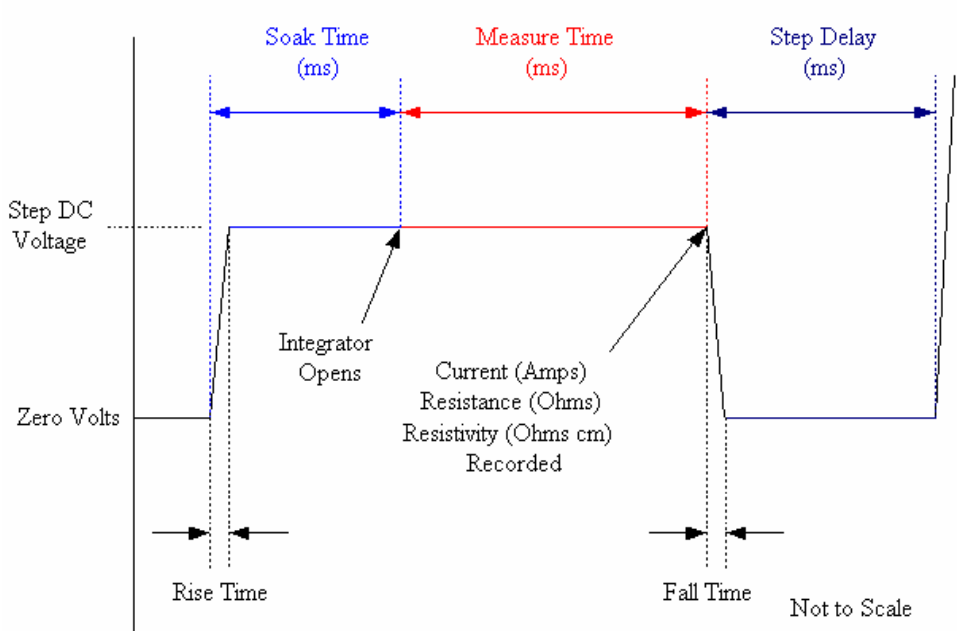

Figure 2.11: *Schematic diagram of a single voltage step used to obtain one of the points of an I/V curve.*

Unfortunately, most of the films studied reach electrical breakdown for low electric fields, which does not allow the measurement of reliable I-V curves with this method. Instead, I-V curves were obtained from the calculations carried out to fit the experimental J-E loops as explained before. We obtain I-V leakage currents from the fitting of experimental data to equation 2.4 and 2.5, and electrical breakdown voltages are determined.

2.4. Piezoelectric characterization.

Considering piezoelectric material characterization, the resonance technique, which is widely used for bulk samples, is not applicable for thin films. The technique measures the natural frequency of a sample, which is determined by its fundamental vibration

modes. In thin films, due to the clamping with the substrate, the vibration frequency is very low and, therefore, it is impossible the characterization by this technique. The difficulties arising from these low frequencies have yet to be solved.

Using the converse piezoelectric effect, the electric field induced displacements of the sample are measured. Since the small thickness of thin films limits the voltage applicable to the samples, the displacements are in the angstrom range. The non-linear piezoelectric response of ferroelectric materials for different applied electric field requires an even higher resolution of about 1-10pm. Interferometric techniques are one approach to achieve such high resolutions.

In this thesis macroscopic piezoelectric hysteresis loops were obtained using a Double Beam Laser Interferometers (aixDBLI System of the University of Twente, see Figure 2.11) and a fiber-optic, double-beam incidence Mach– Zehnder interferometer (University of Oporto). In these two equipments, the principal difference is that, in the DBLI, the optical path is through polarizing beam splitter (PBS) and in the other interferometer is through optic fiber. But the operating principle is the same. The double beam interferometry is one of the best options for the measurement of piezoelectric behavior in thin films, where the induced displacements are small and, besides, the film is attached to a substrate. Though measuring with a single beam yields a high resolution (10^{-5} up to 10^{-4} angstrom), the motion of the sample along the beam path, e.g. due to sample bending, influences the measurement. With a double-beam setup, the bending of the sample is detected by a beam reflecting on the sample backside, and it can be eliminated. However, it must be noted that the resolution is decreased in the double beam interferometer due to the longer beam path and additional optical components used. Despite of this, the typically achieved resolution is

approx. 10^{-2} Angstrom, which is still sufficient to measure the thin film deformations induced by the electric field.

The optical path of the double-beam laser interferometer used in this work is shown Fig. 3.12, where it is possible to observe the scheme of the fiber-optic double-beam incidence Mach– Zehnder interferometer. The laser is equipped with an optical isolator and a fibre-optic plot, in order to avoid reflections and to maximize the optical input power. Then, a directional coupler is used to provide the reference and signal waves. In the case of the DBLI the division of the beam was performed with PBS [13]. In the two interferometer used the piezoelectric response is calculated using the optical path differences [14].

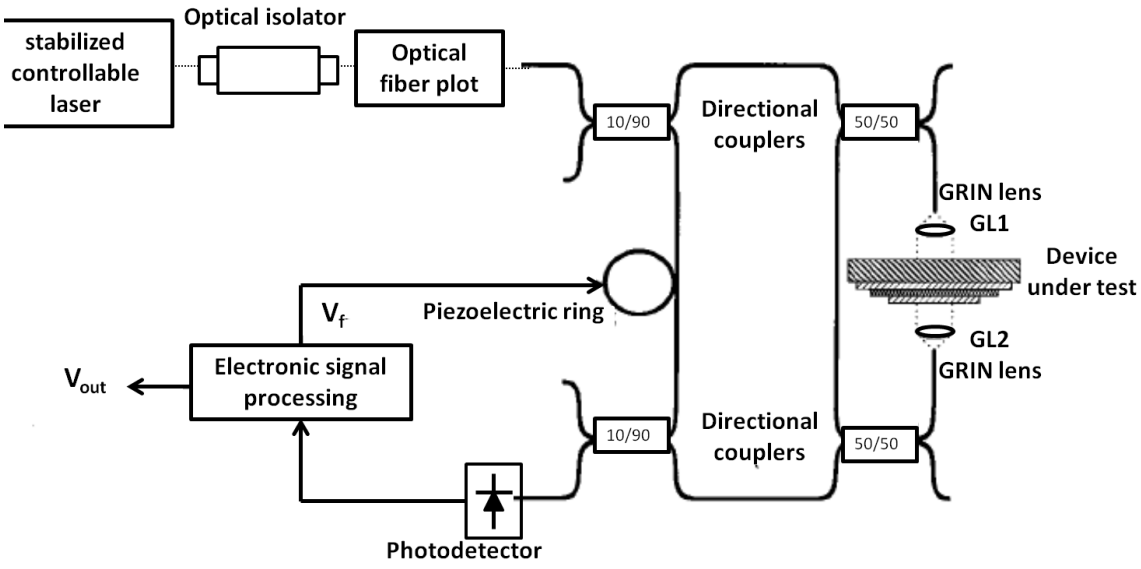

Figure 2.12: *Schematic diagram of the optical path in fiber optic system.*

The piezoelectric coefficient is measured from the deformation induced in the film by an alternating electric field (high frequency from 1 kHz to 7.5 kHz and small amplitude 0.5 V). The resulting displacement, detected by the photodetector after subtracting sample

bending, is analyzed with a lock-in amplifier. To obtain the piezoelectric hysteresis loops, the DC bias is applied as pulses of increasing and decreasing values, while the piezoelectric coefficient is measured when the bias is applied (Figure 2.13). Simultaneously, we measure the capacitance and we obtain the corresponding C-V loops.

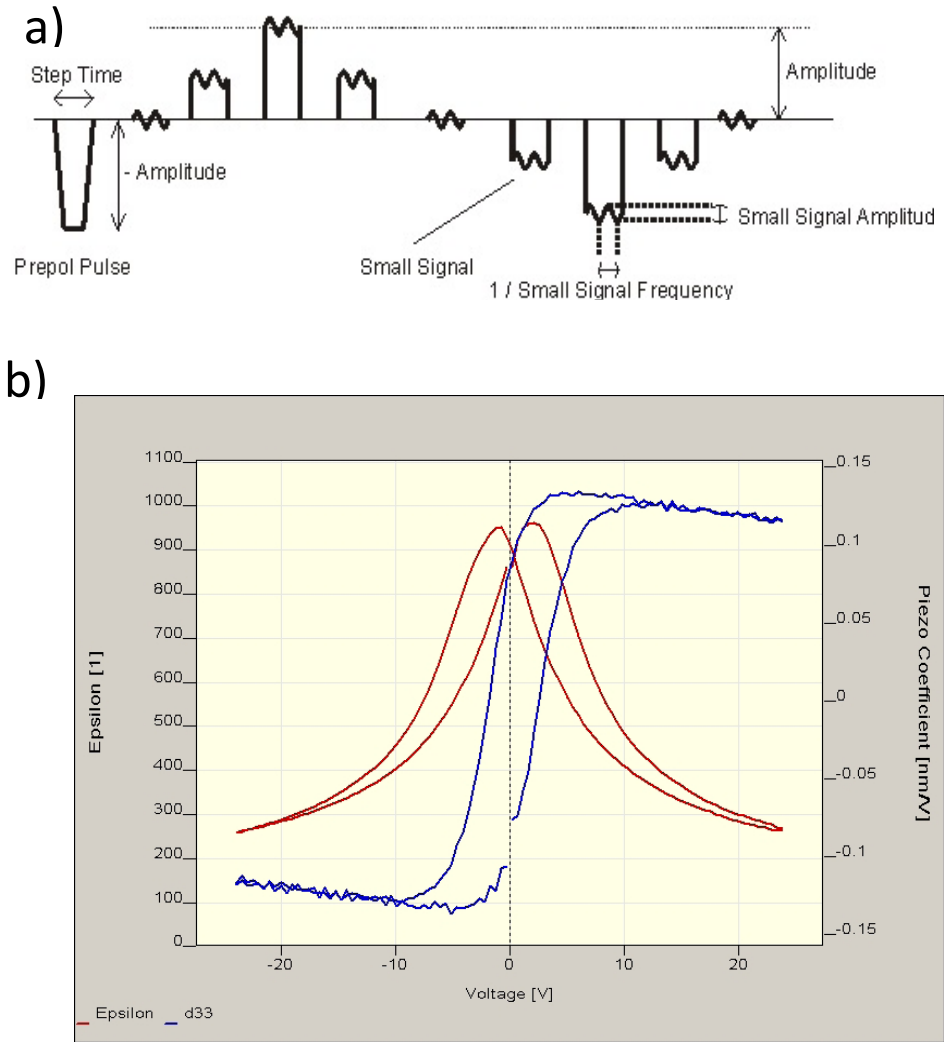

Figure 2.13: *a) Combination of electrical pulses used for the measurement of piezoelectric hysteresis loops, and simultaneous C-V curves , b) example of the piezoelectric loop and C-V curve measured for a PZT film.*

2.5. Magnetic characterization.

Magnetization vs. magnetic field curves at different temperatures of the multilayer composite films were performed using a commercial SQUID DC-magnetometer (Quantum Design) equipped with a 5 T superconducting coil and a helium cryostat allowing temperature control between 1.8 K and 400 K. The magnetic field was applied parallel to the film surface and the diamagnetic contributions from the substrate were eliminated by fitting the high field data to a straight line with a negative slope.

SQUID consists of a superconducting loop with one or two non-superconducting links inserted (the so-called Josephson junction). These devices give rise to an output voltage signal, which is a periodic function of the flux threading the superconducting loop. This geometry is known as DC-SQUID (constant bias current). The magnetometer includes a SQUID detection system and a precision temperature control unit in the bore of a high field superconducting coil. The sample locates inside a set of pick-up coils, which in turn are placed inside the superconducting coil which provides a uniform dc-magnetic field at the sample location. The magnetized sample is then displaced inside the set of pick-up coils inducing a current proportional to the variation of the magnetic flux. The signal is detected and amplified by means of the SQUID sensor (the superconducting loop with the weak link) in form of voltage. The magnetic moment of the sample is thus proportional to the voltage variations that the SQUID detects, which can resolve magnetic moments in the order of 10^{-6} emu. All the system is placed inside a helium cryostat which refrigerates the superconducting coil and allows precise temperature control.

2.6. References.

[1] D. Alonso- Sanjosé, R. Jiménez, I. Bretos, and M. L. Calzada, J. Am. Ceram. Soc., 92 [10] 2218–25 (2009).

[2] D. Pérez-Mezcua, R. Sirera, I. Bretos, J. Ricote, R. Jiménez, L. Fuentes-Cobas, R. Escobar-Galindo, D. Chateigner, and M. L. Calzada, J. Am. Ceram. Soc. 97, 1269 (2014)

[3] C. Gutiérrez-Lázaro, I. Bretos, R. Jiménez, J. Ricote, H. El Hosiny, D. Pérez-Mezcua, R.J. Jiménez-Rioboó, M. García-Hernández, M.L. Calzada, J. Am. Ceram. Soc. 96, 3061 (2013).

[4] P. Ramos, "Estudio de la ferroelectricidad en láminas delgadas de titanato de plomo modificados, obtenidas por sol-gel" PhD Thesis. Universidad Autónoma de Madrid (1996)

[5] D. Rivero, L. Pardo, R. Jiménez, Revista Cubana De Física 26, 169 (2009)

[6] R. Jiménez, C. Alemany, M.L. Calzada, A. González, J. Ricote, J.Mendiola, Appl. Phys. A: Mater. Sci. Process. 75, 607 (2002)

[7] S.L. Miller, R.D. Nasby, J.R. Schwank, M.S. Rodgers, P.V. Dresendorfer, J. Appl. Phys. 68, 6463 (1990)

[8] R. Jiménez, C. Alemany, A. González, M.L. Calzada, J. Mendiola, Integr. Ferroel. 47, 227 (2002)

[9] H.Hu, S.B. Krupanidhi, J. Mater. Res. 9 1484 (1994)

[10] T.P. Juan, S., Chen, J. Y. Lee, J. Appl. Phys. 95, 3120 (2004)

[11] A. Rose, Phys. Rev. 97, 1538 (1955)

[12] R. Jiménez, A. González, C. Alemany, M.L. Calzada, Bol. Soc. Esp. Ceram. Vidr. 41, 22 (2002)

[13] Manual Double Beam Laser Interferometer (aixDBLI), Version 1.5.4.0, (2012).

[14] J. R. Fernandes, F. A. de Sa, J. L. Santos, E. Joanni, Rev. Sci. Instrum., 73, 2073, (2002).

CHAPTER-III

FUNCTIONAL PROPERTIES OF $(Bi_{0.5}Na_{0.5})_{1-x}Ba_xTiO_3$ *(BNBT) SINGLE PHASE THIN FILMS AND CERAMICS*

In this chapter, the main results of the functional properties (ferroelectric, dielectric and piezoelectric) of solution derived BNBT bulk ceramics and thin films are described. The aim of this Chapter is the analysis of the functional behavior of BNBT for its integration in microdevices. Materials with compositions close to the morphotropic phase boundary of this solution are studied in order to determine which of them shows the most appropriate ferroelectric behavior. In addition, the comparison between bulk ceramics and thin films (prepared from the same precursor solutions) allows us evaluating the influence of the grain size and film residual stress on the properties. The volatility of Bi and Na may cause problems during the preparation of thin films and in this chapter we analyze the impact that the use of excess in the precursor solutions has on the ferroelectric behavior of the films. Table 3.1 summarizes the BNBT materials studied in this chapter.

Table 3.1: *Nomenclature for the BNBT materials studied in this chapter.*

Nomenclature of $(Bi_{0.5}Na_{0.5})_{1-x}Ba_xTiO_3$ materials					
	x=0.035	*x=0.055*	*x=0.08*	*x=0.10*	*x=0.15*
Bulk ceramics	*BNBTc3.5*	*BNBTc5.5*	--	--	--
Thin films with 10 % of Bi, Na excess	--	*BNBT5.5xs*	--	*BNBT10.0xs*	*BNBT15.0xs*
Thin films without excess.	*BNBT3.5*	*BNBT5.5*	*BNBT8.0*	*BNBT10.0*	--

3.1 Ferroelectric properties of BNBT ceramics.

In figure 3.1 it is possible to observe the ferroelectric loops obtained in BNBT bulk ceramics with compositions close to the MPB: x=0.035 and 0.055. Similarly to the results reported in other works, the composition with the largest ferroelectric properties is that with x = 0.055:BNBTc5.5 (P_r=31.3 $\mu C \cdot cm^{-2}$).This composition is at the MPB. It can also be observed that these ceramics present square hysteresis loops with high coercive fields. For BNBTc3.5 the value of the remnant polarization is lower: P_r=20.5 $\mu C \cdot cm^{-2}$.

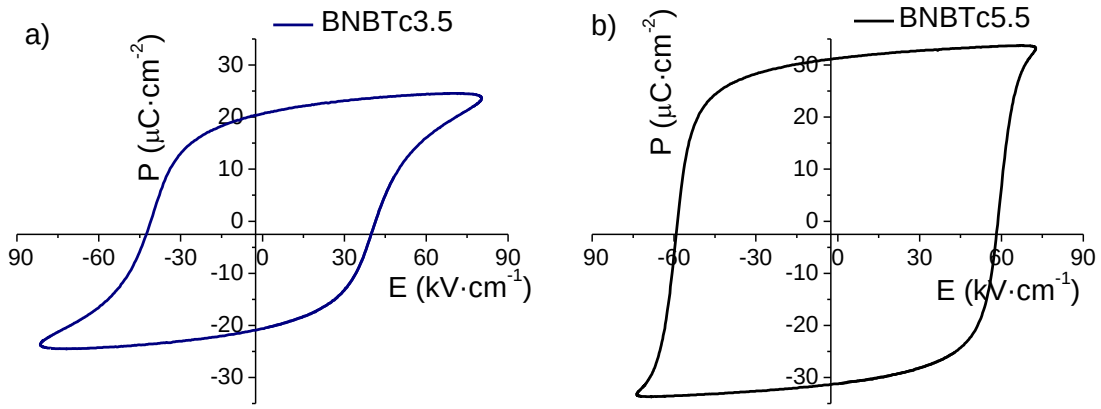

***Figure 3.1**: Ferroelectric loops of lead-free ceramic of BNBT for different compositions; a) BNBTc3.5, b) BNBTc5.5*

In order to study the evolution of the electric properties with temperature, the measurement of the dielectric permittivity at various frequencies was performed. We focus on the sample BNBTc5.5 because it shows the larger values of the polarization. The figure 3.2 shows the real and imaginary part of the dielectric permittivity on heating, after poling the sample with a high electric field, and on cooling, after

reaching the paraelectric state. In the heating run, curves of figure 3.2, two anomalies for the real part are observed at T=219^{0}C and T=320^0 C. The precise temperatures were determined from the first derivative of the real permittivity with respect to the temperature (inset figure 3.2 a). The anomaly at 219^0 C can also be observed in the curve of the imaginary part of the permittivity (figure 3.2 b), which is related with the depolarization temperature [1]. This temperature is independent of the frequency, which is a common feature of normal ferroelectric-related phase transitions. The second anomaly observed at 320^{0}C in the figure 3.2a corresponds to the phase transition to a paraelectric state.

Upon cooling the ceramic from the paraelectric phase, significant differences are observed with respect to the heating behavior (figure 3.2 c, d). There are also two anomalies in the cooling curves of the unpoled ceramics but they differ from the anomalies observed in the heating curves. In the case of the cooling curves it is possible to observe a shifting in the temperature of the maximum permittivity and dispersion with the frequency. This behaviour observed in the cooling curves of the real and imaginary part of the permittivity (Figure 3.2 c, d) is typical of a relaxor phase transition. The curve of the temperature of the maxima vs. the measurement frequency of in the anomaly of low temperature can be fitted to the Vogel-Fulcher law (inset of figure 3.2 d), in order to calculate the freezing temperature T_f=186 ^{0}C, that coincides with the peak observed in the derivative of the real part of the permittivity with the temperature (inset figure 3.2c), the relaxing time $\tau_0=1.05\cdot10^{-8}$s and the activation energy E_a=0.17 eV. In this curve it is not possible to show more than four points for the Vogel-Fulcher fitting, because for low frequency (lower than 50 kHz) the conductivity processes are overlapped with the maximum of the permittivity.

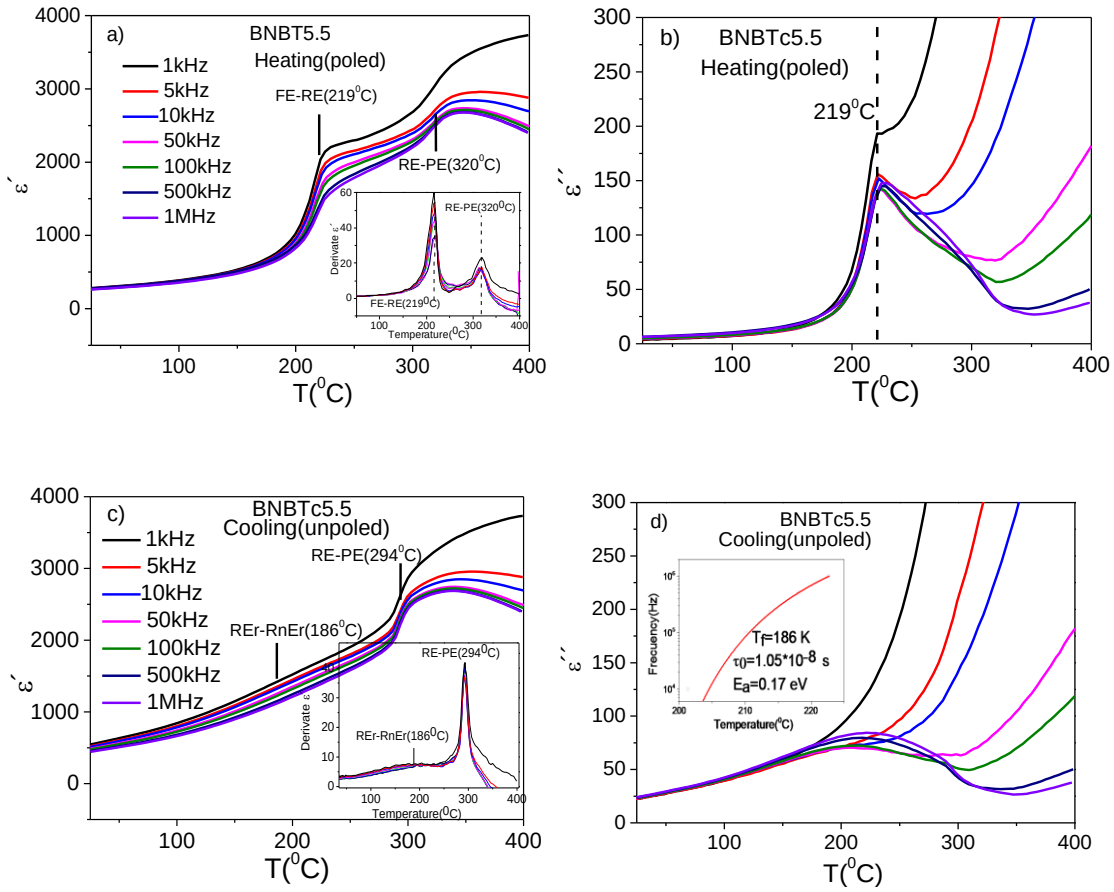

Figure 3.2: *Behavior of the real and imaginary parts of the relative dielectric permittivity for the BNBTc5.5 bulk ceramic: a,b) heating, b,c) cooling.*

This behavior observed in the imaginary part of the permittivity corresponds to the non-ergodic to ergodic relaxor at T_f, similar to that reported by different authors for compositions close to the MPB [1, 2, 3]. But it is possible to observe that the depolarization temperature obtained in these ceramics T_d=219 ^{0}C is higher than the previously reported in works where the ceramic are obtained through a conventional solid oxide route, T_d = 105 ^{0}C [4]. However, it is similar to the value reported in another work, where the sol-gel method is used to synthesize the ceramic, T_d=210 ^{0}C [1]. This can be related to the fact that by the sol-gel method it is possible to obtain an enhanced microstructure and the ferroelectric phase induced under electric field is

more stable, due to the larger ferroelectrics domain, which reduce the presence of the depolarization fields.

The difference observed between BNBTc5.5 poled and unpoled ceramics is an evidence of the canonical relaxor ferroelectric character of this composition. In this type of materials, the application of a large enough electric field during poling transforms the non-ergodic relaxor phase into a long range polarization ferroelectric phase. Regarding the polarization of this ceramic, the value in the sample in the MPB is similar to the reported in the literature, near to 30 $\mu C \cdot cm^{-2}$ for compositions in the MPB [1, 4]. The principal difference with respect to the ceramic obtained by conventional solid oxide route, is the depolarization temperature (T_d), which is higher in this case of the ceramic prepared by sol-gel .This makes these ceramics more suitable for integration in electromechanical devices.

3.2 Ferroelectric properties at room temperature of BNBT thin films.

Figure 3.3 shows the corrected P-E hysteresis loops of BNBT films obtained at room temperature. Among the films prepared from solutions without any excess (figure 3.3a), the film with a composition close to the Morphotropic Phase Boundary, BNBT5.5, has the highest values of the polarization of all the films analyzed (Tables 3.2 and 3.3).

The ceramic with this composition, close to the MPB, BNBTc5.5 also shows the highest polarization values of the two ceramics studied as expected. Saturation values in ceramics and films are similar (Table 3.2), however the remnant polarizations are different (Table 3.3). There is a loss of remanence in the films, as it can be seen in Table

3.4 where the values of P_r/P_s are given. This does not allow us to take full advantage of the functional properties of BNBT films.

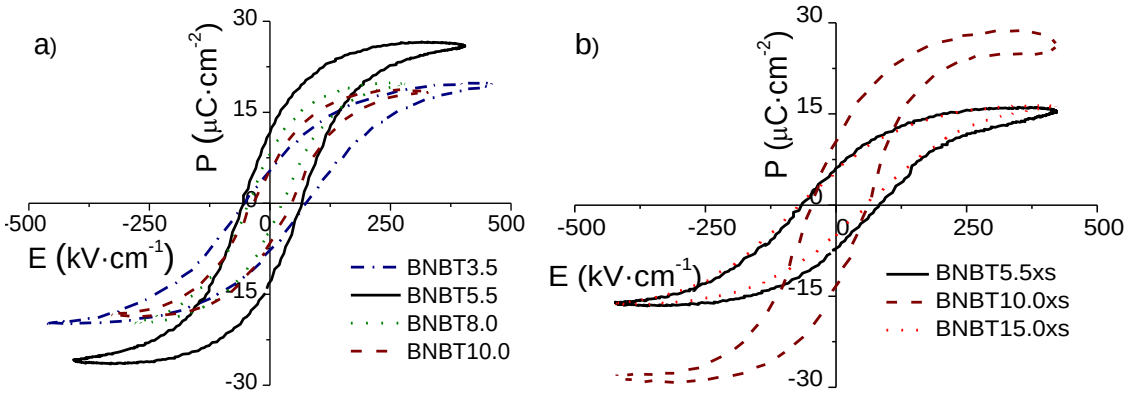

Figure 3.3: *Corrected P-E hysteresis loops of BNBT films measured at room temperature and 1 kHz, for different $BaTiO_3$ contents: a) without any excess (BNBT) ; b) with Bi and Na excess (BNBTxs) .*

The loss of remanence in thin films can be attributed to a stabilization of a relaxor-like phase due to the drastic grain size reduction produced in thin films. This grain size effect has been reported previously on similar perovskite systems with intrinsic chemical inhomogeneities like $Pb(Mg_{1/3}Nb_{2/3})O_3$-$PbTiO_3$ or $Pb(Zn_{1/3}Nb_{2/3})O_3$-$PbTiO_3$, where grain size reduction leads to the stabilization of phases in which the ferroelectric long range order is destroyed [5,6]. The main size effect identified in these relaxor-based solid solutions is a slowing down of the kinetics of the ferroelectric to relaxor transition [7], until the high temperature relaxor state stabilizes for the smallest, nanometric grains in ceramics [8,9] and thin films [10,11].The nature of the phase transition will be discussed in the following subsections.

Table 3.2: *Saturation polarization values measured at room temperature for BNBT ceramics and films*

BNBT ceramics	P_s ($\mu C \cdot cm^{-2}$)	*BNBT films*	P_s ($\mu C \cdot cm^{-2}$)	*BNBTxs films*	P_s ($\mu C \cdot cm^{-2}$)
BNBTc3.5	*24.5*	*BNBT3.5*	*19.8*	--	--
BNBTc5.5	*33.8*	*BNBT5.5*	*26.5*	*BNBT5.5xs*	*16.2*
--	--	*BNBT8.0*	*19.7*	--	--
--	--	*BNBT10.0*	*18.3*	*BNBT10.0xs*	*27.6*
--	--	--	--	*BNBT15.0xs*	*16.3*

Table 3.3: *Remnant polarization values measured at room temperature for BNBT ceramics and films*

BNBT ceramics	P_r ($\mu C \cdot cm^{-2}$)	*BNBT films*	P_r ($\mu C \cdot cm^{-2}$)	*BNBTxs films*	P_r ($\mu C \cdot cm^{-2}$)
BNBTc3.5	*20.5*	*BNBT3.5*	*6.7*	--	--
BNBTc5.5	*31.3*	*BNBT5.5*	*12.3*	*BNBT5.5xs*	*6.6*
--	--	*BNBT8.0*	*6.3*	--	--
--	--	*BNBT10.0*	*6.4*	*BNBT10.0xs*	*11.9*
--	--	--	--	*BNBT15.0xs*	*5.4*

If we assume that a relaxor phase is stabilized in BNBT films, we should consider that the polarization values after the electric field is removed drop significantly, as the polar nano-regions oriented in the direction of the field return to a random state. This means that, for this kind of materials, the remnant polarization values obtained from conventional hysteresis loops (unrelaxed) differs strongly from those of remnant loops (after 1 s relaxation), whereas this difference is almost zero for normal ferroelectrics.

Indeed, the remnant hysteresis loops of the BNBT films (Figure 3.4) show much reduced values of the remnant polarization than the conventional loops of Figure 3.3.

Table 3.4: *Comparison of the remanence (P_r/P_s) of BNBT ceramics and films*

BNBT ceramics	P_r/P_s	*BNBT films*	P_r/P_s	*BNBTxs films*	P_r/P_s
BNBTc3.5	*0.8*	*BNBT3.5*	*0.3*	--	--
BNBTc5.5	*0.9*	*BNBT5.5*	*0.5*	*BNBT5.5xs*	*0.3*
--	--	*BNBT8.0*	*0.3*	--	--
--	--	*BNBT10.0*	*0.3*	*BNBT10.0xs*	*0.4*
--	--	--	--	*BNBT15.0xs*	*0.3*

The occurrence of asymmetric remnant hysteresis loops is related to imprint effects, mainly due to self-polarization effects that cannot be overcome with the electrical cycling. This effect is larger for the BNBT3.5, 8.0, and 10.0 than for the BNBT5.5 film, in which it is almost zero. This suggests a more efficient polarization switching in this film, when the initial polarization state of the film is changed. The same efficiency is observed for the BNBTxs films, with symmetric loops. Comparing values of Figures 3.3 and 3.4, BNBT3.5, BNBT5.5 and BNBT8.0 films around 70% of their P_r after 1s of relaxation, less than BNBT10.0, that loses around 95% of its initial polarization. The relaxation of the polarization is also strong for the BNBTxs films: 80%, 75%, and 86%, for the BNBT5.5xs, BNBT10.0xs, and BNBT15.0xs films, respectively. Based on these results, it can be inferred that the stability with time of the FE polarization is low in these films, as it must be in relaxor ferroelectric materials that develop long range polarization under the application of an electric field.

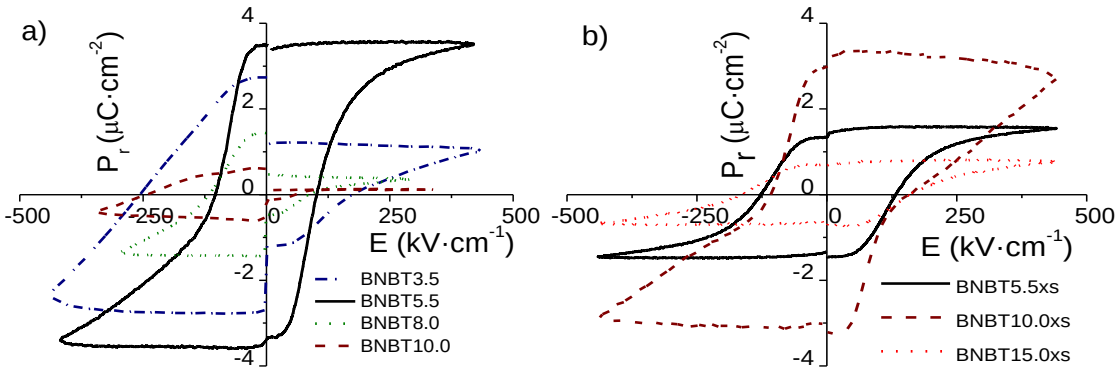

***Figure 3.4**: Remnant hysteresis loops of a) BNBT and b) BNBTxs films.*

Results from films prepared from solutions with excesses (BNBTxs) follow a different trend to BNBT films: the maximum polarization value corresponds to the composition with 10% $BaTiO_3$, far from the reported MPB. Besides, it must be noted that the electric behavior of the films prepared from solutions with and without Bi^{3+} and Na^{+} excesses, but with the same nominal composition, is different, when in principle there is no reason for them to be. These results suggest a compositional shift of this MPB when excesses are used in the precursor solutions. A thorough compositional and structural comparative study of these thin films reported in [12] concludes that the Bi^{3+} and Na^{+} excesses remain to a large extent in the bulk film, i.e., these elements do not volatilize as easily as expected during films processing. And they end up occupying A site positions at the perovskite crystals. As a result, Ti ions are transferred from $BaTiO_3$ to $(Bi_{0.5}Na_{0.5})TiO_3$ and a subsequent compositional variation.[12] Therefore, there is not any compositional shift of the MPB, but a change in the nominal composition of the films prepared from solutions with excesses, which is also accompanied by the presence of free BaO and the formation of secondary phases and interfaces, which affects the electrical behavior of these films as it is discussed below [12].

In the case of the BNBTxs films, the non-switching contributions to the FE loop are more important, due to the effect of a larger conductivity in the P-E loops. In Fig. 3.5 a), the experimental loops of the BNBT5.5 and BNBT10.0xs films are plotted in order to show the differences between the non-ferroelectric contribution of films prepared from solutions with and without excesses. The BNBT10.0xs film presents more rounded ferroelectric hysteresis loops than BNBT5.5, which indicates larger contributions to the P-E loop. This is seen more clearly in figure 3.5b, where the calculated non-ferreoelectric contributions to the polarization for the two films are compared. The differences observed can be attributed to the reported increase of surface roughness and porosity when the films are prepared from solutions with excesses. This causes that in this film there are more available conductivity paths, and this is accompanied by a compositional inhomogeneity that contributes to the increase of the conductivity and leakage currents. The origin of this enhanced conductivity may be related to the fact that not all of the excesses of these elements are lost by volatilization; part of them are incorporated in the crystalline structure [12], and the rest either remains in grain boundaries, as secondary phases or contributes to the formation of thick interfacial regions within the bottom electrode.

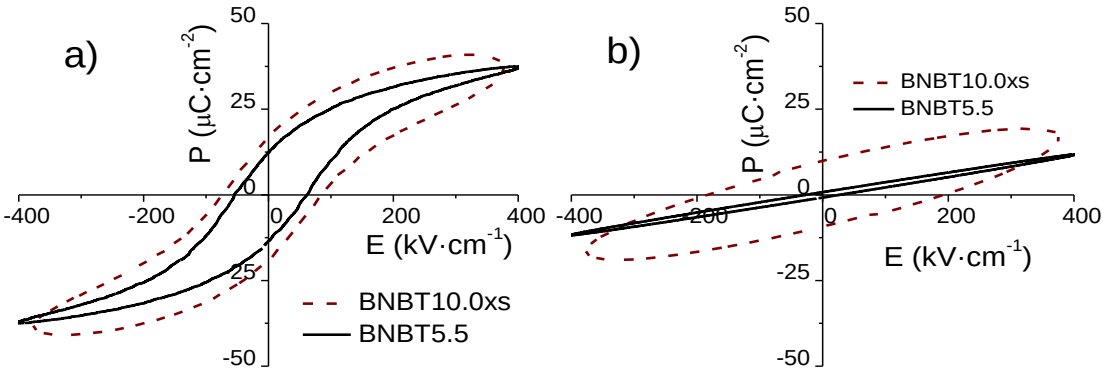

Figure 3.5: *a) Experimental P-E hysteresis loops for the BNBT5.5 films measured at 1 kHz. b) Calculated non–ferroelectic contributions to the polarization loops.*

3.3 Piezoelectric characterization of BNBT films.

The piezoelectric properties of the BNBT films have been analyzed through the d_{33} hysteresis loops (Figure 3.6) obtained by double beam interferometry. Unfortunately, the maximum applied electric field could not be higher than 220 kV·cm^{-1} in any film, which means that all the measured loops are undersaturated and, therefore, the results obtained are not conclusive. The BNBT5.5 and BNBT8.0 films present the largest response, with d_{33}^{eff} remnant values of 18 and 19 pm·V^{-1}, respectively, whereas BNBT3.5 film has a lower value of ~11 pm·V^{-1} (Fig. 3.6(a)). These results corroborate the trend that in films with a composition closer to the MPB, larger functional properties are obtained. Besides, the difference between saturated and remnant values of the piezoelectric coefficient is another evidence of the loss of remanence of the BNBT films. The results for films obtained from solutions with excesses, BNBT5.5xs and BNBT10.0xs, shown in Figure 3.6(b), show the difficulties to obtain functional properties in these films. The effective application of electric fields in films with compositional inhomogeneities and the presence of large conductivity and leakage currents (current injection) produce deformed and unreliable piezoelectric loops.

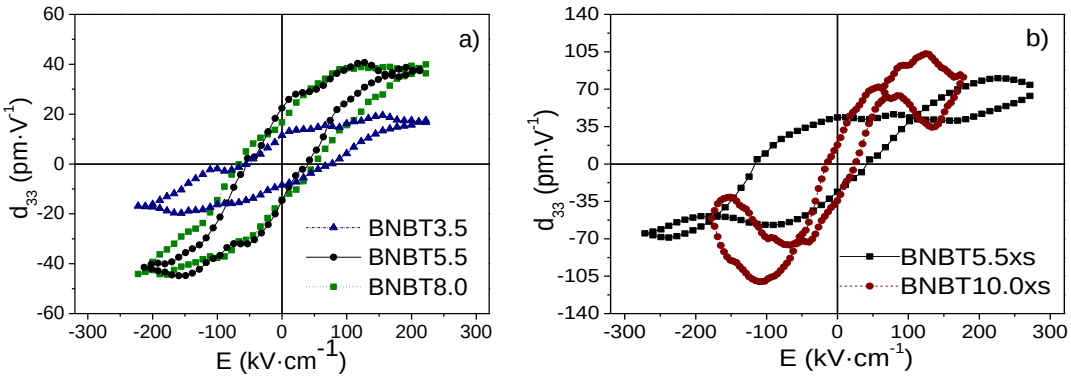

***Figure 3.6**: Macroscopic piezoelectric hysteresis loops for. a) BNBT3.5, BNBT5.5 and BNBT8.0 and b) BNBT5.5xs and BNBT10.0xs films.*

3.4 Evolution of ferroelectric properties of BNBT films with the temperature.

3.4.1. Polarization behavior with temperature.

The behavior of the ferroelectric polarization as a function of temperature under switching conditions was studied for each film, by measuring the hysteresis loops with increasing temperature. In Figure 3.7 a representative example of the evolution of corrected P-E hysteresis loop with temperature is shown. A reduction of both the remnant (P_r) and the saturation polarization (P_s) is observed as the temperature increases. Moreover, the coercive field (E_c) decreases as the temperature increases. This is the general behavior for all the BNBT films studied in this work.

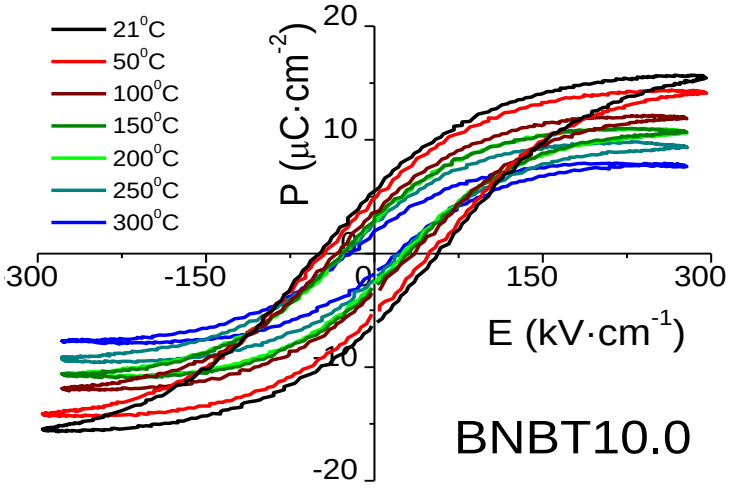

Figure 3.7: *Corrected ferroelectric hysteresis loops as a function of the temperature for the BNBT10.0 film.*

The evolution of P_r and E_c with temperature for the BNBT and BNBTxs films is plotted in Fig. 3.8 and 3.9. The P_r and E_c present a continuous reduction on increasing temperature, with a kink, where the drop of the P_r against the temperature is stronger.

To determine the precise temperature at which this change occurs, the derivative of the interpolated P_r versus T curves is calculated, i.e., the pyroelectric coefficient (γ = dP/dT) (insets of Figs. 3.8 and 3.9). The minimum value of the pyroelectric coefficient for the temperature range studied corresponds to the depolarization temperature of the material T_d [13]. The temperatures are collected in Table 3.5. On further increase in the temperature above the depolarization temperature, P_r slowly drops to zero, as it corresponds to relaxor ferroelectrics. The polarization disappears when the transition temperature to the paraelectric phase is reached. Unfortunately, the high contributions of the conductivity to the P-E loops prevent the observation of the ferroelectric polarization vanishing at the highest temperatures in these curves.

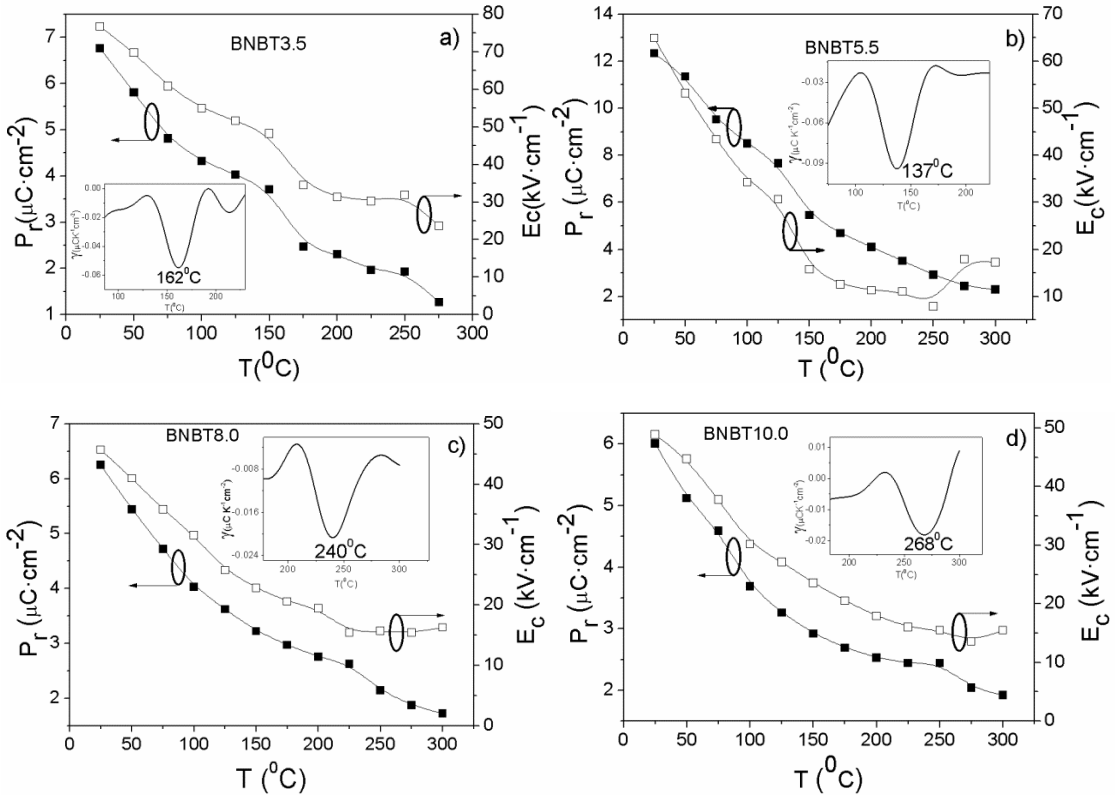

Figure 3.8: *Behavior of the remnant polarization (P_r) and coercive field (E_c) with the temperature for a) BNBT3.5, b) BNBT5.5, c) BNBT8.0, d) BNBT10.0 films. Insets show the evolution of the calculated pyroelectric coefficient as a function of the temperature.*

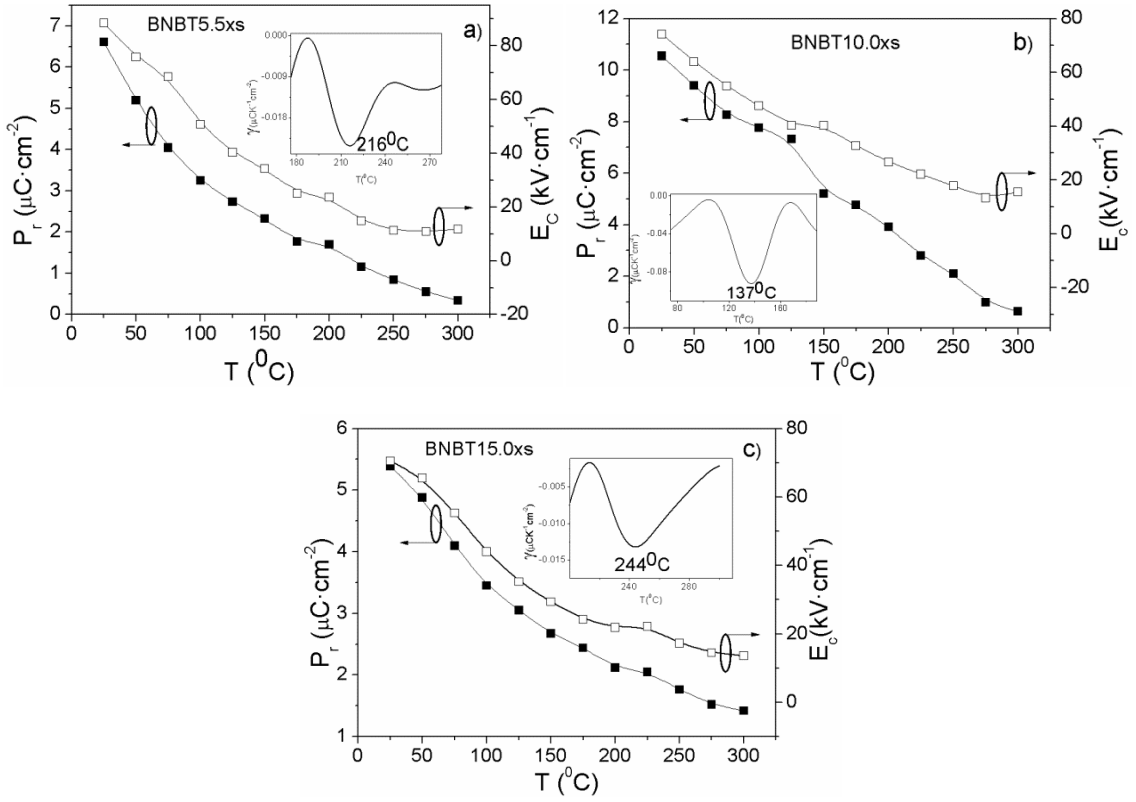

Figure 3.9: *Behavior of the remnant polarization (Pr) and coercive field (Ec) with the temperature for, a) BNBT5.5xs, b) BNBT10.0xs, c) BNBT15.0xs films. Insets show the evolution of the calculated pyroelectric coefficient as a function of the temperature.*

Table 3.5: *Depolarization temperatures of BNBT films.*

BNBT films	*T_d (^{0}C)*	*BNBTxs films*	*T_d (^{0}C)*
BNBT3.5	*162*	--	--
BNBT5.5	*137*	*BNBT5.5xs*	*216*
BNBT8.0	*240*	*BNBT10.0xs*	*137*
BNBT10.0	*268*	*BNBT15.0xs*	*244*

3.4.2 Low field, dielectric behavior with temperature.

We have mentioned that the application of a large electric field may induce a long range polarization ferroelectric phase. Therefore, the study of low field dielectric

behavior with temperature will provide information about the phase distribution without the influence of large electric fields, that may disturb it. The variation of both, real and imaginary parts of the dielectric permittivity, with the temperature is shown in Fig. 3.10 for BNBT5.5 and BNBT10.0xs films. These samples were selected for a more detailed analysis due to the fact that they have the largest polarization values (Tables 3.2 and 3.3) and allow a discussion on phase transitions of compositions close to the MPB. The results obtained can be compared to those shown in Figure 3.3 for BNBTc5.5 ceramic. The dielectric response of these films is similar, being the main difference the large conductivity contributions found in the BNBT10.0xs film, that causes a different behavior and higher values of the dielectric losses in this film.

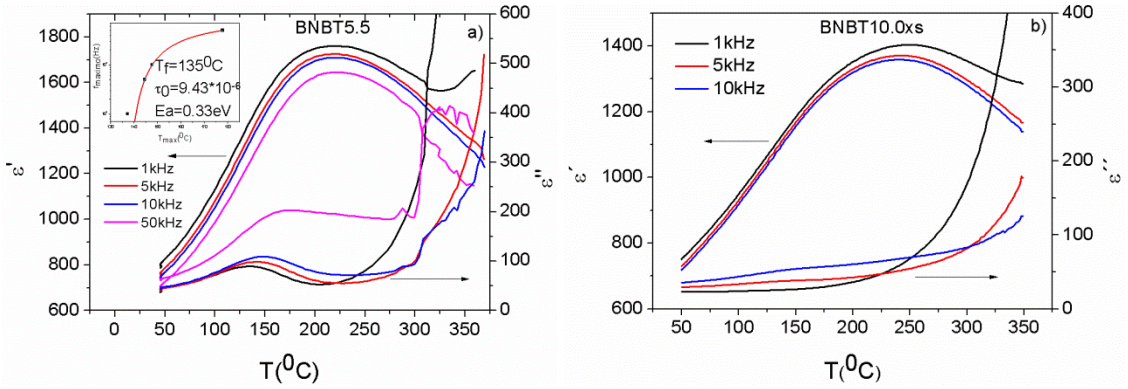

Figure 3.10: *Behavior of the real and imaginary part of the relative dielectric permittivity for: a) BNBT5.5, b) BNBT10.0xs. Inset of a) shows the Vogel-Fulcher fitting.*

The real part of the dielectric permittivity of the BNBT5.5 film presents a broad maximum at 220°C without frequency shift on heating [Fig. 3.10(a)]. For the dielectric loss, a maximum at lower temperatures (130-180^{0}C) is observed, which shifts to higher temperatures and larger loss values with frequency. This situation is similar to the one observed for unpoled BNBTc5.5 (Figure 3.3), where these two anomalies were attributed to a high temperature transition into a paralectric phase and to a low temperature non-ergodic-ergodic relaxor phase transition. The temperatures of both

transitions are lower in thin films, as expected due to the decrease of the grain size. The ferroelectric to paraelectric transition temperature goes from 320^0C in the BNBTc5.5 ceramic to 220^0C in the BNBT5.5 film. Similarly, the characteristics of the relaxor transition are analyzed through the fitting to the Volger– Fulcher expression of the temperatures of the maxima of the dielectric loss for the different measurement frequencies (inset of Fig. 3.10(a)). A freezing temperature of the polar nanoregions (PNRs) T_f = 135°C is obtained, with an activation energy of 0.33 eV and a relaxation time τ_0 = 9.43 10^{6} s. The freezing temperature is lower than the one found for BNBTc5.5, but the activation energy is larger. The relaxation time is quite high, and much larger than the one calculated for BNBTc5.5. It must be noted that the calculation of this parameter has a large fitting error due to the limited frequency window used in the measurements. The existence of T_f indicates a transition from a non-ergodic to ergodic relaxor phase in BNBT thin films. Below T_f, at room temperature, the P-E loops indicate that there is not a low temperature ferroelectric phase corresponding to a non-canonical relaxor. Therefore, we can conclude that BNBT films are canonical relaxors, like BNBTc5.5.

The reason behind the relaxor-like behavior of the $(Bi_{0.5}Na_{0.5})_{1-x}Ba_xTiO_3$ solid solution can be related to the complex domain structure of the $Na_{0.5}Bi_{0.5}TiO_3$ phase. Recent transmission electron microscopy studies (TEM) [14] demonstrate a strong tilting and chemical Bi/Na disorder found in this phase, producing a shortening of the coherence length of the structure, which cause a stabilization of the relaxor character . Due to this relaxor character, the effect of the grain size on the stability of the PNRs (Chapter I) domains should be strong, as previously demonstrated for the PMPT solid solution, in which a relaxor-like character appears with the decrease of the grain size [6]. Therefore, in thin films, the influence of the small grain sizes effect, the stabilization of

the ferroelectric phase with time is not possible, even for compositions with small phase coexistence. These phenomena can be understood considering in these compounds a two-stage process for the FE to RE transition [15].

The enhancement of the switched domains randomization in thin films is produced by intrinsic size effect as boundary conditions and small grain size, in addition to extrinsic effect as electrode/FE interfaces "dead-layers", and depth profile compositional/structural differences that lead to large extrinsic depolarization fields, in addition to that resulting from the internal random fields (See section of grains size effect in the Chapter I).

The T_f value of 135°C matches well with the temperature of the minimum in the pyroelectric coefficient for this film, 137°C. This supports the idea that the observed kink in the evolution of P_r with temperature must be related with a transition from a nonergodic to an ergodic relaxor state.

The dielectric behavior as a function of the temperature for the BNBT10.0xs sample is presented in Fig. 3.10(b). The real part of the dielectric permittivity presents a broad maximum centered at 241°C, which is attributed to a transition into a paraelectric phase. As in BNBT5.5, the evolution of the dielectric loss with temperature shows a maximum around 130^0C that shifts to higher temperatures on increasing the frequency. In this case, the large conductivity contribution to the losses masks the Volger–Fulcher behavior, and makes impossible any good fitting to obtain T_f. But the overall behavior of the permittivity and the temperatures of the anomalies observed are very similar to those of BNBT5.5, supporting the idea of the compositional shift of the MPB for the films obtained from solutions with Bi^{3+} and Na^{+} excess, and that BNBTxs10.0 is close to the MPB.

Similar behaviors are also observed for the other BNBT and BNBTxs films, but, with higher noise affecting the results of the measurements, due to their high conductivities (Figures 3.11 and 3.12). But in all cases the transition temperature into the paraelectric phase could be determined and are summarized in Table 3.6.

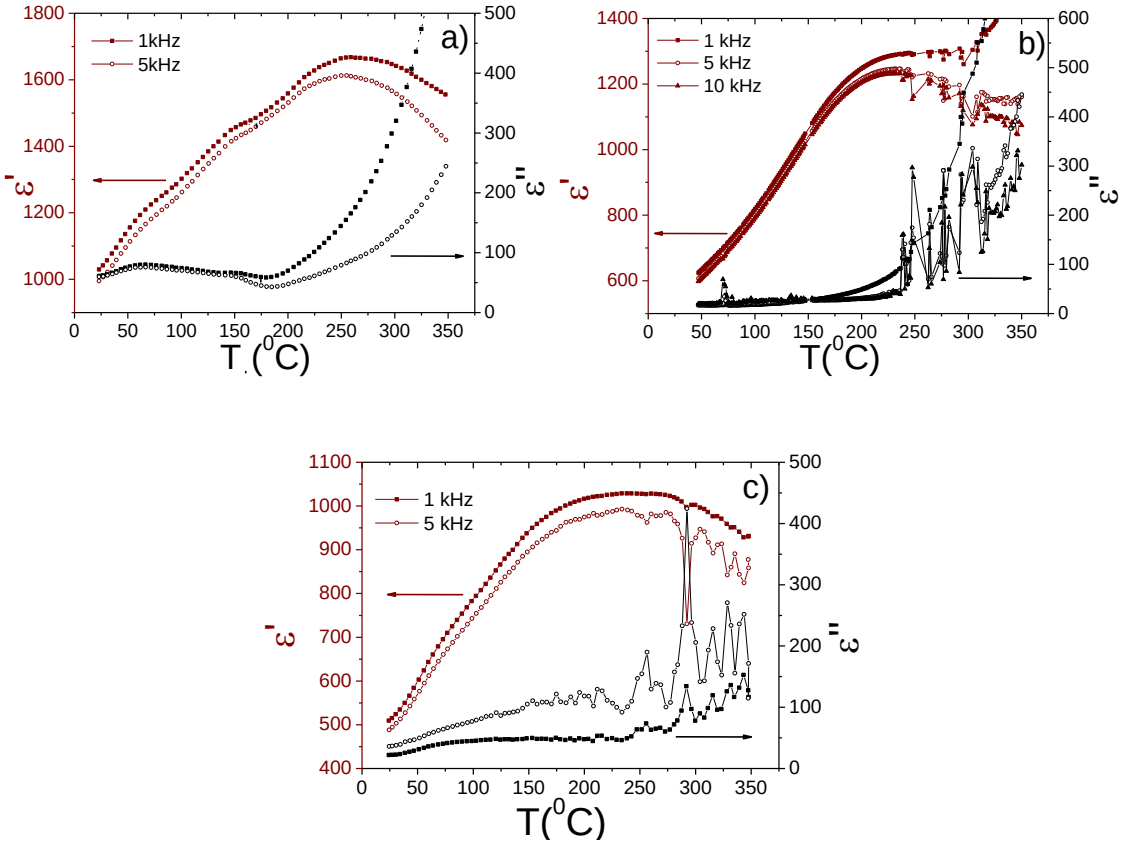

***Figure 3.11**: Behavior of the real and imaginary part of the relative dielectric permittivity for: a) BNBT3.5, b) BNBT8.0 and c) BNBT10.0.*

***Table 3.6:** Temperatures of the transition into the paraelectric phase of BNBT films.*

BNBT films	T_P (^0C)	*BNBTxs films*	T_P (^0C)
BNBT3.5	*227*	--	--
BNBT5.5	*220*	*BNBT5.5xs*	*240*
BNBT8.0	*228*	*BNBT10.0xs*	*241*
BNBT10.0	*258*	*BNBT15.0xs*	*264*

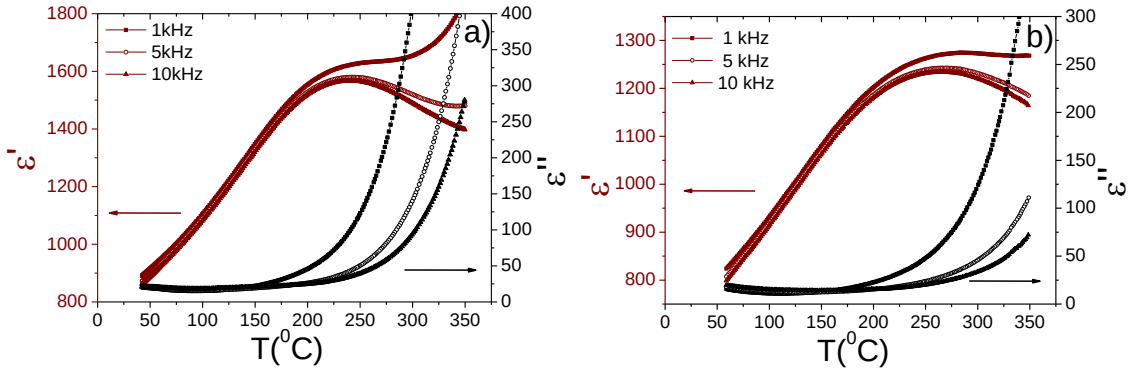

Figure 3.12: *Behavior of the real and imaginary part of the relative dielectric permittivity for: a) BNBT5.5xs, b) BNBT15.0xs*

The variation in the dielectric permittivity with temperature of the BNBT3.5, BNBT8.0, and BNBT10.0 films also shows broad maxima at 227°C, 228°C, and 258°C, respectively, with maxima of the dielectric losses clearly visible at 10 kHz for intermediate temperatures, but not observable at low frequencies due to conductivity. For the films obtained from solutions containing Bi^{3+} and Na^{+} excesses, larger contributions from conductivity are observed, obtaining broad maxima of the dielectric permittivity at 240°C and 264°C for the BNBT5.5xs and BNBT15.0xs films, respectively. A maximum in the dielectric losses at intermediate temperatures is only observed here for the BNBT10.0xs film at 10 kHz (Figure 3.10(b)). The similarities between the dielectric behavior of the BNBT and BNBTxs films (is more evident in the films with best ferroelectric properties BNBT5.5 and BNBT10.0xs) allow us to state that the minimum in the pyroelectric coefficient associated with the drop in P_r can be related to the nonergodic to ergodic transition in relaxor ferroelectric materials, at least for these thin films.

It has to be noted the coincidence between T_d and T_f in the films with compositions close to the MPB. In this MPB, the free energies of the rhombohedral and tetragonal phases should almost be equal, so the easy conversion between both phases can produce anticipation in the splitting of the polar domains to yield PNRs and give rise to the ergodic relaxor state. It is complicate to try to extract more information from the characterization of polycrystalline thin films, but the proximity of the T_d of the BNBT10 and BNBT15.5xs thin films to the T_m can be related to a larger stability of the tetragonal polar phase, for the compositions far from the MPB, that keeps the nonergodic state up to temperatures close to ferroelectric to paraelectric transition.

3.5 Phase diagram of BNBT films.

A phase diagram is proposed for $(Bi_{0.5}Na_{0.5})_{1-x}Ba_xTiO_3$ films, using the depolarization temperatures (T_d) calculated from the P-E hysteresis loops (Table 3.5) and the transition temperatures to the paraelectric phase (T_p) obtained from the permittivity curves (Table 3.6). The position of the MPB, i.e. the transition from the rhombohedral to the tetragonal phase at room temperature as the $BaTiO_3$ content increases, was previously determined for both BNBT and BNBTxs films [12]. The results are superimposed to the phase diagram reported by Takenaka et al for bulk ceramics [16] in Figure 3.13. The films prepared from solutions with the nominal composition, BNBT films, present a phase diagram similar to that reported for bulk ceramics (filled symbols in Fig. 3.13), with the MPB in the vicinity of x~0.055. The relaxor-to-paraelectric transition is observed however at lower temperature (~100°C lower). The reduction of phase transition temperatures is usually observed in thin films and it is attributed to a size effect. But the most important difference with Takenaka's phase diagram is the identification of the nature of the phases. The antiferroelectric intermediate phase

between the low temperature ferroelectric and the high temperature paraelectric proposed in that work is found to be an ergodic relaxor phase that evolves from a low temperature nonergodic relaxor phase. According to our results, the low temperature phases are better described as nonergodic relaxors, regardless whether they are rhombohedral or tetragonal. The stabilization of the relaxor phase due to the reduced grain size of the films produces this effect.

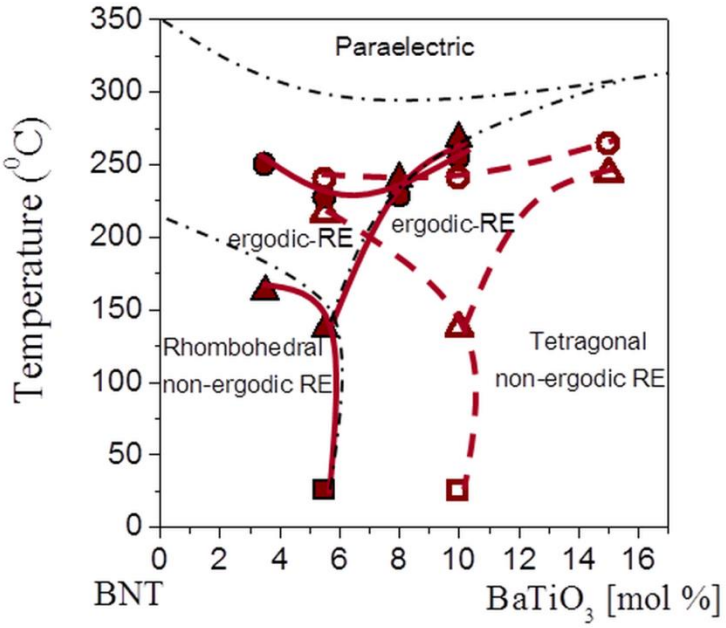

Figure 3.13: *Phase diagram of the $(Bi_{0.5}Na_{0.5})_{1-x}$ Ba_xTiO_3 thin films studied in this work. The filled and open squares are obtained from a structural study of the films at room temperature [12] for the BNBT and BNBTxs films, respectively. The filled and open triangles indicate the depolarization temperatures. The filled and open circles indicate the temperatures at the maximum of the broad dielectric anomaly, for the BNBT and BNBTxs films, respectively. Lines are drawn as a guide for the eye. The dashed dot lines correspond to the phase diagram reported in [16].*

Regarding the films prepared from solutions with Bi^{3+} and Na^{+} excess, BNBTxs, (open symbols in Fig. 3.13) the whole phase diagram is compositionally shifted to higher concentrations of $BaTiO_3$ content. As it has been discussed before, this is an apparent shift, not only of the MPB but also of all transition boundaries as it can be seen in the

figure. All this is due to the partial incorporation of the excesses in the crystal phases, which produces a transfer of Ti ions from $BaTiO_3$ to $(Bi_{0.5}Na_{0.5})TiO_3$. Therefore the mol% of $BaTiO_3$ in the film does not correspond to the nominal values introduced, but to lower ones, and free BaO and secondary phases are formed in these films. It can be concluded that the use of excesses in the precursor solutions does not affect the phase diagram of the BNBT films. It only modifies de nominal $BaTiO_3$ content in the composition of the films.

3.6 Conclusions on the behavior of BNBT films.

From the results shown in this chapter we can obtain a series of conclusions on the functional behavior of this important family of lead free thin films.

Firstly, the use of Bi and Na excess in the precursor solutions produces an apparent compositional shift of the MPB in the phase diagram. This is in fact due to the incorporation of Bi and Na in the crystalline structure, which produces a transfer of Ti ions from $BaTiO_3$ to $(Bi_{0.5}Na_{0.5})TiO_3$. But some of these excesses remain in the film leading to inhomogeneous film profiles, responsible for the enhanced conductivity and leakage currents of these films. All this disturbs the functional behavior of the films, as it has been shown for their piezoelectric properties, which make them unsuitable for applications. We can conclude that the use of excess in the precursor solutions is not only unnecessary but also must be avoided to obtain reliable films.

BNBT films show a non-ergodic relaxor phase at room temperature for all the compositions analyzed, which suffers a transformation to a high temperature ergodic relaxor phase for compositions below x=0.08 (8% $BaTiO_3$ content). The position of the MPB in the phase diagram of the films is the same as for bulk materials. The best

properties are found for compositions close to the MPB, with the highest values of the polarization.

The main drawback for the effective integration of these films in a device is their low remanence. The application of an electric field on the ergodic relaxor phase results in the inducement of a long range polarization that almost disappears when the field is removed. The small grain size of these films is the main cause of the stabilization of this relaxor state and subsequent poor remnant properties of BNBT films. In chapter 5 we will discuss the integration of these promising lead free films in composites in order to circumvent this problem and be able to take full advantage of their functional properties.

3.7 References

[1] L.Pardo, E.Mercadelli, Á.García, K.Brebøl and C.Galassi, IEEE Transactions on Ultrasonics, 58,9, 1893-1904 (2011).

[2] C. Xu, D. Lin, and K. W. Kwok, Sol. Sta. Sci , 10 [7] 934-40, (2008).

[3] M. Cheng, G. Hanzheng, P. B. Scott, T. Xiaoli, Phys. Rev. Lett. 109, 107602, (2012).

[4] W. Jo, S. Silke, E. Sapper, L. A. Schmitt, H. J. Kleebe, A. J. Bell, and J. Rödel, J. Appl. Phys., 110, 074106, (2011).

[5] J. Carreaud, J. M. Kiat, B. Dkhil, M. Algueró, J. Ricote, R. Jimenez, J. Holc, M. Kosec, Appl. Phys. Lett. 89, 252906 (2006)

[6] M. Algueró, J. Ricote, R. Jiménez, P. Ramos, J. Carreaud, J.M. Kiat, B. Dkhil, J. Holc M. Kosec, Appl. Phys. Lett. 91, 112905, (2007)

[7] R. Jiménez, H. Amorín, J. Ricote, J. Carreaud, J. M. Kiat, B. Dkhil, J. Holc, M. Kosec, M. Algueró, Phys. Rev. B 78, 094103 (2008)

[8] M. Algueró, T. Hungría, H. Amorín, J. Ricote, J. Galy, A. Castro, Small 3, 1906 (2007)

[9] H. Amorín, R. Jimenez, T. Hungria, A. Castro, M. Algueró, Appl. Phys. Lett. 94, 152902 (2009)

[10] M. Alguero, M. Stewart, M. G. Cain, P. Ramos, J. Ricote, and M. L. Calzada, J. Phys. D: Appl. Phys., 43, 205401, 7pp (2010).

[11] H. Hitham, R. Jimenez, J. Ricote, A. Alguero, and M. L. Calzada, Thin Solid Films, 519, 6467–71 (2011).

[12] D. P. Mezcua, R. Sirera, I. Bretos, L. F. Cobas, R. E. Galindo, D. Chateigner, J. Ricote, R. Jiménez, and M. L. Calzada, J. Am. Ceram. Soc., 97 [4] 1269–1275 (2014)

[13] E. Sapper, S. Schaab, W. Jo, T. Granzow, and J. Rödel, J. Appl. Phys., 111, 014105, 6pp (2012).

[14] I. Levin ,M. I. Reaney, Adv. Funct. Mater., 22, 3445–52 (2012).

[15] W. Jo, J. Daniels, D. Damjanovic, W. Kleeman, J. Rödel, Appl. Phys. Lett., 102, 192903, (2013).

[16] T. Takenaka, K. Maruyama, K. Sakata, Jpn. J. Appl. Phys., 30, 2236–2239 (1991).

CHAPTER-IV

FUNCTIONAL PROPERTIES OF $BiFeO_3$ (BF) SINGLE PHASE THIN FILMS.

In this chapter, the main results of the functional properties of BiFeO3 (BF) thin films, for different crystallization conditions are described, in addition to the effect that the doping of the films have on these properties. The aim of this chapter is to present the properties of the BF films in order to identify its advantages and disadvantages for their possible application in microelectronics devices. To find the optimum processing conditions for which the films have the desired/required properties for this aim, the introduction of Bi excess in the precursor solutions, different crystallization temperature and the effects of the doping with different percent of Ca^{2+} in the ferroelectric properties are evaluated. The possible reductions in the high contributions of the leakage current found in BF films are studied, in addition to the behavior of the polarization with the change of the preparation conditions and doping. Table 4.1 summarizes the different BF thin films studied in this chapter.

***Table 4.1**: Nomenclature used for the BF films.*

Nomenclature of $BiFeO_3$ thin film			
	Crystallization 400ºC	*Crystallization 450ºC*	*Crystallization 500ºC*
Thin films without excess.	*BF400*	*BF450*	*BF500*
Thin films with 5 % of Bi excess	*BF400xs*	*BF450xs*	*BF500xs*
			doped 3% Ca *BCF3*
			doped 5% Ca *BCF5*

4.1 Pure $BiFeO_3$ thin films

Firstly, we will show the structural and microstructural features of pure BF films. Bi is a volatile element that can be lost during film crystallization at high temperatures, which produces extensive defective regions in the crystal. Introducing an excess of Bi in the precursor solution will promote the volume fraction of defect-free, well crystallized crystals within the BF films. Besides, the use of Bi excess does not produce the segregation of measurable distinct phases according to the X-ray diffraction data of these films (Figure 4.1). The crystalline perovskite phase (rhombohedral R3c crystal structure, JCPDS-ICDD 86-1518 file) is detected for all films, with only small traces of a secondary crystalline phase ($Bi_{25}Fe_4O_{39}$) observed for the films crystallized at 500ºC (BF500 and BF500xs). This nanocrystalline phase, $Bi_{25}FeO_{39}$ (JCPDS 46-0416 file), is usually stabilized during processing at temperatures below 447ºC [1]. Therefore, it should be also present in the films prepared at lower temperatures, but probably it is not diffracting due to its low crystallinity.

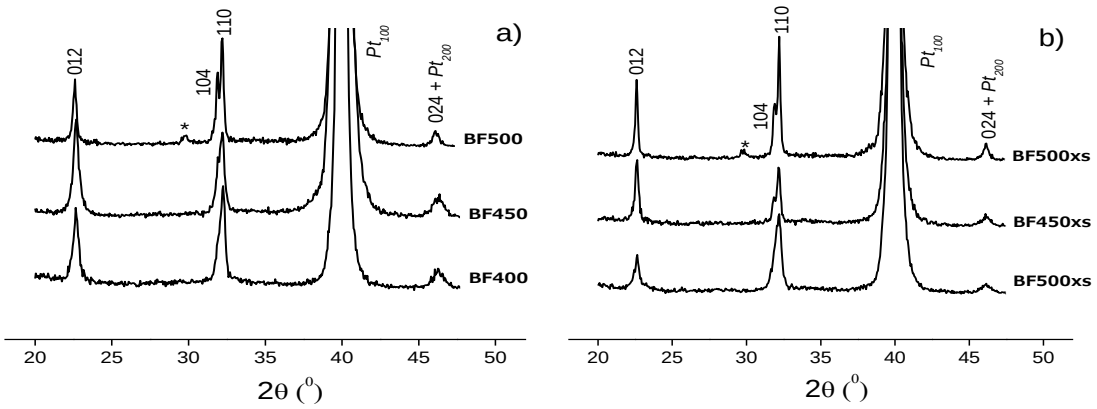

Figure 4.1: *X-Ray diffraction patterns of BF films crystallized at different temperatures from solutions a) without any excess and b) with 5% Bi excess. *$Bi_{25}Fe_4O_{39}$.*

The defective regions can be distributed within the grains, forming for example core-shell structures, as it has been proposed previously for films with volatile element [2]. This distribution is in agreement with the observed microstructures of the films (SEM micrographs of Figure 4.2, which do not show any differentiated grains that may suggest the existence of defective and flawless grains within the film.

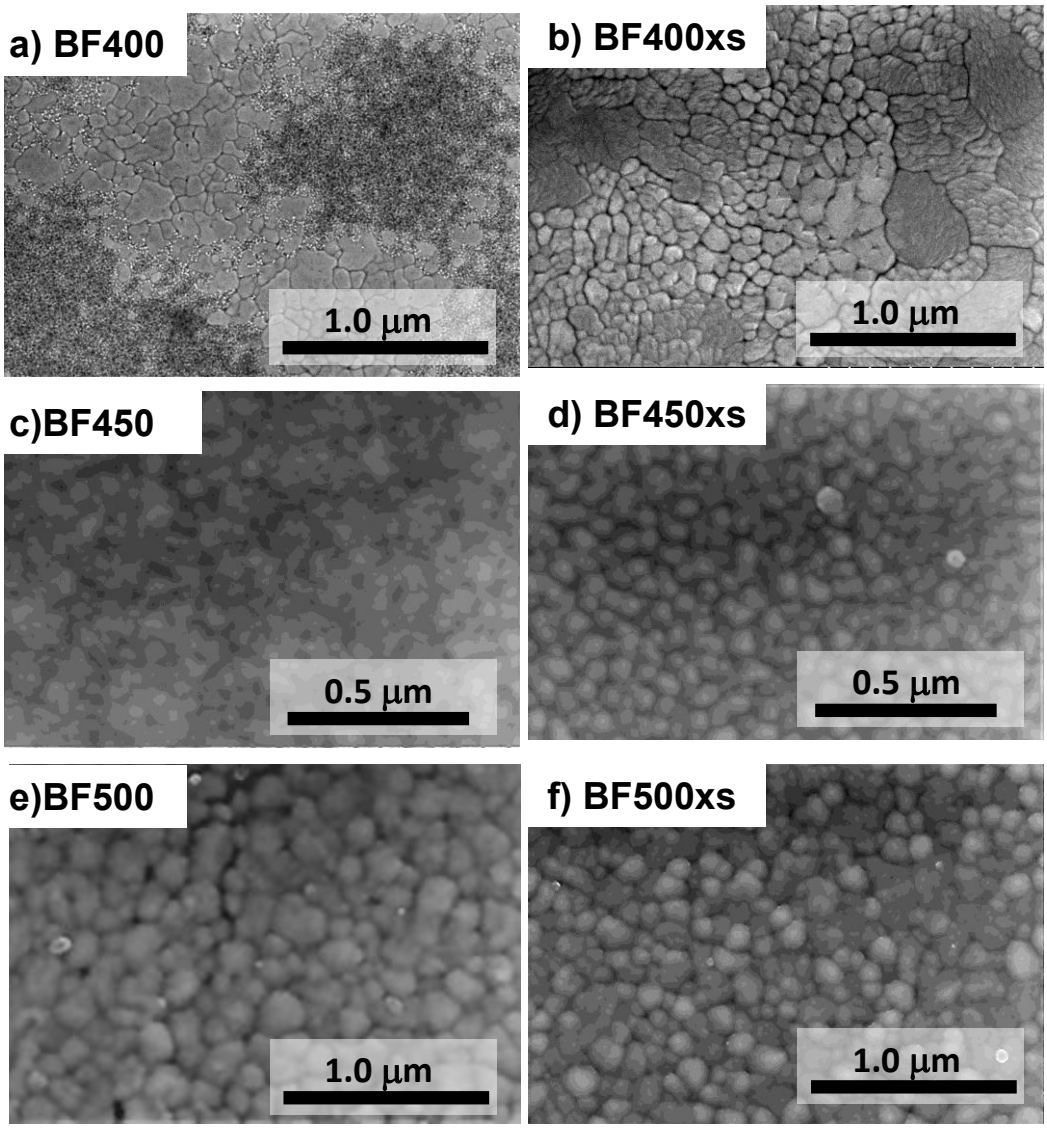

Figure 4.2: *SEM micrographs of the surface of BF films crystallized at different temperatures from solutions a),c) ,e)without any excess and b), d), f) with 5% Bi excess.*

The existence of crystalline Bi defective regions in the films is corroborated by the variations of the conduction mechanisms observed in the films prepared with and without Bi excess. In addition, these defective regions in the films does not affect significantly the grain size variations caused by the different crystallization temperatures used (Figure 4.2), which is similar for the films prepared from solutions with and without Bi excess. The decrease of the grain size, with the appearance of fine grained regions, as the crystallization temperature is lowered, is correlated with the smaller polarization values obtained for the films crystallized at 450 and 400^{0}C. Therefore, we conclude that the optimum temperature for the preparation of BF films is 500^{0}C.

4.1.1 Ferroelectric properties.

In the BF films it was impossible to measure the ferroelectric properties at room temperature due to the high leakage contributions in these thin films [3]. Therefore, the ferroelectric characterization needs has to be performed from low to room temperature, in order to be able to switch the polarization without the occurrence of electrical breakdown due to the large electric fields applied. For all films studied in this chapter the temperature was lowered first to 150K and then, the amplitude of a sinusoidal electric field used for the P-E hysteresis loop measurements was increased slowly up to the point that switching is produced. Then, the temperature is increased successively in step of 25 ^{0}C and the electric conditioning is repeated. Under no circumstances the electric field exceeded the one applied at 150K, to prevent the dielectric breakdown. This procedure prevents any irreversible resistivity degradation and acts as an electrical conditioning treatment of the BF films. However, due to the increase of the leakage current with the temperature, when the electric conditioning is repeated for different temperatures, the dielectric breakdown can appear at a given temperature.

The temperature at which this occurs is different for films prepared with different crystallization temperatures, showing the influence of the processing parameters on the leakage current behavior of BF films.

Figure 4.3 shows the experimental J–E curves/loops obtained at different temperatures for BF films crystallized between 400 and 500^{0}C (400^{0}C (BF400),450^{0}C (BF450),500^{0}C (BF500)). From them we calculate the P-E hysteresis loops, where all non-ferroelectric contributions have been removed. This fitting of the current loops through a phenomenological model allows extracting more information about the dielectric behavior [4]. For the sake of comparison we show only those measured at 200 K, the maximum temperature at which all films can be measured without electrical breakdown. Here we show the results of the films prepared from solutions without any Bi excess. We observe the characteristic maxima of the current curves related to the switching of the ferroelectric polarization for all the films. In addition, for the film crystallized at the lowest temperature, BF400, we can observe that the switching present higher non-ferroelectric contributions than in the other two films. Leakage currents, that can be identified by a no-lineal behavior in the J-E lops at high electric field, are part of these non-ferroelectric contributions and are present for the films crystallized at the three different temperatures, being lower for the film crystallized at 500 ^{0}C. However, electrical breakdown in this film occurs at a lower temperature (225K) than in BF400 and BF450 (275 K). This evidences that not in all cases the electric breakdown is directly related with the leakage current magnitude. In the P-E loops obtained at 200 K (figure 4.3), a high remnant polarization (P_r) is observed for all samples, whose values are collected in Table 4.2 together with other parameters calculated from the fitting of the loops . The highest value of P_r is obtained for the BF500 film: P_r= 57.1 μC·cm^{-2} and the P_r/P_s rate is 0.9 approximately. This value of

polarization is amongst the highest reported for lead-free materials in thin film form [5]. For lower crystallization temperatures, this remnant polarization decreases down to P_r= 28.8 μC·cm^{-2} with the saturation in P_s=36.4 μC·cm^{-2} (P_r/P_s ~0.8) for the film BF450 and P_r= 7.4 μC·cm^{-2} and P_s= 11.2 μC·cm^{-2} (P_r/P_s ~0.7) for BF400, film. These values prove that the BF500 sample has the highest polarization retention at zero field, reaching 90% of the saturation polarization.

Table 4.2. *Results of the density current hysteresis loops measured at 1 kHz of BF films from solutions without Bi excess.*

$BiFeO_3$ thin films		Results from the loop fittings at 200 K and 1 kHz				
Precursor solution	Crystallization temperature	Remnant polarization P_R (μC/cm²)	Saturation polarization P_S (μC/cm²)	(P_R/P_S)	Coercive field E_C (kV/cm)	BIAS (kV/cm)
No Bi(III) excess	400°C	7.4	11.2	0.7	401	-333
	450°C	28.8	36.4	0.8	370	213
	500°C	57.1	63.6	0.9	180	53

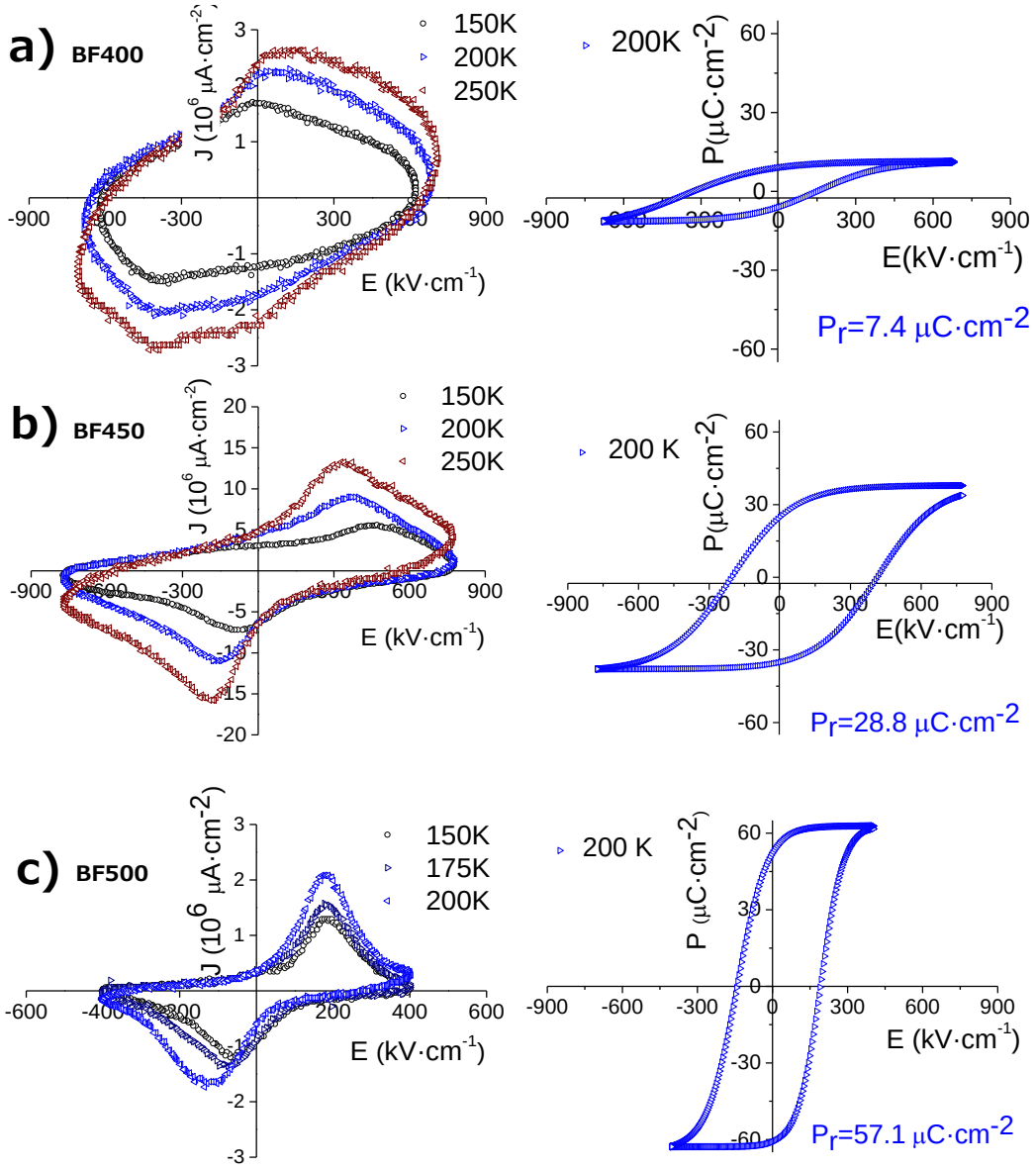

Figure 4.3: *Current vs. electric field hysteresis loops measured at different temperatures together with the corresponding corrected P-E hysteresis loops measured at 200 K for BF films form solutions without excess and crystallized at different temperatures; a) 400^{0}C, b) 450^{0}C, c) 500^{0}C.*

The evolution of the saturation polarization values with increasing measuring temperatures for BF thin films prepared from solutions without Bi excess are presented in Figure 4.4. BF400 presents a saturation value of P_s = 5.3 μC·cm^{-2} at 150K, increasing to 11.2 μC·cm^{-2} at 200K, and slightly reducing its value at 250K to 11.0

$\mu C \cdot cm^{-2}$. The results for BF450 (Figure 4.4) follow the same behavior, with maximum value P_s = 43.0 $\mu C \cdot cm^{-2}$ at 225K. The same occurs for BF500 film, with the largest maximum value, P_s = 60.0 $\mu C \cdot cm^{-2}$ at 200K.

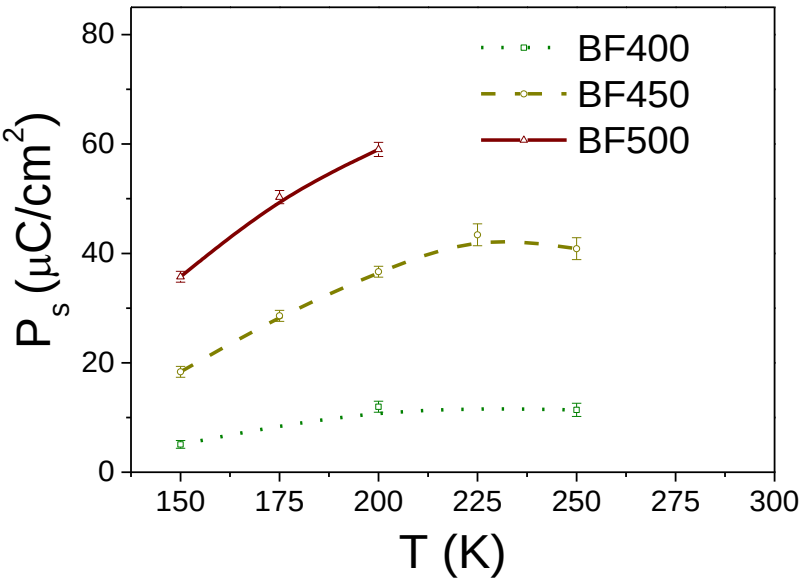

Figure 4.4: *Behavior of the saturation polarization for BF films prepared from solutions without any Bi excess.*

For the films prepared from solutions with Bi excess and crystallized at the same temperatures as those of the previous set of films (400^0C (BF400xs), 450^0C (BF450xs), 500^0C (BF500xs)), we observe the evolution of the ferroelectric behavior in figure 4.5 through the J-E hysteresis loops measured at different temperatures and the corrected P-E hysteresis loops. A simple inspection of the ferroelectric switching in the current loops shows the typical behavior of polarization switching. The contribution from non-linear leakage currents increases significantly with the measuring temperature, with respect to the films prepared from solutions without Bi excess (Figure 4.3). Another important aspect is that the polarization of the films prepared with excess can be switched at room temperature when crystallized at 400 and 450ºC (Figure 4.5). In the film crystalized at 500 ^{0}C, ferroelectric switching is achieved at higher temperature

than in the film crystallized at the same temperature but from a solution without Bi excess. However, the dielectric breakdown occurs when a large enough electric field is applied at temperatures larger than 225K, preventing the switching at room temperature (Figure 4.5 c). This occurs despite the well-defined switching curves observed at 150-175K. Nonetheless, the film BF500xs has the highest remnant polarization P_r=66.0 μC·cm^{-2} amongst all the BF films here studied. In the films crystallized at 450^{0}C and 400^{0}C the remnant polarization is only P_r=52.5 μC·cm^{-2} and P_r=7.8 μC·cm^{-2}, respectively, but polarization can be switched at room temperature. A comparison of the different dielectric parameters obtained from the fitting of the current loops in the thin films with excess of Bi is collected in table 4.3. BF500xs has the highest P_r/P_s about 0.9, meaning that this sample retains the 90 % of the polarization. The two other films retain 70 % the BF400xs and 80% the BF450xs.

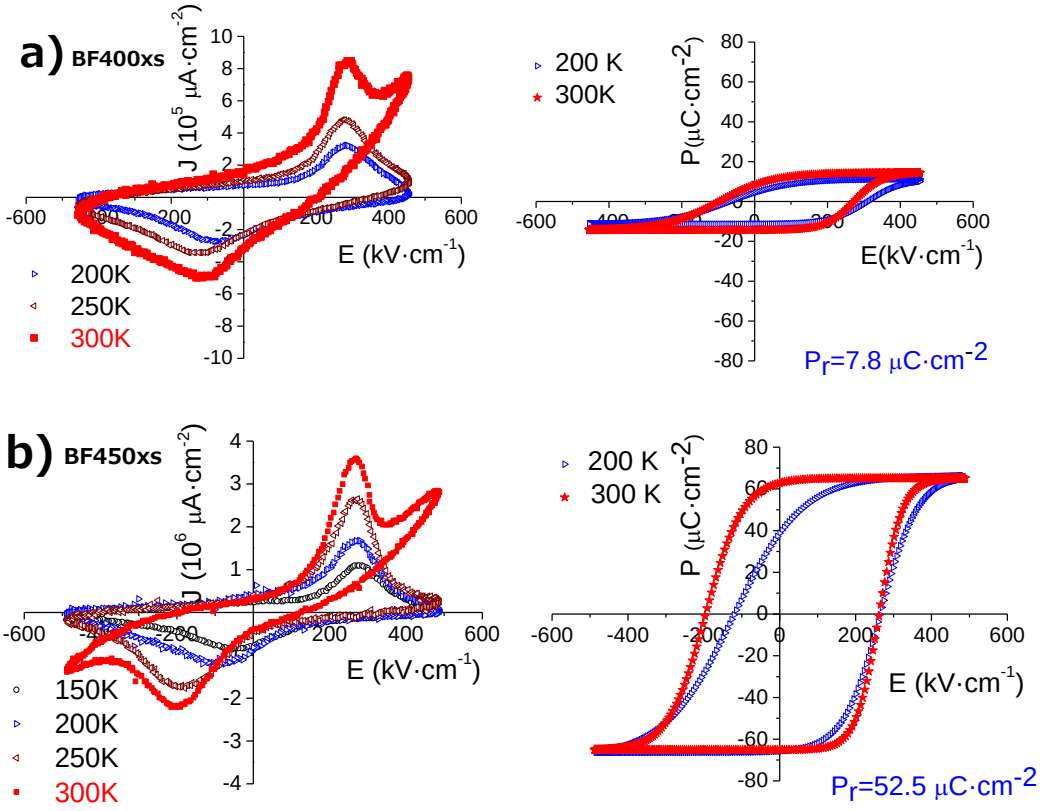

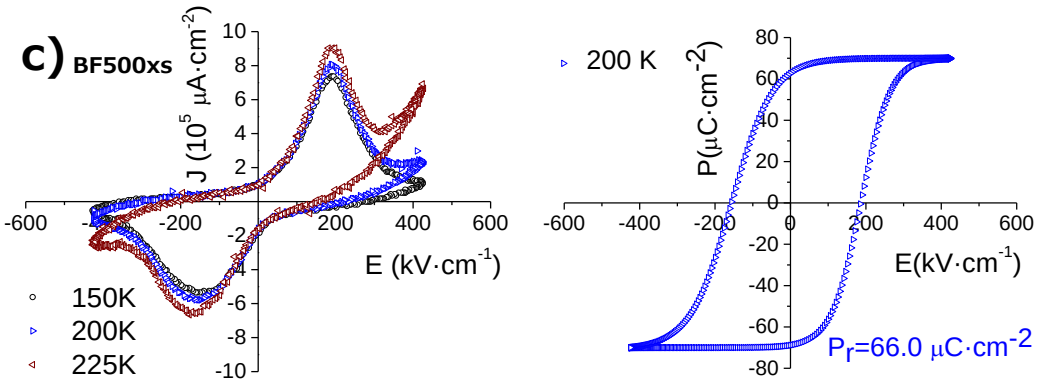

Figure 4.5: *Current vs. electric field hysteresis loops measured at different temperatures together with the corresponding corrected P-E hysteresis loops measured at 200 K for BF films obtained from solutions with Bi excess and crystallized at different temperatures; a) 400^{0}C, b) 450^{0}C, c) 500^{0}C .*

Table 4.3. *Results of the density current hysteresis loops measured at 1 kHz of BF films from solutions with Bi excess.*

$BiFeO_3$ thin films		Results from the loop fittings at 200 K and 1 kHz				
Precursor solution	Crystallization temperature	Remnant polarization P_R (μC/cm²)	Saturation polarization P_S (μC/cm²)	(P_R/P_S)	Coercive field E_C (kV/cm)	BIAS (kV/cm)
5mol% Bi(III) excess	400°C	7.8	11.2	0.7	282	214
	450°	52.5	65.6	0.8	270	181
	500°C	66.0	70.2	0.9	192	28

Figure 4.6 shows the behavior of the saturation polarization for the films prepared from solutions with Bi excess. The general trend is similar to that observed for the films obtained from solutions without any Bi excess (figure 4.4), being the main difference the higher values obtained for the maximum polarization in these films. In the BF400xs film, the value of the maximum is P_s = 17.0 μC·cm^{-2} at a temperature closer to room temperature (275K) than the one observed for the BF400 film (200K). At room

temperature, the value of the polarization is 12.8 μC·cm^{-2}. In the BF450xs, the maximum value is also at 275K (P_s=71.3 μC·cm^{-2}), and at room temperature, decreases to P_s=62.1 μC·cm^{-2}. The BF500xs film (Figure 4.6) presents a reduction from P_s = 80 μC·cm^{-2}at 150K to 69 μC·cm^{-2}at 225K, but exhibits the highest value in the maximum of all thin films studied.

In general, it can be observed that the films obtained from solutions with Bi excess show higher polarization values than those from solutions without any excess. In addition, we only achieve switching at room temperature for the BFxs films, despite their high leakage current values. If we compare the evolution of the saturation polarization with the measurement temperature for all films (Figures 4.4 and 4.6) we observe a tendency to show a maximum value in all of them. The temperature at which this maximum is reached depends on the processing parameters of the film: crystallization temperature and the use of Bi excess in the precursor solution.

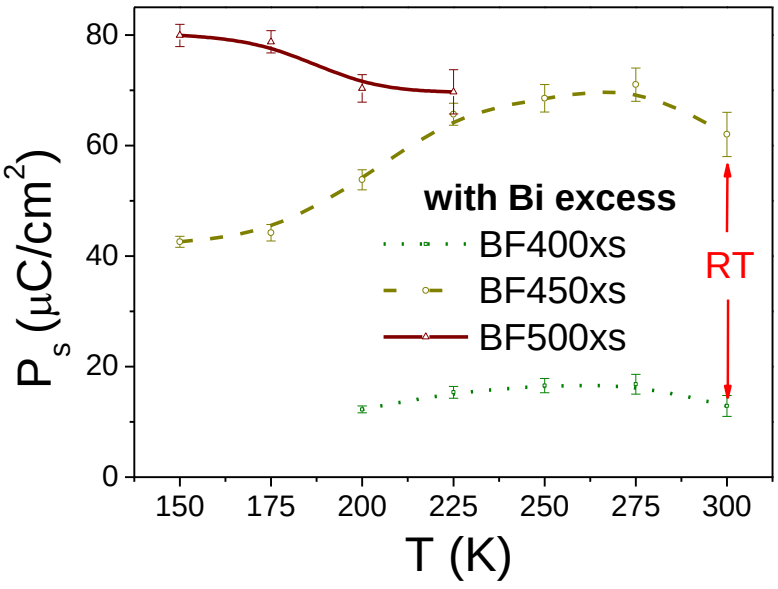

Figure 4.6: *Behavior of the saturation polarization for BF films prepared from solutions with Bi excess.*

In figure 4.7 the absolute values of the BIAS voltage observed in the hysteresis loops is plotted against the measuring temperature. It is clear that the values of the bias decreases as the crystallization temperature increases. We can directly compare these BIAS values since the film thickness do not vary significantly among samples. Besides, a tendency to show a minimum value at a certain measuring temperature can be also observed. This temperature is different for all the films, and more data are necessary to find any correlation with the processing parameters of the films.

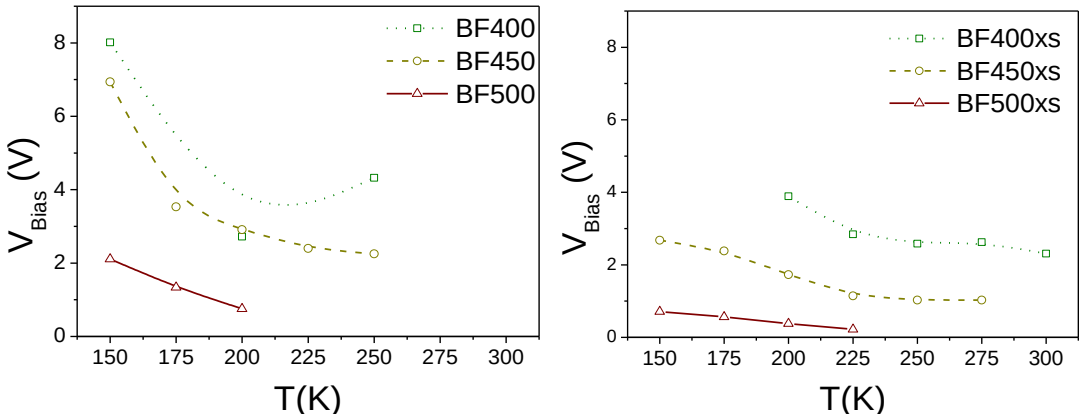

Figure 4.7: *Evolution of the bias voltage with the measuring temperaturefor films prepared from solutions a) without excess and b) with Bi excess.*

The studies performed in the microstructure of the BF films with and without excess [6] (Figure 4.2) show that the size of the grains and the probable columnar growth in the films crystallized at 500ºC seems to hinder the formation of the interface phenomena that causes the appearance of internal BIAS in the films, which is maximum for the films with a fine grained phase crystallized at 400ºC (figure 4.7). The nature of these interfaces seems rather inhomogeneous and the electric BIAS created, as it can be seen in Table 4.2 and 4.3. These results indicate that the maximum crystallization temperature of the films, 500 ^{0}C, without forming secondary phases is the optimum temperature in order to prevent the BIAS voltage development in these films.

The decrease of the polarization observed for the highest measuring temperatures in some of the BF films (Figures 4.4 and 4.6) can be attributed to the appearance of significant electrical conduction in the films. It must be pointed out that this behavior cannot be attributed to the fact that the material is closer to the ferroelectric-to-paraelectric phase transition for the highest measuring temperatures, which will cause a decrease in the polarization. For $BiFeO_3$ this takes place at quite high temperature (1170 K) and it should produce only slight changes in the ferroelectric properties in the temperature interval used in our measurements. Instead, the large increase of the conductivity at large electric fields will reduce the effectiveness of the applied electric field, causing a subsequent decrease of the polarization values. The effect will be enhanced for those films whose current intensity vs. voltage (I-V) curves show strong non-linearities when the measuring temperature increases. This will be analyzed in the next section.

Finally, we compare the ferroelectric response of these films at 200 K (Tables 4.2 and Table 4.3). All the measured capacitors have been subjected to the same electrical conditioning and, thus, the electrical situation of all films is comparable. Apart from the differences of the polarization values of the films prepared from solutions with and without Bi excess, already discussed, it is clear that the increase of the crystallization temperature, which in both cases produces films with larger and better crystallized grains, leads to an increase of the polarization values and of the remanence of the films, accompanied by a strong decrease of the coercive fields.

4.1.2 Leakage currents.

The study of the leakage currents in bismuth ferrite thin films is very important to evaluate their possible integration in microelectronic devices. The electrical current density vs. voltage (J-V) curves are obtained from the fitting of the J-E hysteresis loops

of Figures 4.3 and 4.5, as explained in the experimental procedure of Chapter II, and they are presented in Figures 4.8 and 4.9, for the films prepared from solutions without and with Bi excess, respectively. It must be noted that these curves are not derived from typical measurements under D.C. conditions, due to the difficulty due to the difficulty of performing these measurements in thin films with high leakage currents. As a result, the values of the currents obtained here cannot be analyzed quantitatively; they are not steady current curves.

In order to consider the possible correlations between the current behaviour and ferroelectric switching, the current density, J, is plotted vs. the ratio between the voltage and the coercive voltage, V/V_c (Figure 4.8 and 4.9), for all films. It is known that the ferroelectric polarization has an important effect on the lowering of the Schottky barrier [7], and thus conductivity may be affected by the polarization switching at V_c. The possible differences among curves, due to different V_c in the films, are eliminated in this representation. As we have observed in Figures 4.3 and 4.5, there may be some asymmetry of the coercive voltages for each loop branch (positive and negative). This creates also differences in the subsequent changes of the polarization states at the interfaces, which must be taken into account. Therefore, the value of the corresponding coercive field for each branch is used.

In the J-V curves for the BF400 film (Figure 4.8 a), we observe an ohmic response for all voltages, which can be seen more clearly in the inset, where a linear, instead of a log scale, is used for J. This linear behavior, as pointed out by Scott [8], can be related to the Simmons modified Schottky currents, which present a linear dependence with the field at the so-called low field region of the J-V dependencies. The J-V curves of the film crystallized at 450ºC (BF450) (figure 4.8 b) follow the same trends observed in the film crystallized at 400ºC, differing only in a small slope change at 250K observed at higher

voltages in the positive branch. For the film crystallized at 500ºC (BF500) (figure 4.8 c), although a similar behavior is observed, some differences are noticed. The slope change at 200K is more evident in this film, which indicates that, as the crystallization temperature increases, the non-linearities appear at lower voltages.

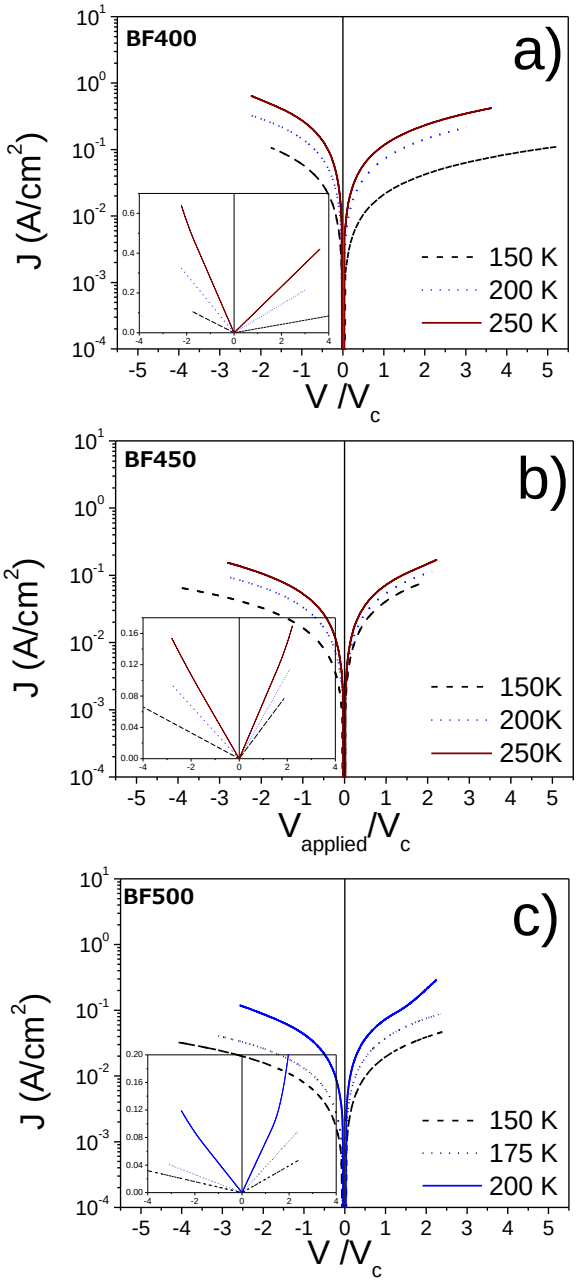

Figure 4.8: *J-V curves for the films prepared from solutions without Bi excess crystallized at different temperatures: a) BF400. b) BF450. c) BF500.*

For the films prepared from solutions with Bi excess, it can be observed that the J-V curves are linear up to 250K for BF400xs (Figure 4.9a). At 300K, the response is non-linear only in the negative branch for all the voltages applied. The BF450xs film (Figure 4.9 b) presents ohmic behavior without any evident change below 250K. At 250 K, a sharp slope change in the J-E curve occurs for voltages 1.5 times the coercive voltage, showing a non-linear behavior for voltages above it. This non-linearity dominates the leakage currents for most voltages at 300K. In the negative branch the threshold voltage is close to 0.5·V_c, while the positive branch shows non-linear behavior for all voltages. This asymmetry is similar to the one found for the curve of BF400xs film at 300 K. The BF500xs film shows non-linear behavior even at 150K (Figure 4.9c) for voltages larger than twice the coercive voltage. For successive increases of the temperature, the voltage at which non-linearities appear decreases progressively: below twice V_c for 175 K, around V_c for 200K, and 0.7 times V_c for 250 K.

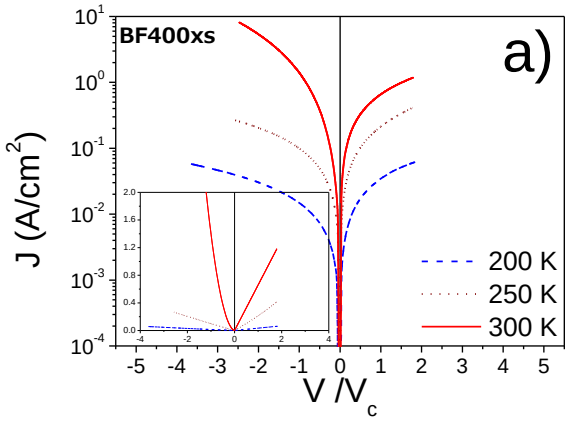

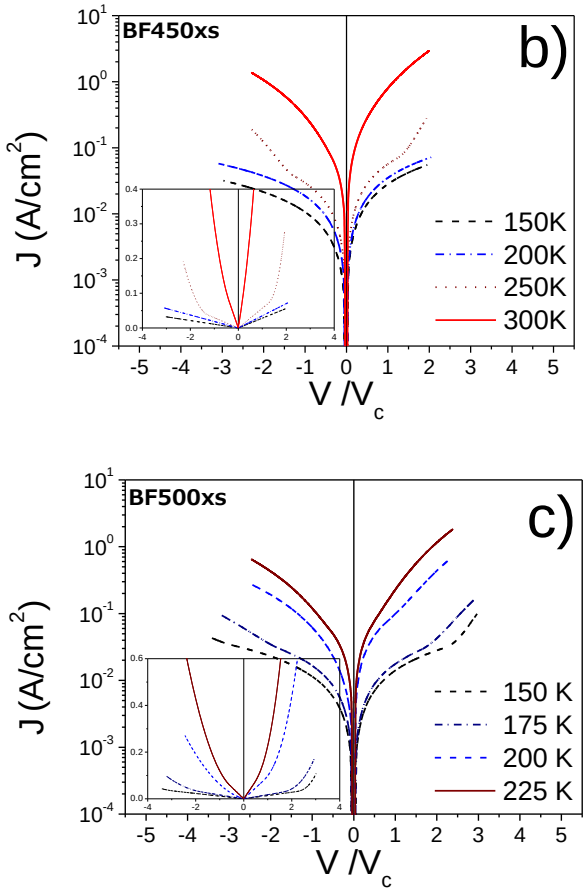

Figure 4.9: *J-V curves for the films prepared from solutions with Bi excess and crystallized at different temperatures: a) BF400xs, b) BF450xs and c) BF500xs.*

The occurrence of non-linear leakage contributions in a short time interval (as it corresponds to the frequency at which the hysteresis loops are measured) must be associated to the appearance of electrical degradation mechanisms in the material. Below a threshold voltage V_0, conduction varies linearly with the voltage, but above it other phenomena produce significant non-linear contributions to the current response. The transition region (characterized by a sharp current increase) can be attributed to a reversible breakdown of one of the Schottky barriers, and thus the introduction of new charge transport mechanisms [9]. The appearance of non-linear leakage currents (and the mechanisms that lead to them) occurs at lower voltages the higher the measurement

temperature used, as it can be seen clearly in BF500xs (Figure 4.9 c). The evolution of the leakage currents with the temperature can be related to a Simmons modified Schottky mechanism [8]. This appears when the charge injection from electrodes is controlled by the interface properties while the carrier transport through the bulk of the film is limited by the slow mobility of carriers. On increasing the measuring temperature there is an increase in the switched ferroelectric polarization and a reorganization of the point defects due to the depinning of the ferroelectric domains, that favours the bulk carriers mobility, increasing the overall conductivity and promoting the appearance of non-linear contributions at lower voltages, as observed.

The results show that non-linearities are rarely observed in the BF films prepared from solutions without any excess, and only when the processing temperature goes up to 500ºC. The crystallization temperature of the films has a strong effect on the occurrence of non-linear behavior. The measurement temperature at which the first non-linearities are observed is lower for the films processed at higher temperatures; in BF400xs appear at 275K, in BF450xs at 250K and at 150K to BF500xs.

The appearance of non-linear leakage currents has been reported before for $BiFeO_3$ films [10-12] but their evolution with the temperature has not been analyzed. The effect of the leakage currents can be large and occurs near to the limit at which irreversible degradation occurs in the sample. Therefore, in table 4.4 we collect both the temperatures at which non-linear currents appear and the temperatures of the dielectric breakdown of the BF films. Non-linear leakage currents become significant for even lower measuring temperatures as the films are crystallized at higher temperatures. Dielectric breakdown also happens at lower temperatures for those same films. We have already discussed that the large grain size and low porosity achieved in these films lead to an increase of the polarization. The activation of the non-linear conduction

mechanisms when the electric field increases, in the so called transition region, is related to the breakdown of one of the Schottky barriers. The height of this barrier decreases with the polarization of the film. The films crystallized at 400ºC and 450ºC have lower polarizations and, therefore, the barrier is not broken easily, and the non-linear currents only appear for the highest temperatures (above 250K). Unlike them, the films crystallized at 500ºC, with large grains and large polarizations, show non-linear conductivity behavior at temperatures as low as 150K. Similarly, we discuss the films prepared from solutions without Bi excess, which present lower values of the polarization and, in principle, more defects, as discussed before. This situation does not favor the easy breakdown of the Schottky barrier, and therefore, the appearance of non-linear currents is very limited and only significant for the highest temperature of the film crystallized at 500ºC.

Table 4.4. *Temperatures at which the non-lineal leakage currents appear and temperatures of the dielectric breakdown of the bismuth ferrite films.*

$BiFeO_3$ thin films		Results from the loop fittings at 200 K and 1 kHz	
Precursor solution	Crystallization temperature	Temperature of appearance of non-linear currents (K)	Temperature of dielectric breakdown (K)
No Bi(III) excess	400°C	Higher than 250	275
	450°C	Higher than 250	275
	500°C	200	225
5mol% Bi(III) excess	400°C	275	Not present (until 300 K)
	450°	250	Not present (until 300 K)
	500°C	150	250

The temperatures at which the dielectric breakdown takes place follow a similar trend to those of the appearance of non-linear currents (Table 4.4). It is observed that the dielectric breakdown occurs at lower temperatures for the films that contain more

defects: those prepared at the highest crystallization temperatures and from precursor solutions without any excess. In the latter case, the current is not limited by the bulk, which may form current paths along less crystallized regions, and dielectric breakdown occurs without the previous development of extensive nonlinear currents. The connectivity is related to the crystallization temperature and, while for the films crystallized at 400ºC, apparently large grains are surrounded by a fine grained phase (connectivity 0–3), this evolves to an increased crystallinity and a connectivity 1-3 in the films crystallized at 450ºC. This heterogeneous phase distribution points out to the development of current channels [13], leading to dielectric breakdown at lower temperature in these films. The improvement of the crystallinity in the films prepared from solutions with Bi excess limits the effects of this connectivity. The hysteresis current loops of the film crystallized at 400ºC from a solution without any excess show less defined switching maxima than the same film from a solution with Bi excess (Figure 4.3 a and Figure 4.5 a). The shape of these maxima, together with the high coercive fields, indicates a worse connectivity of the ferroelectric phase for the films prepared without Bi excess. As the thickness of all films is quite similar, the connectivity of the ferroelectric phase must be related to the relative amount of well crystallized phase in the films. The addition of a volatile element for the preparation of ferroelectric thin films like $PbTiO_3$, also results in the improvement of their properties when crystallized at low temperatures [14]. It is assumed that the crystals form a core–shell structure with a less crystalline/amorphous phase in the shell, which will be thicker if the disappearance of the volatile element (Bi of Pb) is not compensated by the addition of an excess in the precursor solution.

4.2 Ca^{2+} doped $BiFeO_3$ thin films.

In the previous section we have shown that BF films have large leakage currents that make difficult its integration in devices. We have proved that the large polarization values obtained in these films (up to 60 $\mu C \cdot cm^{-2}$) contributes to the low working temperatures at which these non-linear leakage currents are significant. Besides, for the preparation of a successful multilayer composite, as those with lead containing layers [15] it seems necessary to have a saturation polarization in BF films similar to that of BNBT (12 $\mu C \cdot cm^{-2}$). Therefore, we need to find BF based thin films with lower polarization values. This can be achieved through doping [3].

Doping BF films with 3 and 5 % of Ca and crystallized a 500 ^0C produce single phase films, according to the X ray diffraction data shown in figure 4.10. The crystalline perovskite phase (rhombohedral R3c crystal structure, JCPDS-ICDD 86-1518 file) is detected for two doped films without any visible secondary phase.

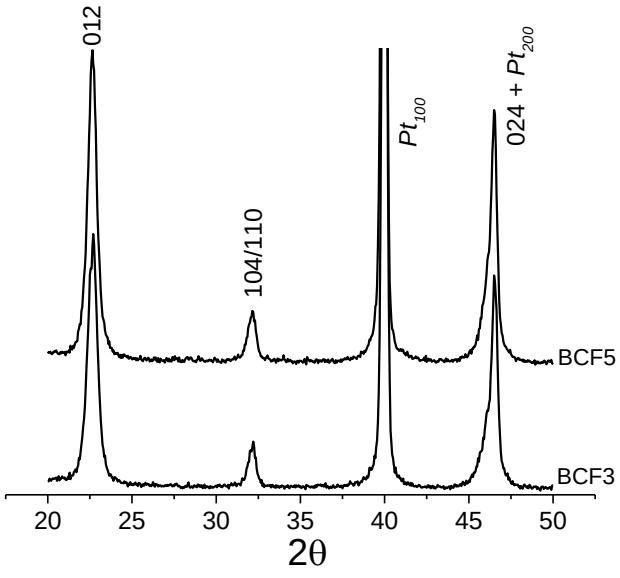

Figure 4.10: *X-Ray diffraction patterns of BF films crystallized at 500 ^0C doped with 3 and 5 % of Ca^{2+}.*

In the microstructure it is possible to observe very small grain that form agglomerates, which make very difficult to calculate the grain size in these films doped with Ca (figure 4.11). The size of this small grain is 22 nm approximately while that in the well-defined grain of BF500xs the size is about 100 nm. This effect of the decreasing grains size with the Ca doping, and the influence in the ferroelectric properties, had been studied previously in the perovskite of lead titanate $PbTiO_3$ [16,17]and has been attributed to the high melting temperature of the Ca in comparison to the volatile elements Pb and Bi present in these films. Another difference of doped BF films with respect to the pure ones is that they present higher porosity caused by the abrupt release of the volatiles elements of the thin films, which indicate that it is necessary to optimize the preparation process in order to improve the microstructure (figure 4.11). However the more significant effect is the strong decrease in the grain size that can be reflected in ferroelectric properties.

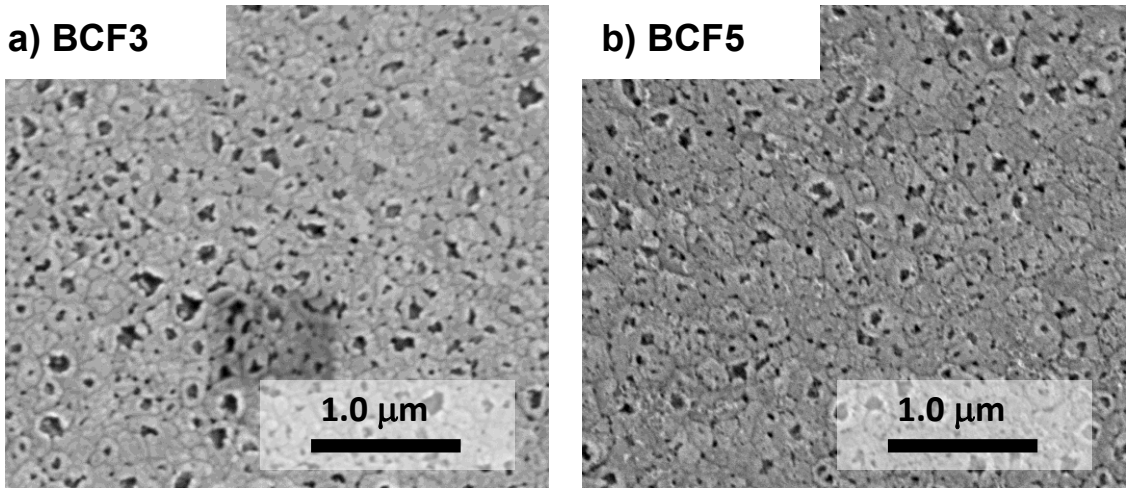

Figure 4.11: *SEM micrographs of the surface of Ca doped BF films, a) BF3 and b) BF5.*

In figure 4.12 the J-E hysteresis loops measured at different temperatures for Ca doped BF films are shown. The corresponding P-E hysteresis loops at 200 K are also shown. We observe that BCF3 film has larger remnant polarization than BCF5 film, but much lower than those of pure BF films. For the BCF3 film, the remnant polarization is P_r*=19.8 μC·cm*$^{-2}$ *and* P_r*=16.5 μC·cm*$^{-2}$ *for BCF5, similar to those of the BNBT layers reported in chapter III. As a consequence, the dielectric breakdown in both films takes place at higher temperatures than in the pure BF films (figure 4.5c). Besides, the leakage currents obtained for the doped BF films are lower than those for the undopel films. We can conclude that Ca doping produces the BF based films we are looking for.*

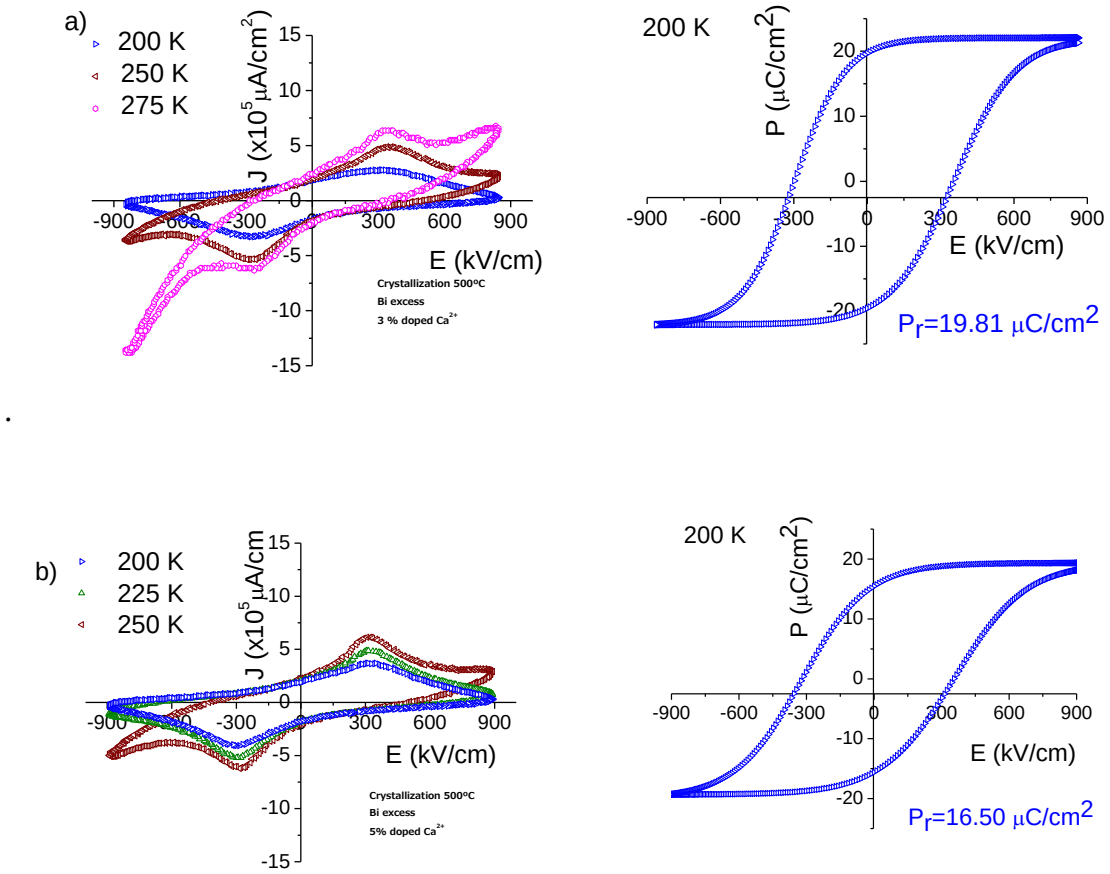

Figure 4.12: *J-E hysteresis loops measured at different temperatures and the corresponding P-E hysteresis loop at 200 K for doped BF films:, a) BCF3, b) BCF5.*

The incorporation of Ca in the crystalline structure of $BiFeO_3$ results in a decrease of the number of oxygen vacancies, which are mostly responsible for the conductivity of these crystals [10]. The decrease of the remnant values of the polarization in Ca doped BF films can be attributed to the replacement of Bi in the perovskite structure, which is the origin of the higher polarization in these crystals and the grain size effect present in this films [3].

Figure 4.13 shows the J-E curves measured using a DC field for a pure BF film, BF500xs, and for the two Ca doped films, BCF3 and BCF5. It must be noted that the large leakage current values of pure BF films makes this type of measurements very difficult without provoking irreversible degradation, as it can be seen in the abrupt change of values of Figure 4.13a for the BF500xs film, after the initial application of large electric fields.

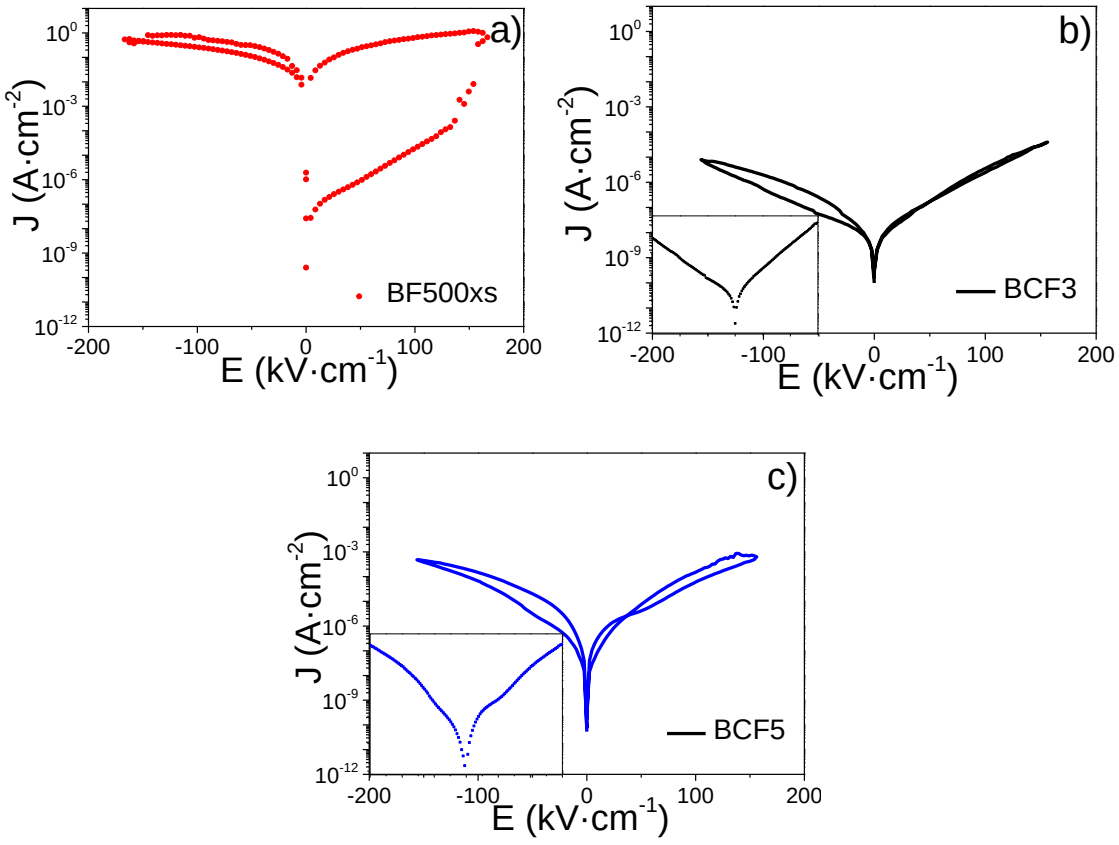

Figure 4.13: *J-E curves for BF500xs, BCF3 and BCF5 films.*

Ca doping reduces the film conductivity (compare the current density values) and prevents the irreversible degradation at high electric fields. The lowest value of current is achieved for the BCF3 film, besides, in this film it is not possible to distinguish the slope change in the J-E loops, as observed in BCF5(see inset Figure 4.13 b and c, where the low electric field region has been magnified in the J-E loops), which is related with the presence of the leakage currents. These characteristics make BCF3 films the best candidate for its integration in devices working at room temperature and also as a component with BNBT for multilayer composite films, as it will be shown in the next chapter.

The behavior of the Ca doped BF films is also in agreement with the Simmons modified Schottky mechanism. The decrease on the vacancy number and grain size, due to the introduction of the Ca in the structure in the bismuth site, decreases the leakage current in both doped samples with respect to the BF500xs. Besides, these samples do not have the problem of the irreversible dielectric breakdown that appears in the BF500xs (see figure 4.12), which indicates that the height of Schottky barrier decreases with the introduction of Ca as dopant in the bismuth ferrite perovskite due to the presence of less charge carrier and conductivity paths. Therefore, it is possible to obtain thin films with less conductivity problem, more suitable for integrating in microelectronic devices.

4.3 Conclusions on the behavior of BF films.

From the results shown in this chapter we have obtained a complete picture of the electrical behavior of $BiFeO_3$ films, which allows us to draw conclusions on the large influence of the processing parameters on the polarization and conductivity characteristics of these films.

1. *The use of Bi excess in the BF thin films produce lower amount of defects in the microstructures and larger polarization. In addition, these films with excess despite not having high leakage current values, present dielectric breakdown for lower temperature than the films with Bi excess. This indicates that the leakages current are not necessarily directly related with the dielectric breakdown.*
2. *When low crystallization temperatures are used, the thin films have inhomogeneous grain size with possible core-shell structures, which yields lower polarization values for films (with and without Bi excess) crystallized at low temperature. Therefore the higher polarization values have been obtained for the film crystallized at 500 ºC, in particular BF500xs.*
3. *The films with higher polarization values still present some problems, such as high leakage currents, degradation of the dielectric properties in the sample and dielectric breakdown at low temperature. These problems have been improved by doping the BF thin films with Ca. The substitution of Bi with 3% of Ca in the structure of the BF film apparently decreases the vacancy number and improve the leakage current problem, decreases the possible presence of the resistivity degradation and increases the temperature where the dielectric breakdown appears.*

BF films have a large number of possible applications; however, it is limited mainly because of the appearance of large non-linear leakage currents, together with a dielectric breakdown at low temperatures. Despite in this chapter we have been able to improve these problems, we still are not able to switch the polarization at room temperature in most of the samples. In addition these high conductivity values prevent the possible use of the enhanced latent ferromagnetism found in these BF thin films [18]

combined with the ferroelectric properties at room temperature, with the aim of achieve their integration in multifunctional devices.

In chapter 5 we will discuss the integration of these promising lead free films in composites in order to circumvent any of these problems, and, thus, to take full advantage of their multiferroic properties.

4.4 References.

[1] S.M. Selbach, M.A. Einarsrud, T. Grande, Chem. Mater. 21, 169, (2009).

[2] C. de Dobbelaere, M.L. Calzada, R. Jiménez, J. Ricote, I. Bretos, J. Mullens, A. Hardy, M. van Bael, J. Am. Chem. Soc. 133, 12922,(2011).

[3] G. Catalan, J. F. Scott, Adv. Mater., 21, 2463–2485, (2009).

[4] R. Jiménez, C. Alemany, M.L. Calzada, A. González, J. Ricote, J. Mendiola, Appl. Phys. A: Mater. Sci. Process. 75, 607, (2002).

[5] J. Rödel, W. Jo, K. T. P. Seifert, E.M. Anton, T. Granzow, J. Am. Ceram. Soc. 92 1153–1177,(2009).

[6] A. Perez-Rivero, M. Tomczyk, R .Jiménez, I. Bretos, J. Ricote, P.M. Vilarinho and M.L. Calzada. J. Mater. Sci.: Mater. Electron. DOI 10.1007/s10854-015-3150-9, (2015).

[7] I. Pintillie, I. Vrejoiu, D. Hesse, G. Le Rhun, M. Alexe, Phys. Rev. B,75, 104103, (2007).

[8] J.F. Scott, J. Phys. Condens. Matter, 26, 142202, (2014).

[9] A. Sigov, Y. Podgorny, V. Vorotilov, A. Vishnevskiy, Phase Trans. 86, 1141, (2013).

[10] M. Alexe, C. Harnagea, D. Hesse, U. Gossele, Appl. Phys. Lett. 75, 1793, (1999).

[11] G.W. Pabst, L.W. Martin, Y.H. Chu, R. Ramesh, Appl. Phys. Lett. 90, 072902, (2007).

[12] I. Bretos, R. Jiménez, C. Gutiérrez-Lazaro, I. Montero, M.L. Calzada, Appl. Phys. Lett. 104, 092905, (2014).

[13] L. Pardo, J. Mendiola, C. Alemany, J. Appl. Phys. 84, 5082, (1988).

[14] C. de Dobbelaere, M.L. Calzada, R. Jiménez, J. Ricote, I. Bretos, J. Mullens, A. Hardy, M. van Bael, J. Am. Chem. Soc. 133, 12922, (2011).

[15] H. El Hosiny Ali, R. Jiménez, J. Ricote, J. Pérez de la Cruz, J.R.A. Fernandes, M.L. Calzada, Thin Solid Films 520, 7205-7211, (2012).

[16] R. Jimenez , I. Bretos, J. Ricote, C. Alemany, M.L. Calzada, J. Mendiola , J. Euro. Ceram. Soc. 25 ,2319–2323 , (2005).

[17] I. Bretos, J. Ricote, R. Jimenez, L. Pardo, M.L. Calzada, Appl. Phys. A 89, 967–973, (2007).

[18] C. Gutiérrez-Lázaro, I. Bretos, R. Jimenez, J. Ricote, H. El Hosiny, D.Pérez-Mezcua, R. J. Jiménez Rioboo, M. García-Hernández, and M. L. Calzada, J. Am. Ceram. Soc. 96, 3061,(2013).

CHAPTER-V

MULTILAYER COMPOSITE FILMS

WITH IMPROVED FUNCTIONAL BEHAVIOUR

In order to improve the properties of lead-free, BNBT based films, whose drawbacks were studied in Chapter III, we analyze in this chapter the combination of layers of this material with those of a ferroelectric with large polarization values, $BiFeO_3$, in a 2-2 biphasic multilayer composite film. We look for a lead-free composition and one of the best candidates is bismuth ferrite (BF), as it has been explained before. In thin film form, it presents enhanced polarization and magnetization values as it has been established in chapter-IV, although the low film resistivity is a problem to access this polarization values at room temperature. This can be solved by the application of an electric conditioning treatment [1], and, thus, BF layers show P_r~60 $\mu C/cm^2$ at room temperature. These values make them excellent candidates to be used in a multilayer configuration to induce polarization in the adjacent BNBT layers. Moreover, we can also take advantage of the good ferroelectric and magnetization values of the BF layers for multiferroic applications in the proposed 2-2 biphasic multilayer composites, as the BNBT may act as a point defect buffer for the BF, reducing their leakage currents. Different configurations of multilayer composite films (MLC) were studied in this work. Ferroelectric and magnetic properties of these multilayer composite films are analyzed in this chapter, the mechanisms for the enhancement of the effective remnant polarization and the magnetic properties of the multilayer composite films are discussed.

5.1 Configurations and microstructures of the multilayer composite films.

In this thesis a variety of multilayer composite films were prepared. In all cases we have used thin layers of BNBT and BF, previously studied in Chapters III and IV. In the case

of the BNBT the composition close to the MPB: BNBT5.5 (see Chapter III) due to the fact that it presents the best ferroelectric properties among the films studied. The BF films used in the multilayer composite films are BF500xs (see Chapter IV), prepared under the most appropriate processing conditions to obtain the most adequate properties. We will prepare also MLC films using layers of 3% Ca^{2+} doped BF (BCF), which allows modulating the polarization of BF and make it closer to that of BNBT.

Four different configurations were used in this study: two bilayers and two trilayers as shown in Figure 5.1. As it can be seen in the figure, only the configuration BF/BNBT/BF can induce an internal field in the BNBT layer. Table 5.1 summarizes the multilayer composite films studied in this chapter.

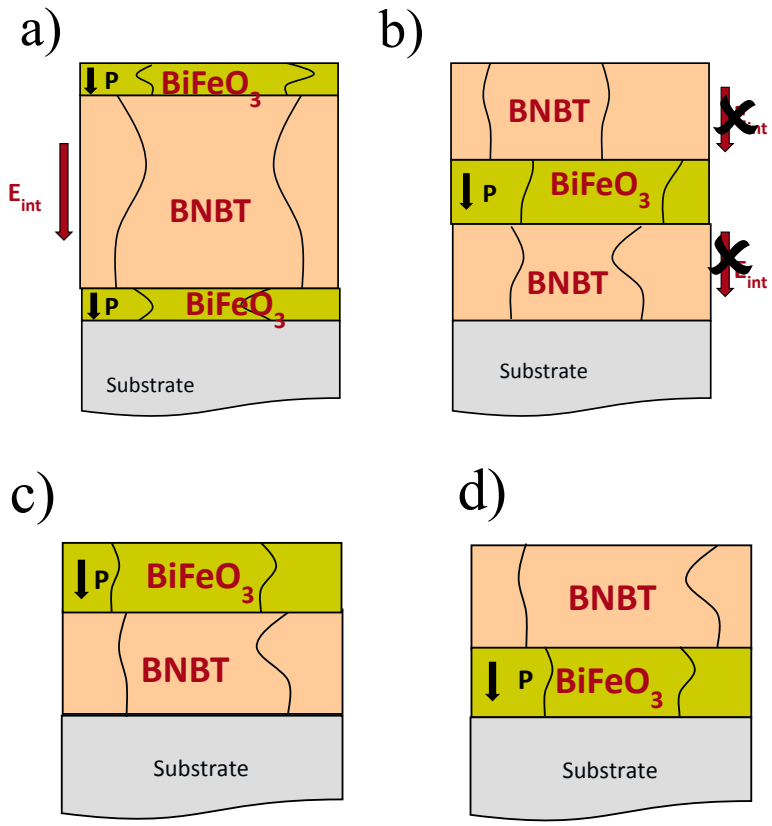

Figure 5.1: *Multilayer composite film configurations studied in this thesis, a) MLC-BNBT, b) MLC-BF, (with either pure or Ca doped layers, c) Bilayer- BF/BNBT and d) Bilayer-BNBT/BF.*

Table 5.1: *Nomenclature used for the MLC films.*

	Layer configuration	*FILM NAME*
Bilayer	*BF/BNBT*	*BF/BNBT*
	BNBT/BF	*BNBT/BF*
Trilayer	*BF/BNBT/BF*	*MLC-BNBT*
	BNBT/BF/BNBT	*MLC-BF*
	BCF/BNBT/BCF	*MLC2-BNBT*
	BNBT/BCF/BNBT	*MLC2-BF*

5.1.1 Phases control and microstructural characteristics.

The study of the phases present in the multilayer composite films has been performed by X-ray diffraction. The patterns show that no significant interdiffusion among the layers occurs as separate peaks coming from the different layers are observed. In a 2θ range about 32^0 coexist the strongest diffraction peaks of the BNBT and BF phases, and convolution of peaks can be studied.

In Figure 5.2 we show the X-ray diffraction patterns of both bilayer composite films, together with those of single phase BNBT and BF films for the sake of comparison. It must be noted that the MPB $(Bi_{0.5}Na_{0.5})_{0.945}Ba_{0.055}TiO_3$ phase contains both rhombohedral and tetragonal crystalline phases [2], but for simplicity we have indexed the reflections corresponding to BNBT on the basis of a pseudocubic (p) unit cell, instead. Regarding the diffraction peaks coming from the BF layers, we observe a small shift of the position of the 104 peak, which, according to the deconvolution carried out (using pseudo-Voigt functions; Figures 5.2b and c)) goes from 31.8^0 for BF/BNBT to

32.0^0. The other two peaks analyzed (110-BF and 110$_p$-BNBT) show the same position for both bilayers.

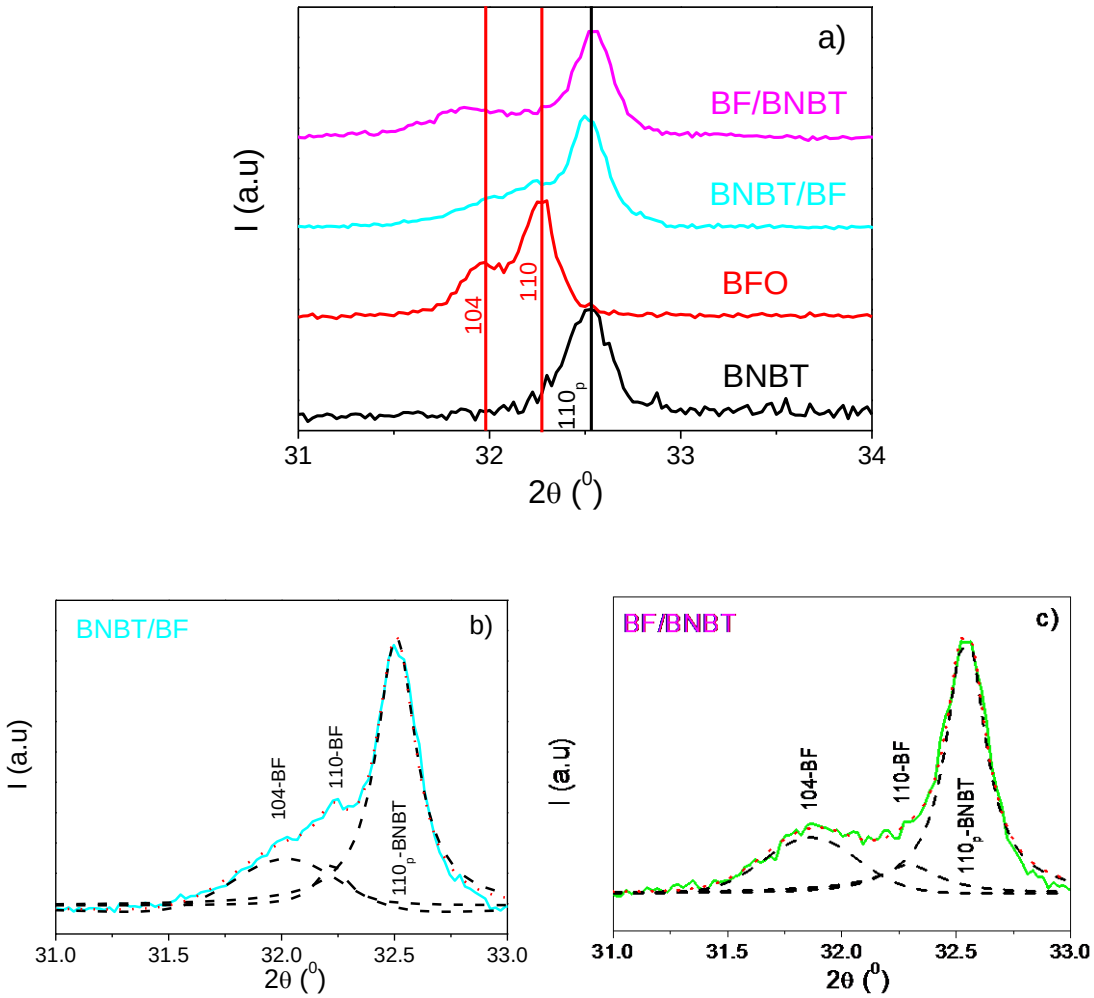

Figure 5.2: *(a) X-ray diffraction patterns about 2θ = 32^0 for the single phase $BiFeO_3$ and BNBT films compared with the bilayer composite films BNBT/BF and BF/BNBT. (b) and (c) show the deconvolution of diffraction peaks for both bilayers. Solid lines correspond to experimental data and dashed lines to the fitting curves.*

Similarly, Figure 5.3 shows the X ray diffraction patterns of trilayer composite films (MLC-BNBT and MLC-BF), compared with the BNBT and BF single phase films. It can be observed that both multilayer composites contain as well the desired crystalline phases: MPB $(Bi_{0.5}Na_{0.5})_{0.945}$-$Ba_{0.055}TiO_3$ and $BiFeO_3$. Only a small peak associated to a

secondary phase appears in the X-ray diffraction patterns, which is also present in the single phase BF films. It is close to $2\theta \sim 29.9^0$, and it can be associated to the iron-rich $Bi_2Fe_4O_9$ secondary phase [3]. The fact that only crystalline phases coming from the individual layers are present indicates again that no significant interdiffusion between the alternating BNBT and BF layers is produced, which shows the high quality of the multilayer composite films prepared. As the diffraction peaks of these two phases are too close, details of the diffraction patterns are shown in Figures 5.3(b) and 5.3(c): experimental data (solid lines) with their corresponding deconvolution into the diffraction peaks from the BNBT and BF layers (dashed lines). Deconvolution of the experimental diffraction peaks was carried out by using also two pseudo-Voigt functions. In the case of the peak situated at $2\theta \sim 32.5^0$, it can be seen that the contribution of the 110_p reflection corresponding to BNBT is significantly larger than those coming from the BF layers. This can be related to the fact that there is some preferential crystallographic orientation in this film, when the BNBT layer is grown on a BF layer.

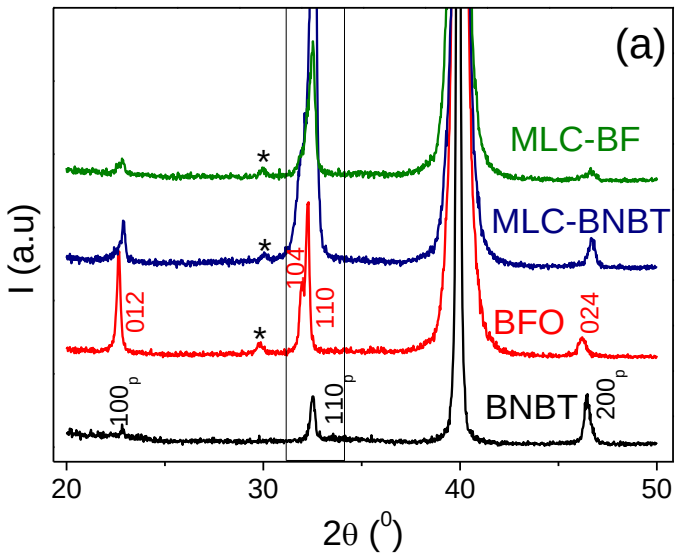

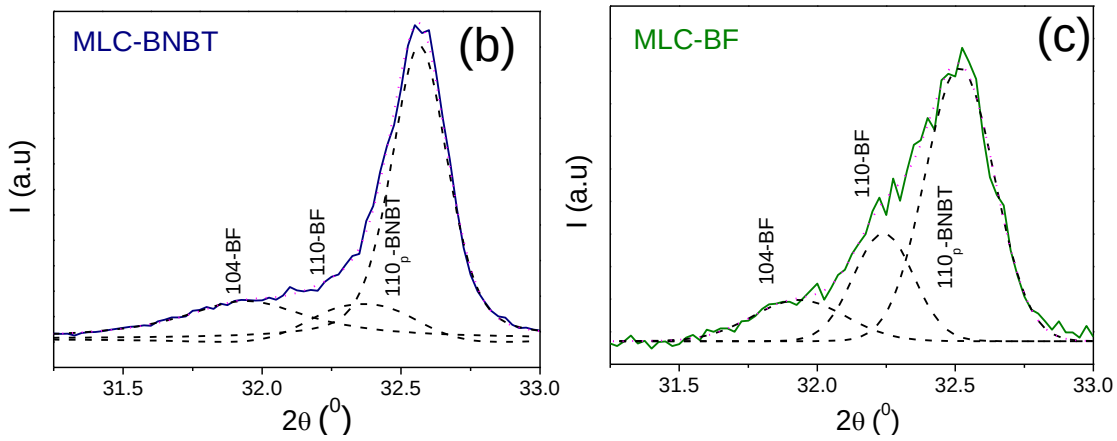

Figure 5.3: *(a) X-ray diffraction patterns of the single phase $BiFeO_3$ and BNBT films compared with the multilayer composite films MLC-BNBT and MLC-BF (*$Bi_2Fe_4O_9$). (b) and (c) show the deconvolution of diffraction peaks for both MLCs.*

In Figure 5.4 we show SEM micrographs of cross sections and top surfaces of the bilayer composite films. From the cross section pictures we can see a columnar-like growth in both of them. Thickness is the same, within the error, for the two bilayers: 415±20 nm for BNBT/BF and 425±20 for BF/BNBT. This is the result of the successive deposition of 6 coatings of BNBT and 3 of BF. From the thickness obtained for single phase films, we calculate that one coating of BNBT produces a layer approximately 60 nm thick, and one coating of BF produces one of 20 nm thick. As we use the same dilution for the precursor solutions and the same processing conditions for both BNBT and BF layers to fabricate the bilayers, this coating thickness are also valid here. The expected final thickness is therefore 420 nm, like the one finally obtained. Therefore, the volume fraction of BNBT is 85 % and that of BF is 15 %. From the number of solution coatings, we can estimate the thickness of the BNBT and BF layers, which are superimposed in the micrographs to show the approximate position of the layer boundaries.

The images of the top surfaces show the microstructural differences of both layers. The top BF layer (Figure 5.4 d) has less porosity than the top BNBT layer (Figure 5.4 c). Besides, the BF layer presents a larger grain size than the BNBT layer.

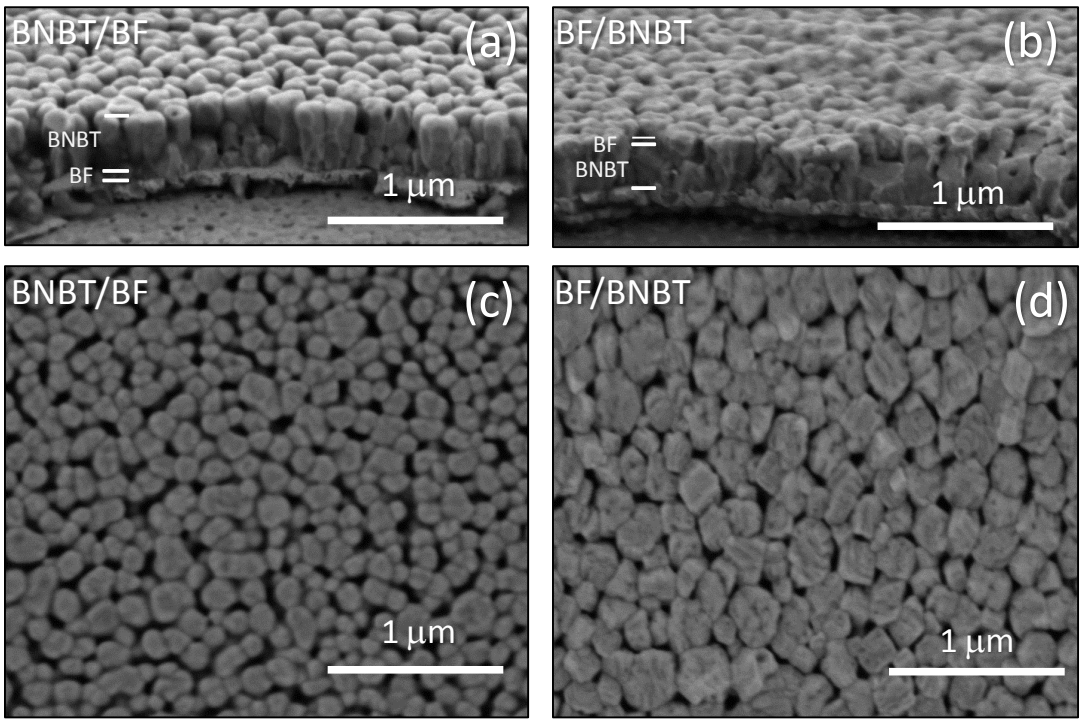

Figure 5.4: *SEM micrographs of: cross sections of (a) BNBT/BF and (b) BF/BNBT films; images of top surfaces of (c) BNBT/BF and (d) BF/BNBT films.*

Similarly, a columnar-like growth was observed in the SEM micrographs of cross sections of multilayer composite films MLC-BNBT and MLC-BF (Figures 5.5a and b). The measured film thickness is very similar: 470±20 nm and 500±20 nm for the MLC-BF and MLC-BNBT, respectively. Again, from the number of solution coatings, we expect a total thickness of 480 nm (6 coatings of BF and 6 coatings of BNBT), which is very close to the thickness obtained, and we can estimate the thickness of the BNBT and BF layers; they are superimposed in the micrographs to show the approximate position of the layer boundaries. Note that MLC-BNBT was obtained with 3 coatings of BF,

followed by 6 coatings of BNBT and other 3 of BF. For MLC-BF, 3 coatings of BNBT were followed by 6 coatings of BF and other 3 of BNBT. In these multilayer composite films the BF layers represent the 25 % of the volume fraction of the multilayer, and BNBT layer the remaining 75 % . It can be seen that there are some observable traces of these boundaries in some regions, which indicates the different microstructure of both types of layers. While BF layers tend to have small pores (see surface image of the top BF layer in the MLC-BNBT film of Figure 5.5(c)), BNBT layers present columns that are more separated, with larger voids between them, as it can be seen in Figure 5.5(d) where the surface of the top BNBT of the MLC-BF film is shown. This is similar to observed in the bilayer composite films (Figure 5.4c and d). Grain size of the on the top BF layer is slightly larger than that of on the top BNBT layer.

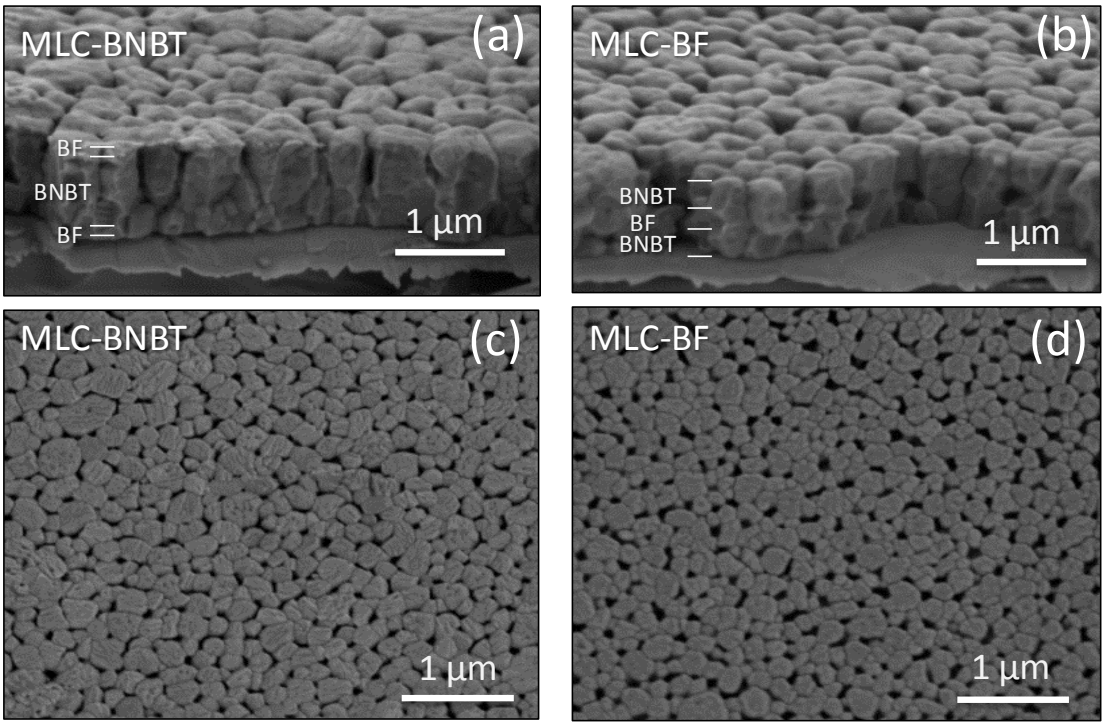

Figure 5.5: *SEM micrographs of cross sections of (a) MLC-BNBT and (b) MLC-BF films; and of top surfaces of (a) MLC-BNBT and (b) MLC-BF films.*

From the structural and microstructural analysis we can conclude that chemical solution methods produce high quality multilayer composite films, without any significant interdifussion among the layers. The layer-by-layer crystallization used leads to a columnar-grain growth. Despite the microstructural differences of the two types of layers used, no large inhomogeneities are observed in the transition from one layer to another in the cross sections, which will facilitate the desired electrical interaction between layers.

5.2 Ferroelectric properties.

5.2.1. Bilayer composite films.

In Figure 5.6 we show the experimental J-E hysteresis loops of bilayer composite films BNBT/BF and BF/BNBT together with their corresponding corrected P-E hysteresis loops. Non-linear leakage currents contribute significantly in the BF/BNBT film as it can be deduced from the shape of its J-E loop, while they are absent in the BNBT/BF film. The fact that the BF was the top layer seems to introduce all the leakage contributions already observed in the single phase BF films, and hinder the polarization in this bilayer (BF/BNBT). When the BNBT acts as a buffer layer in the BNBT/BF film those leakage current contributions disappear. This is an important result, as it shows the role that the BNBT layers play in the multilayer composite films proposed here.

After subtracting all non-ferroelectric contributions, we obtain different polarization values for both bilayers; P_s*=40.7* $\mu C \cdot cm^{-2}$ *and* P_r*=20.7* $\mu C \cdot cm^{-2}$ *for BNBT/BF, and* P_s*=25.2* $\mu C \cdot cm^{-2}$ *and* P_r*=10.9* $\mu C \cdot cm^{-2}$ *for BF/BNBT.*

We can calculate the expected values for the remnant polarization of the multilayer composites (P_r^{MLC}) from the values of the polarization of the individual layers (P_r^{BNBT} and P_r^{BF}) with the following equation that considers a linear additive effect of properties in the multilayer structure[4]:

$$P_r^{MLC} = V^{BNBT} \cdot P_r^{BNBT} + V^{BF} \cdot P_r^{BF} \qquad (5.1)$$

being V the volume fraction of the phases. In the bilayer composite films, V^{BNBT} = 0.85 and V^{BF} = 0.15. Taking the remnant polarization values for single phase BNBT (P_r^{BNBT} = 12.3 μC·cm^{-2}) and BF films (P_r^{BF} = 61.1 μC·cm^{-2}) [3], we can estimate the expected remnant polarization for the bilayer composite films studied in this work: P_r = 19.3 μC·cm^{-2}, which is closer to the value obtained for BNBT/BF, but far from the polarization values of BF/BNBT. This simple equation is valid for high enough applied field and can be considered as a maximum expected value for the remnant polarization in the composite if the properties of the single phases are preserved. Note that from the calculations using equation (1) an error in the estimation of the volume fraction of the layers of 10% produces a variation in the remnant polarization of ± 2 μC·cm^{-2}, which is lower than the observed change. Therefore, some other effect determines the polarization in these bilayer composite films that must be identified.

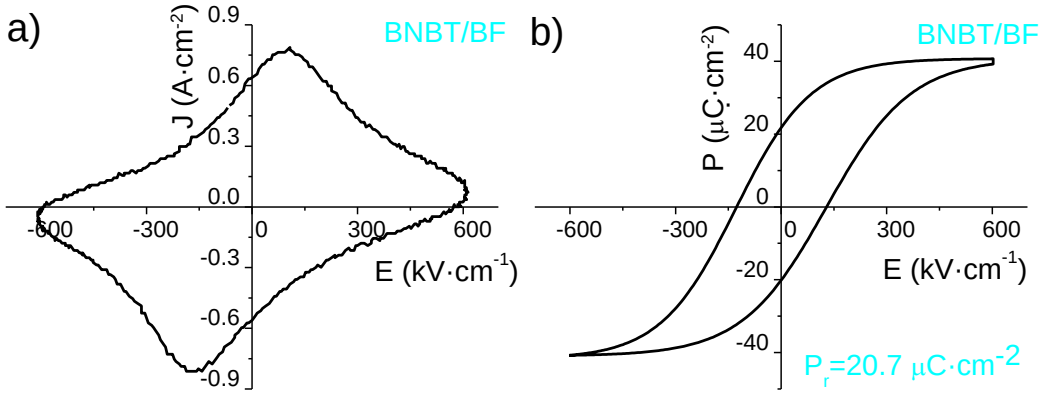

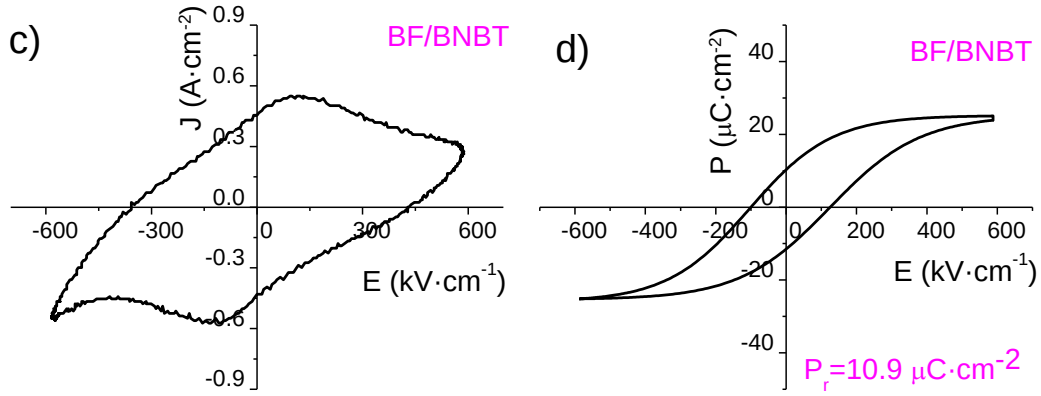

Figure 5.6: *Experimental J-E and corrected P-E hysteresis loops at room temperature of (a, b) BNBT/BF and (c, d) BF/BNBT.*

The remnant loops (see Chapter II- 2.3.2, for a description) also show this difference in the polarization of both bilayers measured 1s after the application of a poling pulse: P_r=11.9 µC·cm^{-2} for BNBT/BF (Figure 5.7a) and P_r=4.0 µC·cm^{-2} for BF/BNBT (Figure 5.7b). These values are below those obtained for the P-E loops of Figure 5.6. This is the consequence of a large relaxation of the polarization in this very short period of time (1 s). This behavior is typical of relaxor ferroelectric materials. As it has been shown in Chapter III, the same behavior appears for BNBT thin films, so this layer is responsible for the quick relaxation of the polarization observed in these bilayers.

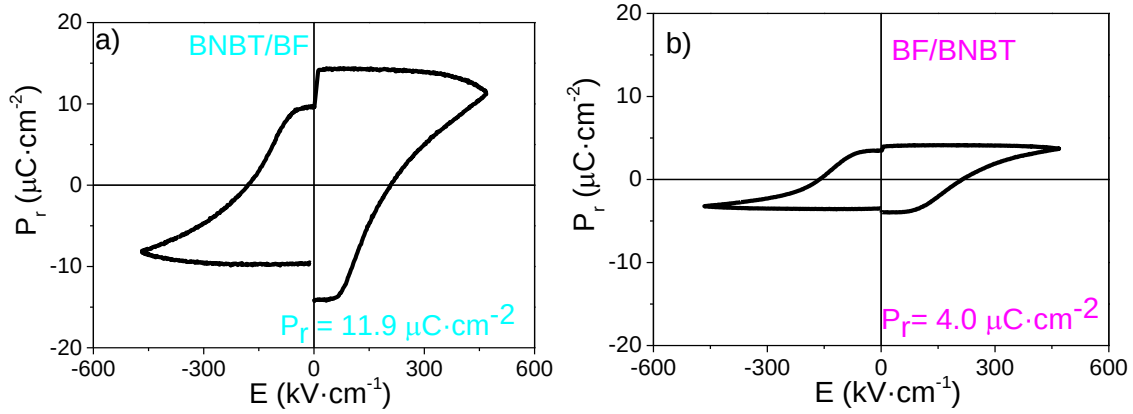

Figure 5.7: *Remnant hysteresis loops of bilayer composite films, a) BNBT/BF, b) BF/BNBT.*

In order to evaluate the behavior of the polarization of the two bilayer composite films with time, a study of the polarization retention was performed at room temperature (Figure 5.8). This value is still much lower than that of BNBT/BF after the same time (7.7 μC·cm^{-2}). But in this case the retention of the polarization is much worse, with 45% polarization loss. This indicates again that the polarization behavior of the BNBT/BF bilayer seems to be dominated by the BNBT layer, prone to have more serious retention problems due to its relaxor ferroelectric character.

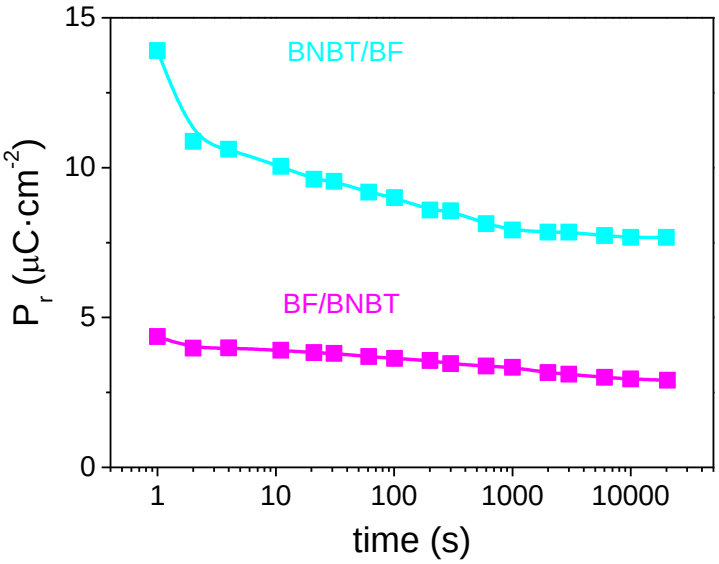

Figure 5.8: *Retention of the polarization for long times of bilayer composite films.*

The presence of the BF layers makes interesting the study of the leakage currents of these bilayers. Figure 5.9 shows the comparison of the J-E curves of BNBT and BF single phase films and the bilayer composite films. Single phase BF film presents values of current density in the range of 10^{-7} to 10^{-5} A/cm^{-2} for small values of the D.C voltage applied. However, when we increase the values of the applied D.C electric field above 140 kV·cm^{-1}, the film suffers a sharp change of its conductivity, already described in chapter IV, with values go up to 0.1-1 A/cm^{-2} (Figure 5.9a). Unlike it, the single phase

BNBT film presents low current values, without any abrupt change at high electric fields, and a linear dependence with the applied field (Figure 5.9b). The bilayer composites have intermediate current density values show a parabolic, non-linear dependence like the BF single phase film, but not any abrupt increase for large electric fields (Figure 5.9c). The combination with BNBT layers seems to prevent the strong resistivity degradation produced by large electric field in the BF films that results in large leakage density currents. The BNBT/BF layer shows lower density current values than BF/BNBT, which is also an indication of the dominance of the BNBT layer (with lower leakage) in the electrical behavior of this bilayer.

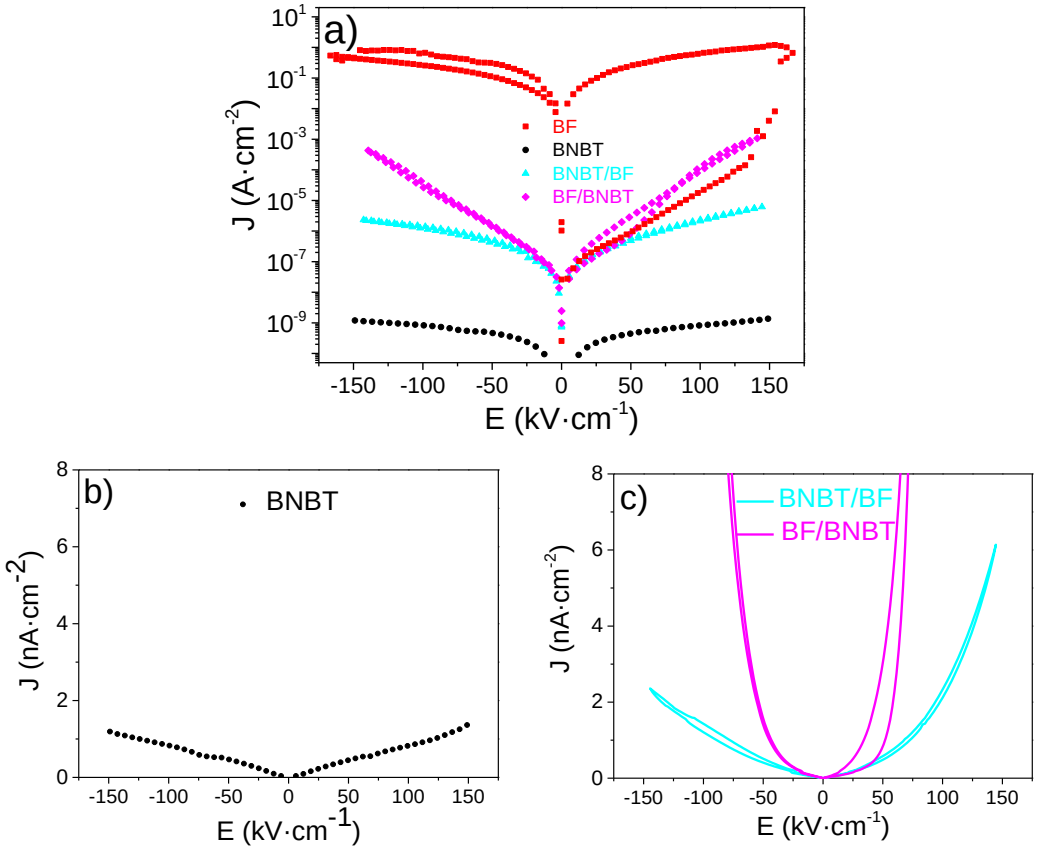

Figure 5.9: *a) J-E curves of the BF and BNBT single phase films compared with those of the bilayer composite films BNBT/BF and BF/BNBT. b) and c) details of the same graph with J in linear scale.*

From the electrical characterization of the bilayer composite films we can conclude that the ordering sequence of the BNBT and BF layers has an impact on the polarization of the multilayer composite film. Not only that, the conductivity is also affected by the fact that the top layer is BNBT or BF. The deposition of a thick BNBT layer on a much thinner BF layer in BNBT/BF makes that decrease the presence of the leakage current and it is possible switching the polarization in the two layers.

5.2.2. Multilayer composite films (MLC).

The behavior of the J-E and corrected P-E hysteresis loops for both multilayer composite films MLC-BNBT and MLC-BF are shown in Figure 5.10, measured at 150K and 300K. In the figures 5.10 a, c show the experimental current vs. electric field hysteresis loops, from which we calculate the P-E loops (Figures 5.10 b, d). It is noticeable that, although it can be seen a small increase with the temperature, leakage currents are strongly suppressed in MLC films in comparison with those reported for the BF500xs single phase film [see Chapter IV]. As it happen with the bilayer composite films, although both MLC films contain the same volume ratio of BNBT and BF phases, the saturation and remnant polarization values differ: MLC-BNBT film show at 300 K, P_s *= 43.6* $\mu C \cdot cm^{-2}$ *and* P_r *= 32.4* $\mu C \cdot cm^{-2}$, P_r/P_s *= 0.7 (Figure 5.9b), while values for MLC-BF film are* P_s *= 40.3* $\mu C \cdot cm^{-2}$ *and* P_r *= 23.5* $\mu C \cdot cm^{-2}$, P_r/P_s *= 0.6 (Figure 5.9d). The remanence is improved respect to that of BNBT single phase film:* P_r/P_s *= 0.5.*

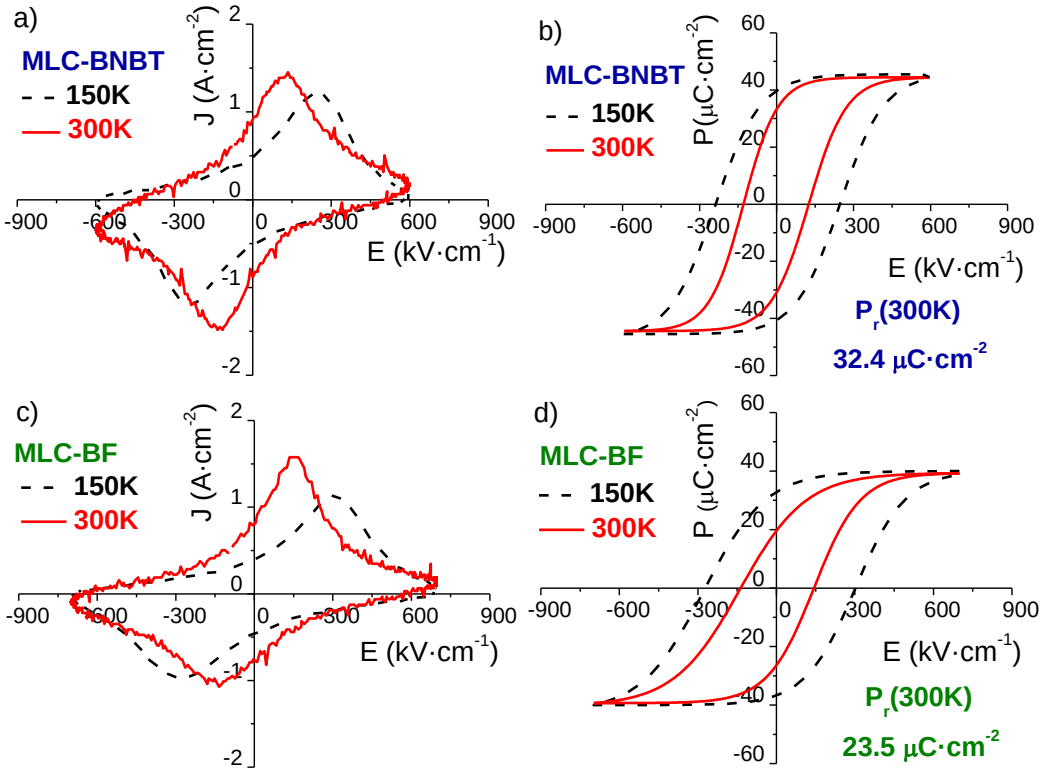

Figure 5.10: *Experimental J-E and corrected P-E hysteresis loops at different temperatures of (a, b) MLC-BNBT and (c, d) MLC-BF.*

The remnant polarization calculated from equation 5.1 for these MLC films is P_r = 24.5 μC·cm^{-2}. From this result we can conclude that in the case of MLC-BF the remnant polarization value obtained (P_r = 23.5 μC·cm^{-2}) corresponds to a simple addition of the properties in the composite film and thus the applied field is large enough to produce the maximum expected remnant polarization. However, the larger value obtained for the MLC-BNBT (P_r = 32.4 μC·cm^{-2}) indicates that other contributions must be considered. The increment of the polarization respect to MLC-BF is of 33%. It should be borne in mind that the difference between the two MLC films is the ordering sequence of the layers and their thickness. In the MLC-BNBT the BNBT layer (380 nm) is sandwiched between two BF layers (60 nm), while in the MLC-BF film the BF layer (120 nm) is between two BNBT layers (175 nm).Thickness may affect the polarization

values of the layers due to a size effect. From the SEM images it can be concluded that the grain size is not much influenced by the different thickness of the layers (Figure 5.5). Therefore, a size effect, although it cannot be discarded completely, it should not be significant.

The behavior at low frequency of single phase BNBT and both MLC films was studied through C-V loops (Figure 5.11). In the three films we observe that the there is a strong difference between the static coercive field obtained from the C-V loops, i.e., at very low frequency (~0.08 Hz) and the coercive field at 1 kHz from the P-E hysteresis loops. In the single phase BNBT film the coercive field decreases 80% approximately when the frequency is reduced, which is similar in both MLC films: 75 %(MLC-BNBT) and 80% (MLC-BF).

A complete study of the variation of the coercive field with the measuring frequency and temperature is shown in Figure 5.12. The values of E_c are obtained from P-E loops measured at different frequencies, and for the value at the lowest frequency we use the value from the C-V loops (Figure 5.11). We can see that, although the BNBT film shows an almost linear dependence with log 1/f, MLC films have a rather abrupt increase of the values of the coercive fields for high frequencies. This dependence of the coercive field with the frequency can be attributed to the depolarization fields resulting from the screening charges that are located in the electrode/ferroelectric interfaces [5]. The differences observed between the single phase BNBT film and the MLC films behaviors must be associated to the different interfaces involved in the latter. Not only the screening charges in the electrode/ferroelectric interfaces play a role, but those in the BNBT/BF interfaces, which at high frequencies, with no time to recombine effectively, generate internal electric fields. Thus, to produce polarization switching larger electric

fields must be applied to counteract these internal fields, and coercive fields show a large increase for high frequencies as shown in Figure 5.11 a.

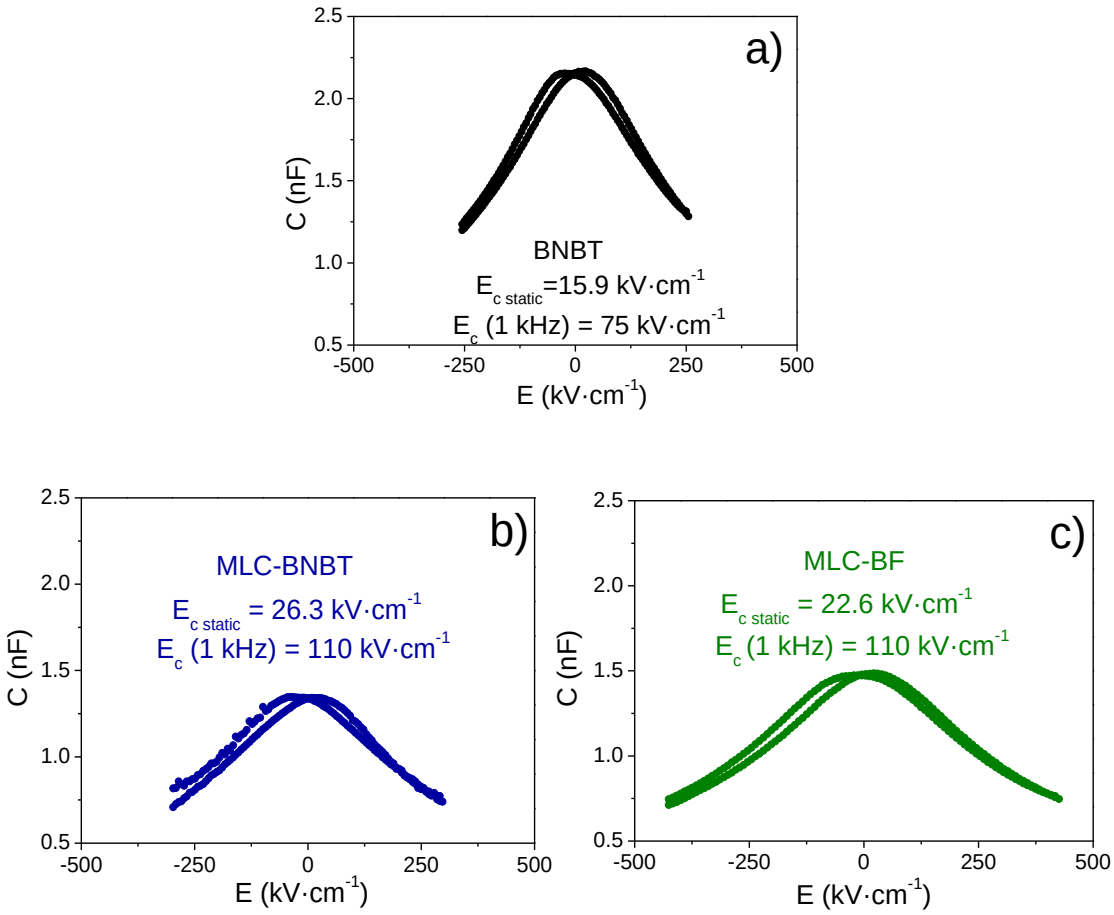

Figure 5.11: *C-V loops of a) single phase BNBT, b) MLC-BNBTand c) MLC-BF films. The values of the coercive fields obtained in these curves ($E_{c\ static}$) is compared with the coercive field measured at 1 kHz*

The coercive field decreases with the increase of the temperature for these films (Figure 5.12 b). As the values of the temperature are larger, the polarization becomes more unstable and therefore the electric field needed to produce its switching decreases. This is more important for relaxor ferroelectric compositions. Figure 5.12 (b) also includes the values calculated considering a bilayer-model film of BNBT and BF layers, which will be discussed later in detail. We can assume that the properties of the BF layers do

not change much in this range of temperatures, as they are far from the $BiFeO_3$ ferroelectric to paraelectric transition temperature (1107 K). The relaxor ferroelectric nature of the BNBT layers mostly accounts for the variations observed. It must be pointed out that there is agreement between the experimental and the calculated values for the coercive fields of the multilayer composite films at 200 and 300 K. But the values measured at 150 K are larger than the calculated ones. This is related to the fact that the BNBT layers in the MLC films suffer an increase of the coercive field at these very low temperatures due to better stabilization of PNRs to produce larger ferroelectric domains. Again, it seems that the BNBT/BF interfaces play an important role in the determination of the coercive fields of the MLC films, and, more generally, in the electrical behavior of multilayer composite films.

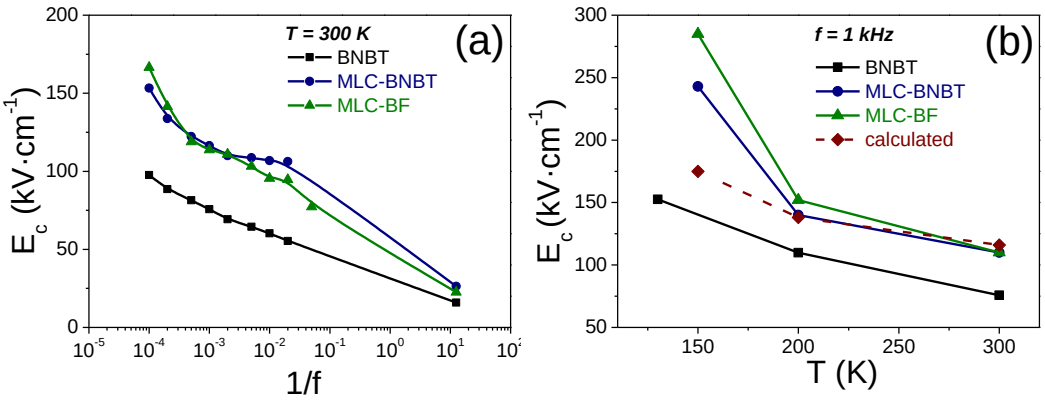

Figure 5.12: *Evolution of the coercive field E_c with the measurement (a) frequency and (b) temperature for single phase BNBT and MLC films.*

The retention of the polarization after 1s of relaxation in both MLCs was studied through remnant hysteresis loops (Figure 5.13). It can be seen that both MLCs present values of P_r below those obtained for the P-E loops of Figure 5.10: P_r=15.8 μC/cm^2 for MLC-BNBT P_r=12.7 μC/cm^2 for MLC-BF. This indicates a relaxation of ~50% in 1 s,

which is much less than the one reported for BNBT single phase film: ~75% (Chapter III). In the case of the MLC-BNBT the remnant polarization (P_r) is larger than that of MLC-BF, as it has been observed before in the conventional P-E loops, but the difference of 33% obtained is reduced to 24% for the remnant loops. Therefore, the evolution with the time after the application of the electric field is key for these multilayer composite films.

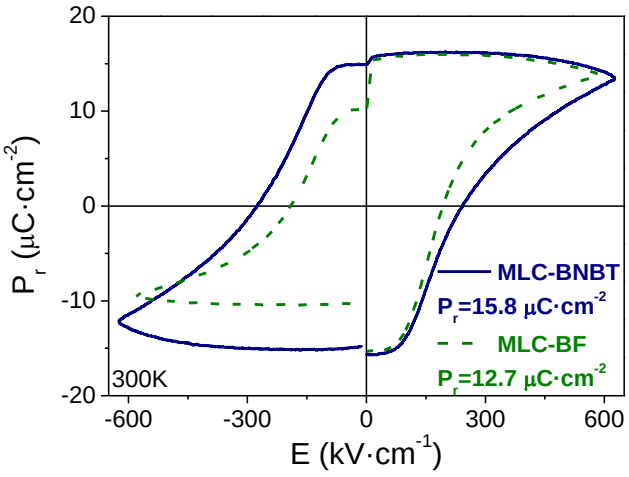

Figure 5.13: *Remnant hysteresis loops of multilayer composite films.*

In a further study of the retention of polarization for longer times (Figure 5.14) we observe that, after an initial large decrease of the values during the first few seconds, the values remain rather stable, with only an additional 15-20% of polarization lost up to 3 hours after poling. The values of the remnant polarization after this time are around 15 μC/cm^{-2} for both MLC films. All of this indicates that the polarization is highly unstable just after the removal of the electric field as expected for relaxor ferroelectrics. The remaining polarization is rather stable with time and with values higher than those of the single phase BNBT films. The fact that both MLC films show similar values after some time after the application of the electric field shows that the

effects of the layer ordering on the ferroelectric properties of the multilayer composite films is lost with time.

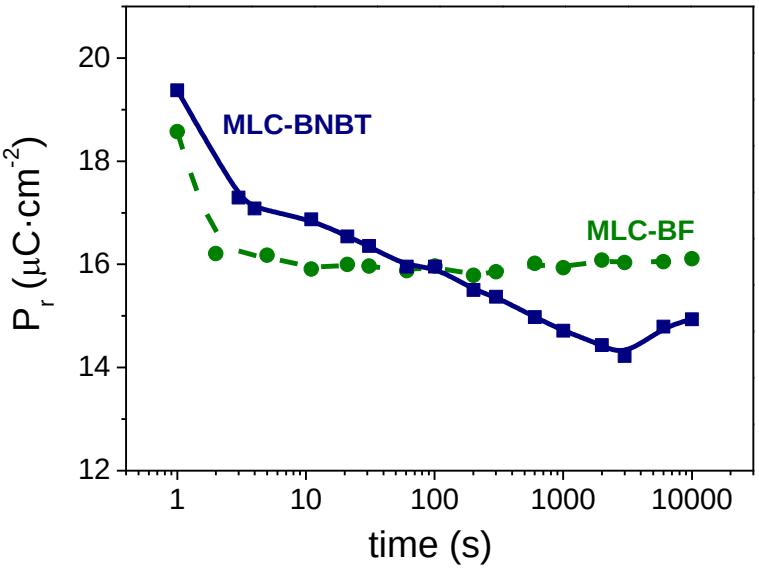

Figure 5.14: *Retention of the polarization for long times of multilayer composite films.*

In order to apply large electric fields, the appearance of leakage currents must be considered. This has been traditionally a problem for BF films, as it can be seen in Figure 5.15, where the behavior of the current density vs. electric field is compared for the single phase and multilayer composite films. The combination of the BF layers with high non-linear leakage currents and the BNBT layers with low linear leakage currents results in MLC films with intermediate current density values. It also prevents any resistivity degradation by large electric fields in the BF layers that results in large leakage density currents. The most effective layer combination from this point of view seems to be that of MLC-BF, where the BF layer is sandwiched between two BNBT layers (6 nA·cm^{-2} at ~150 kV·cm^{-1})(Figure 5.15 b). It must be noted that the control of the leakage currents in BF-based films is essential for their application in magnetoelectric devices.

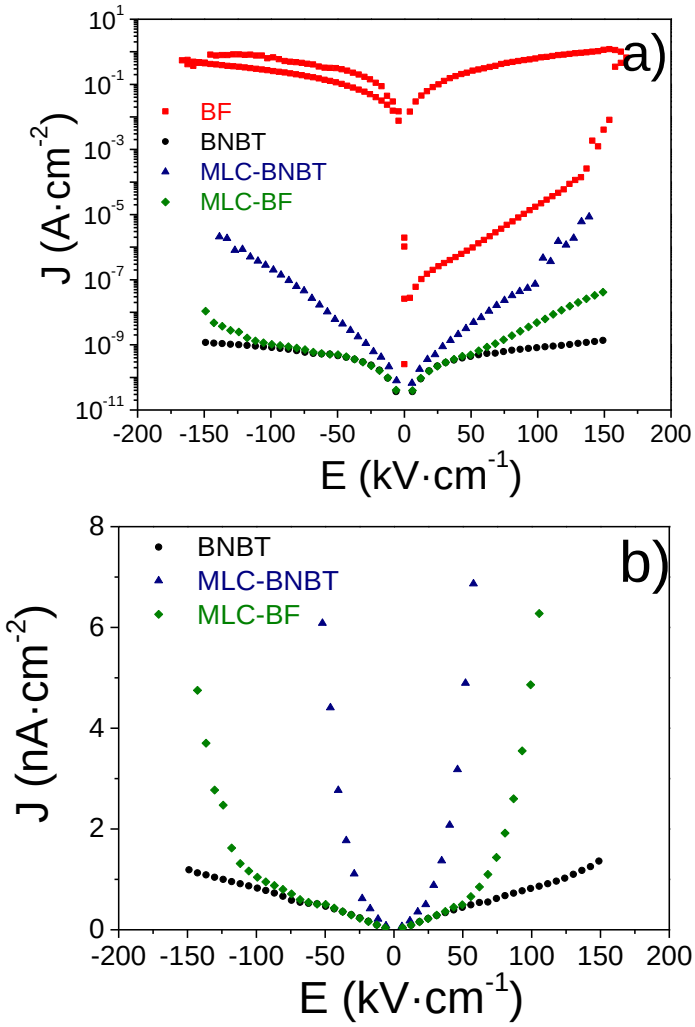

Figure 5.15: *a) J-E curves of the BF and BNBT single phase films compared with those of multilayer composite films MLC-BNBT and MLC-BF. b) Detail of the same graph with J in linear scale.*

From the results of the electrical characterization of the MLC films we can conclude that the combination of BNBT and BF layers in a multilayer composite film produces slightly larger values of the remanence (P_r/P_s) than that of the single phase BNBT film. The ordering sequence of the layers is important, and when the BNBT layer is sandwiched between two BF layers, the polarization values obtained are higher than the expected by sum of polarization. However, the characteristics derived from the relaxor ferroelectric character of the BNBT layers are present in these multilayers, and significant loss of properties sometime after the application of the electric field has been

observed. In any case the remaining polarization values of the MLC films are higher than those of the single phase films. And the control of the resistivity degradation mechanisms of the BF layers is a clear advantage of these MLC films for applications.

5.2.3. Multilayer composite films with Ca doped BF layers (MLC2).

Layers of $BiFeO_3$ doped with 3% of Ca^2 were used in a new set of multilayer composite films (MLC2), with the objective of improving the functionality of the MLC films that contain pure $BiFeO_3$ layers. In this section we will study the impact of the characteristics of the Ca^{2+} doped $BiFeO_3$ (see Chapter IV) on the electrical properties of the multilayer composite films.

The experimental J-E hysteresis loops and their corresponding corrected P-E hysteresis loops of MLC2 films are shown in Figure 5.16. The first effect of the use of Ca modified BF (BCF) layers instead of the pure BF layers can be seen in the J-E hysteresis loops. The shape of the loops show the drastic reduction of the contribution of non-linear leakage currents (compare Figures 5.10 a, c and 5.16 a, c) thanks to the use of these less conductive BCF layers. Similarly to MLC films, the film with the BNBT layer between two BF layers (MLC2-BNBT) presents higher polarization values than that with the BF layer in the middle (MLC2-BF):P_s=24.5 $\mu C \cdot cm^{-2}$, P_r=17.9 $\mu C \cdot cm^{-2}$, P_r/P_s = 0.7 (Figure b) for MLC2-BNBT and P_s=30.3 $\mu C \cdot cm^{-2}$, P_r=14.2 $\mu C \cdot cm^{-2}$, P_r/P_s = 0.5 (Figure d) for MLC2-BF. The remanence is improved respect to that of BNBT single phase film (P_r/P_s = 0.5) for MLC2-BNBT.

From the P-E hysteresis loop at 200 K of the single phase BCF3 film (Chapter IV), we can argue that the value for the remnant polarization at room temperature is $P_r^{BF} \sim 20$ $\mu C \cdot cm^{-2}$. Taking this value, the calculated remnant polarization from equation 5.1 for

the MLC2 films is P_r = 14.2 μC·cm^{-2}. This value is close to that of MLC2-BF, which thus corresponds to a simple addition of the properties in the composite film. The larger value obtained for the MLC2-BNBT (P_r = 24.5 μC·cm^{-2}) indicates that other contributions must be considered. The increment of the polarization respect to MLC2-BF is of 27%. It should be borne in mind that the difference between the two MLC2 films is the ordering sequence of the layers.

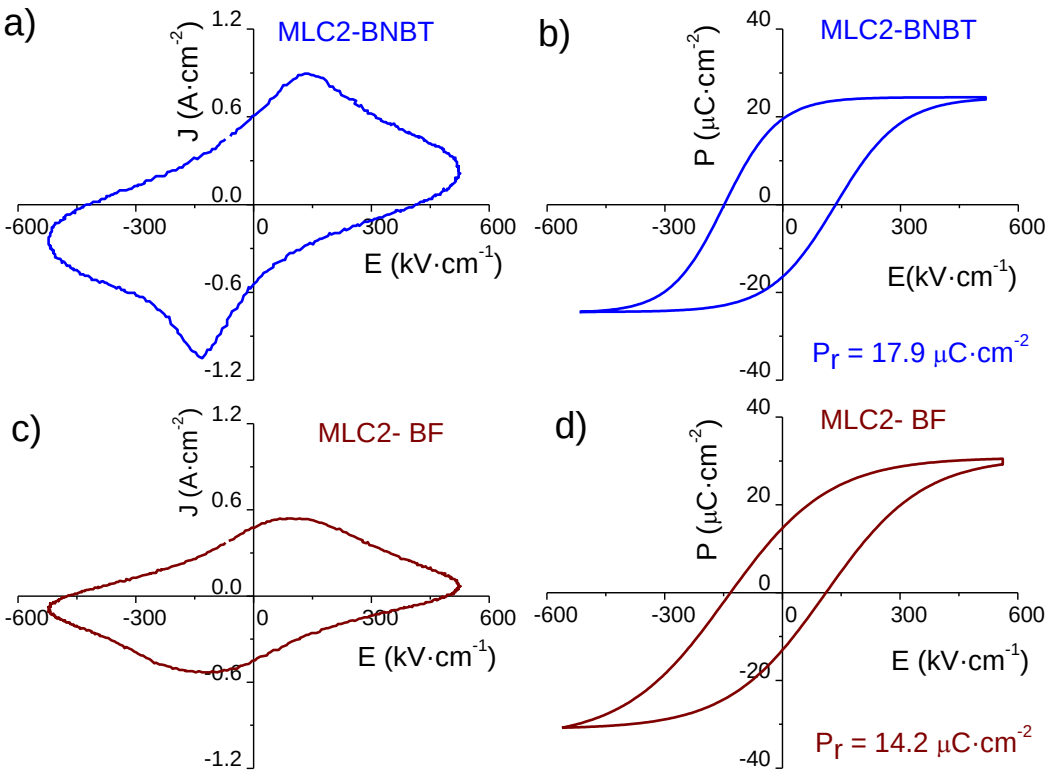

Figure 5.16: *Experimental J-E and corrected P-E hysteresis loops of (a, b) MLC2-BNBT and (c, d) MLC2-BF.*

The behavior at low frequency of MLC2-BNBT and MLC2-BF can be seen in Figure 5.17. The coercive fields obtained are E_c = 44.2 kV·cm^{-1} for MLC2-BNBT and E_c = 56.0 kV·cm^{-1} for MLC2-BF. These values are much larger than those of the MLC films (Figure 5.11). However, it must be taken into account that the coercive fields at 1 kHz

are also larger for MLC2 films (Figure 5.16) If we calculate the variation of the coercive fields with the measurement frequency, we find that in MLC films we obtain more than 75 % of reduction, while for MLC2 films is around 60%. Even with this difference, we can conclude that the stability of the polarization that can be deduced of this comparison is still present in the two sets of MLC films, although some improvement is achieved with the inclusion of the BCF layers in MLC2 films.

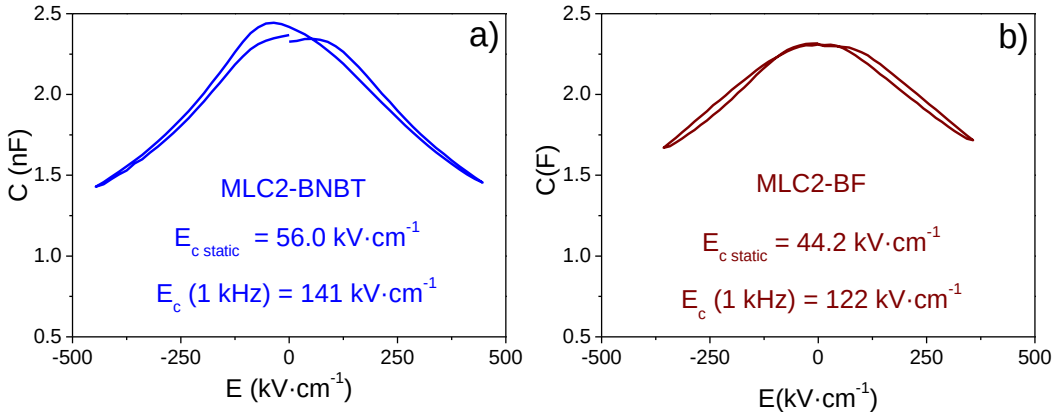

Figure 5.17: *C-V loops of the: a) MLC2-BNBT, b) MLC2-BF.*

The retention of the polarization with time of MLC2 films is shown in Figure 5.18. Comparing these values with those obtained from the P-E loops (Figure 5.16) we find that in the first second 52% of the polarization is lost for MLC2-BNBT and 72% for MLC2-BF. After that, in the two MLC2 films the values remain rather stable with time, without any significant variation for MLC2-BNBT. This stability may be related to the low contribution of non-linear leakage currents in the BCF layers, which will influence the stability of any internal field developed in these layers.

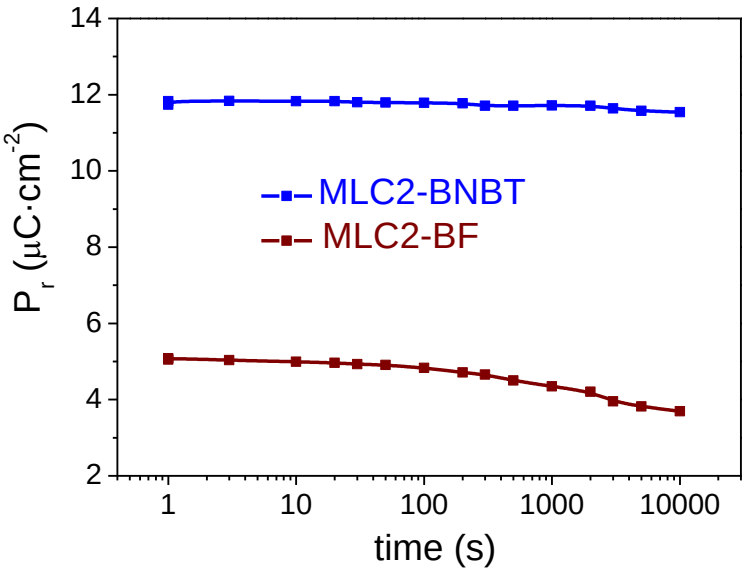

Figure 5.18: *Retention of the polarization for long times of multilayer composite films with Ca doped BF layers.*

In Figure 5.15, it is possible observed the behavior of the current density vs. electric field for two multilayer composites films MLC2-BNBT and MLC2-BF. The combination of the BF doped with Ca layers with lower non-linear leakage currents with BNBT makes that the MLC2 have lower no-linear current values with respect to the MLC films. In this MLC2 it is also prevents resistivity degradation produced by large electric fields in the BF layers that results in large conduction density currents. It is possible observed also that the change of slope related with the apparition of the non-linear leakage current in this MLC2 occurs at higher electric field than in the MLC films, 100 kV·cm^{-2}for MLC2-BF and 75 kV·cm^{-2}for MLC2-BNBT. Similar to the MLC films the most effective layer combination from this point of view seems to be that of MLC2-BF, where the BF doped layer is sandwiched between two BNBT layers (3.5 nA·cm^{-2} at ~150 kV·cm^{-1})(Figure 5.19 b) in this films the no-lineal current is approximately the half of the MLC-BF at high electric field. This demonstrates that the use of BF doped layers in

the MLC2 films improved the leakage current problems present in these multilayer composite films.

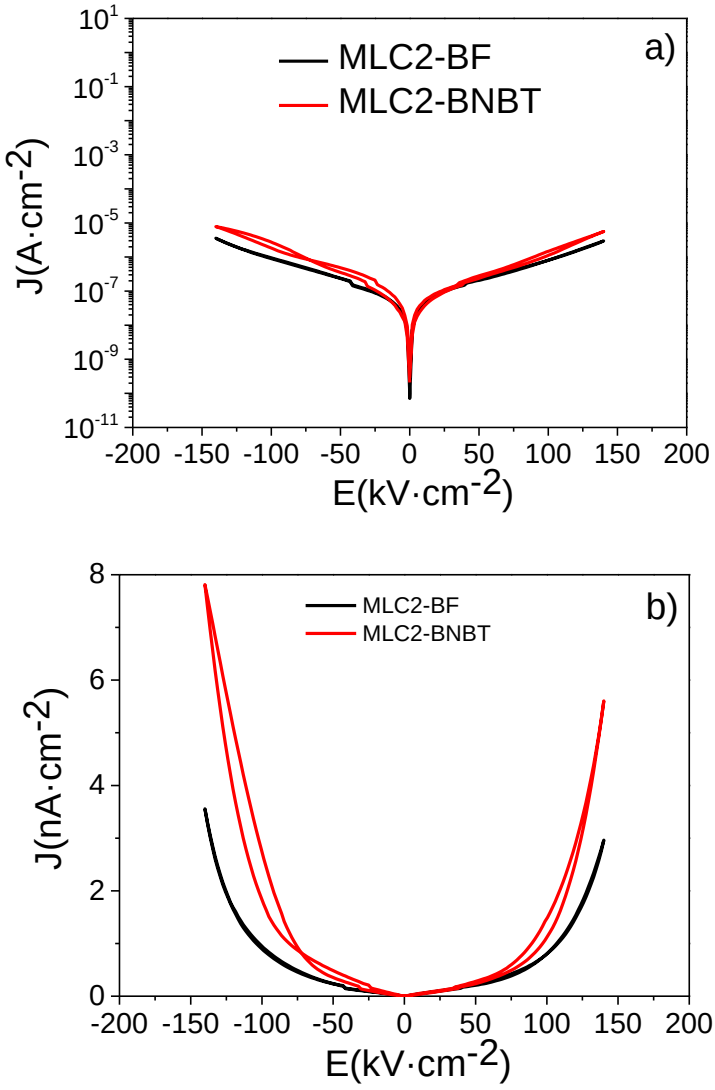

Figure 5.19: *a) J-E curves of the multilayer composite films MLC2-BNBT and MLC2-BF. b) Detail of the same graph with J in linear scale.*

The substitution of the BF for BCF layers results in a reduction of the net polarization values (as BCF present less polarization than BF films). But the effect observed in the MLC films is still present, and the remanence is improved respect that of the single phase BNBT film for the films where BNBT is surrounded by two BCF layers. The reduction of the conduction effects in the BCF layers produces multilayer composite

films with less contribution of non-linear leakage currents. This makes that was possible achieve the full switching in the polarization in thin this MLC2.

5.2.4. Polarization values in multilayer composite films.

The low remnant value of single phase BNBT film (P_r = 12.3 μC·cm^{-2}) is a result of the low remanence of this film (P_r/P_s= 0.5). In the previous sections we have analyzed multilayer composite films with polarization values that allow the fabrication of films containing $(Bi_{0.5}Na_{0.5})_{1-x}Ba_xTiO_3$ with useful remnant properties. All the values are summarized in Table 5.2.

***Table 5.2**. Summary of the polarization values obtained for the multilayer composite films.*

Layer configuration	*FILM NAME*	P_r/P_s	P_r (μC·cm^{-})^2
	Composite calculated polarization value (with BF layers):		*24.5*
BNBT/BF	*BNBT/BF*	*0.5*	*20.7*
BNBT/BF	*BNBT/BF*	*0.4*	*10.9*
BF/BNBT/BF	*MLC-BNBT*	*0.7**	*32.4*
BNBT/BF/BNBT	*MLC-BF*	*0.6*	*23.5*
	(with BCF layers):		*14.2*
BCF/BNBT/BCF	*MLC2-BNBT*	*0.7**	*17.9*
BNBT/BCF/BNBT	*MLC2-BF*	*0.5*	*14.2*

** significant improvement of remanence respect single phase BNBT film*

It can be seen that only specific multilayer configurations achieve the improved remanence searched. In the following section we will analyze the mechanisms that lead to this response.

5.2.5. Analysis of the polarization behavior in MLC films.

To understand properties of the multilayer composite films shown in the previous sections we first calculate the polarization behavior, we should obtain from the simple combination of layers of two different materials. Then, through the comparison with the experimental results, we can discuss the possible interactions between the layers that lead to the final electrical properties obtained. We consider a series circuit to represent the two layers of ferroelectric material that constitutes the multilayer composite film (Figure 5.20). The two elements of the circuit are characterized by its resistance, capacitance and ferroelectric polarization in parallel configuration.

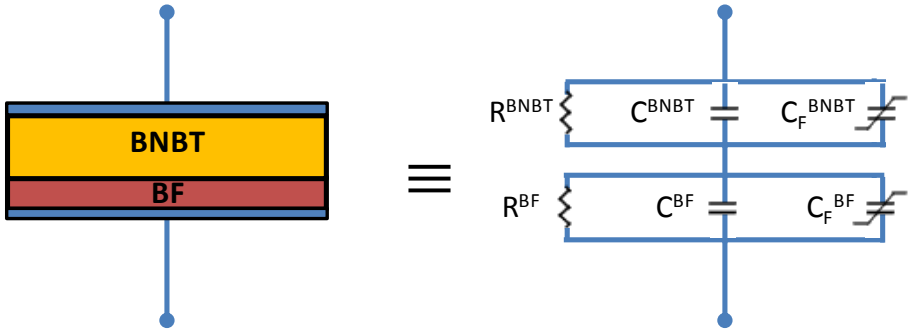

Figure 5.20: *Equivalent circuit used for the calculation of effective properties of multilayer composite films.*

We therefore assume the electric current density continuity through the layers, which leads in our case, with two BNBT and BF layers, to the following equation:

$$J_{BNBT} = J_{BF} = J_T$$

$$\sigma_{BNBT}E_{BNBT} + K'_{BNBT}\frac{dE_{BNBT}}{dt} + \frac{dP_{BNBT}}{dt} = \sigma_{BF}E_{BF} + K'_{BF}\frac{dE_{BF}}{dt} + \frac{dP_{BF}}{dt}$$

$$= \sigma_T E_T + K'_T\frac{dE_T}{dt} + \frac{dP_T}{dt} \qquad (5.2)$$

where J is the current density, σ the conductivity, K' the permittivity, E the electric field and P the polarization. We calculate the polarization hysteresis loop of the multilayer $(\frac{dP_T}{dt})$ *considering that in a series circuit:*

$$V_{BNBT} + V_{BF} = V_T$$

$$E_{BNBT}d_{BNBT} + E_{BF}d_{BF} = E_T d_T \qquad (5.3)$$

being d the thickness of the layers.

To solve this equation we follow the method developed by Y.Y. Or et al. [6], based on the model of polarization behavior proposed by S. Miller et al [7, 8]. We take the coercive field, the remnant and saturation polarization values of each layer and from them we build their P-E hysteresis loops. It is important to establish correctly the initial conditions of the calculations: for the first P-E hysteresis loop, P = 0 for E = 0 at t = 0. This determines the value of P_s*, which will be kept for the following loops. The input values of the layers for the calculations are taken from the results obtained for the single phase BNBT films (Chapter III) and BF films (Chapter IV), and are summarized in Table 5.3.*

From the calculations, P-E hysteresis loops are obtained, which, after subtraction of the non-switching contributions as explained before for the experimental loops [9], yields the effective ferroelectric switching P-E loops, comparable with the experimental corrected P-E hysteresis loops. Also, the distribution of the electric field in the layers is calculated.

Table 5.3. *Parameters of the BNBT and BF layers used in the calculations of the effective ferroelectric properties of the multilayer composite films.*

	P_s ($\mu C \cdot cm^{-2}$)	P_r ($\mu C \cdot cm^{-2}$)	E_c ($kV \cdot cm^{-1}$)	K'	σ (at 1 kHz) ($\Omega^{-1} \cdot cm^{-1}$)
BF layer [Chapter IV]	65	61	300	400	$1 \cdot 10^{-7}$
BNBT layer [Chapter III]	28	12	68	700	$1 \cdot 10^{-7}$

The results of the calculations for two layers with thickness: d_{BNBT} = 360 nm and d_{BF} = 60 nm can be compared with the experimental results obtained for the bilayer composite films (Figure 5.21). The calculated hysteresis loops is similar to that of BNBT/BF, with the coercive field and remnant polarization values close. The main difference is the saturation polarization values. We can consider that there is a good agreement, within the error, between the calculated and experimental values in this bilayer, which validate the assumptions made during the calculations.

However, BF/BNBT presents a completely different behavior, far from the calculated values. This can be due to the fact that the input values used in the calculations are not adequate for any of the layers. In this case the BF layer is grown on top of a BNBT layer, while the single phase BF thin film is deposited directly on the platinised Si-based substrate. It has been shown before that the properties of polycrystalline $BiFeO_3$ thin films depend strongly on the substrate used [10,11]. Besides, the microstructure of the BF layer on BNBT (Figure 5.4 d) and that of a similar BF thin film on $Pt/TiO_2/Si$ [3]

are rather different. Besides the stress state in both cases must be different, which also affects significantly the properties of $BiFeO_3$ films. Therefore, we cannot use the same values of K', σ and P for the calculations of a BF layer deposited on a BNBT layer (BF/BNBT film) and that on the Si-based substrate (BNBT/BF film). We can conclude that the calculations are valid for multilayer composites with BF layers grown directly on the Si substrate.

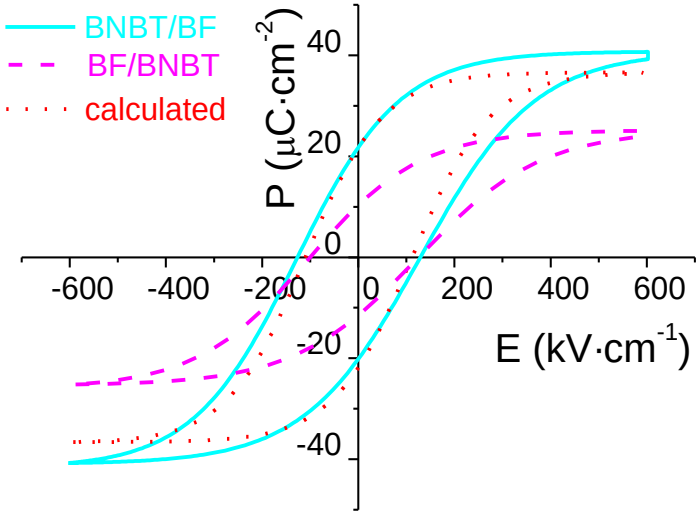

Figure 5.21: *Experimental and calculated P-E hysteresis loops for the bilayer composite films.*

The calculations can be made for two layers with the total thickness of the constituent layers of the MLC films: d_{BNBT} = 360 nm and d_{BF} = 120 nm. The results of the calculations can be compared with the experimental results obtained for the two configurations used (Figure 5.22). For the MLC-BNBT film the calculated P_r and P_s values are quite different to the experimental. The slope of the hysteresis loop close to E_c also differs from the calculated curve (Figure 5.11 a). However, a closer agreement between the calculated and the experimental hystereis loops is found for the MLC-BF. In this case, we have the BF layer deposited on a BNBT layer, as in the BF/BNBT film. But the deposition and crystallization at 650^0C of another BNBT layer on top of it must

modify its microstructure, and the input values for the calculations for the BF layer seem in this case adequate.

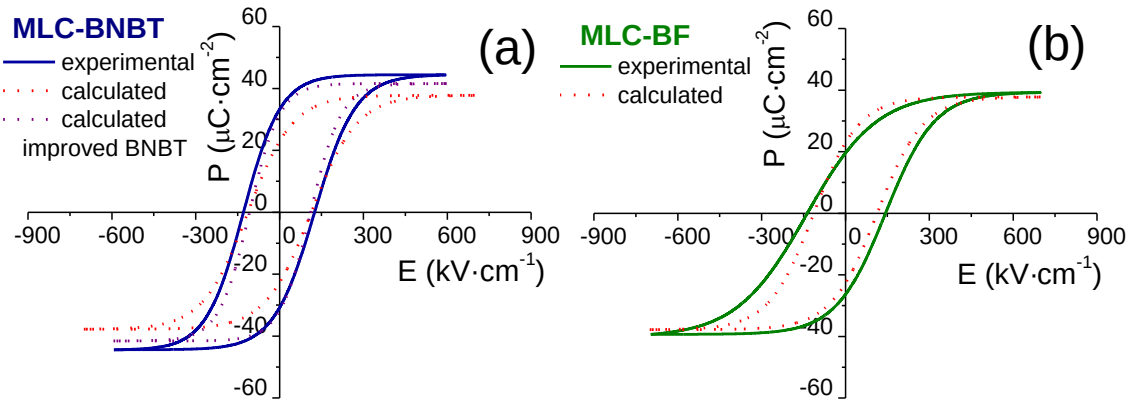

Figure 5.22: *Experimental and calculated P-E hysteresis loops for the multilayer composite films: a) MLC-BNBT and b) MLC-BF.*

It must be pointed out that the calculations do not take into account the ordering sequence of the layers or the presence of interfaces. Therefore, the fact that the experimental P-E hysteresis loops of MLC-BF shows a good agreement with the results of the calculations, but MLC-BNBT not, is an evidence that there is some interaction between layers in the MLC-BNBT film, not considered in the calculations. In fact the calculated hysteresis loop fits better the experimental data when the input parameters for the polarization of the BNBT layer are increased up to P_s *= 40 μC/cm*^{2} *and* P_r *= 25 μC/cm*^{2}*, i.e., values that correspond to a BNBT layer with improved remanence,* P_r/P_s *(Figure 5.22 a). This is the consequence of the extra contribution to the polarization of the BNBT layer induced by the surrounding BF layers that should be related to an enhanced ferroelectric domain stability. The poled BF layers seem to prevent the fast depolarization of the BNBT layer creating an internal electric field, induced by their remnant polarization vectors. Once the external electric field is removed, the BNBT layer is subjected to an internal bias that allows it keeping a larger percentage of the*

saturation polarization. This situation is not possible in the MLC-BF film, as the BNBT layers are not sandwiched between two BF layers.

It is therefore shown that, the ordering sequence of the layers in the multilayer composite films has a significant effect on their ferroelectric behavior. This is not only on the polarization values but also on the switching process. The MLC-BNBT film shows a more square P-E loop than MLC-BF film, i.e., the saturation and remnant polarization values are closer and the coercive field is larger. Switching seems to be dominated by the BF layers in MLC-BNBT films, whose single phase films present square P-E loops, as shown in Chapter IV. For MLC-BF films, the BNBT layers, characterized by slim hysteresis loops (Chapter III), are instead dominant.

As we have discussed, the layer ordering sequence effect on the ferroelectric properties of the films is related to the depolarization fields (E_{dep}) developed after the application of an electric field. It is important to note that in the time scale of a P-E loop at 1 kHz we are dealing with fast depolarization phenomena, which means that the depolarization happens between switching (ns) and 0.1s [12]. One of the causes of the occurrence of strong depolarization fields in films is the existence of dead layers at the interface between the metal electrode and the ferroelectric material, where uncompensated polarization charges are accumulated. For example, the appearance of a 2 nm layer with k'=40 at the interface between the bottom electrode and a PZT film with P_s close to 30 μC/cm^2 results in a depolarization field close to 85 kV/cm [12]. Similarly, the accumulation of polarization charges at the interface between the BF and BNBT layers, caused by their different polarization values can stabilize the polarization of the BNBT layer sandwiched between the BF layers, i.e. reducing the rate of

polarization reversal. This can be seen as an effective inducement of polarization in this layer and, thus, an improvement of the remanence in the MLC-BNBT film.

But the efficiency of the mechanism described for the multilayer composite films is based on the actual distribution of the electric field in each layer. This can be studied using the electric fields obtained in the calculations (Figure 5.23). The electric field in the BNBT layer, E^{BNBT}, follows closely the sinusoidal shape of the applied field with a small phase difference and achieve 10 times the coercive field of the BNBT (marked in the graph), which ensures full switching polarization in this layer. In the case of the electric field in the BF layers, E^{BF}, the fact that the maximum electric field attained is only ~1.4 times higher than the coercive field of BF single phase (marked in the graph) results in the calculated P_S^{BF} = 57 μC·cm^{-2}, which is below the expected saturation value of 65 μC·cm^{-2}.

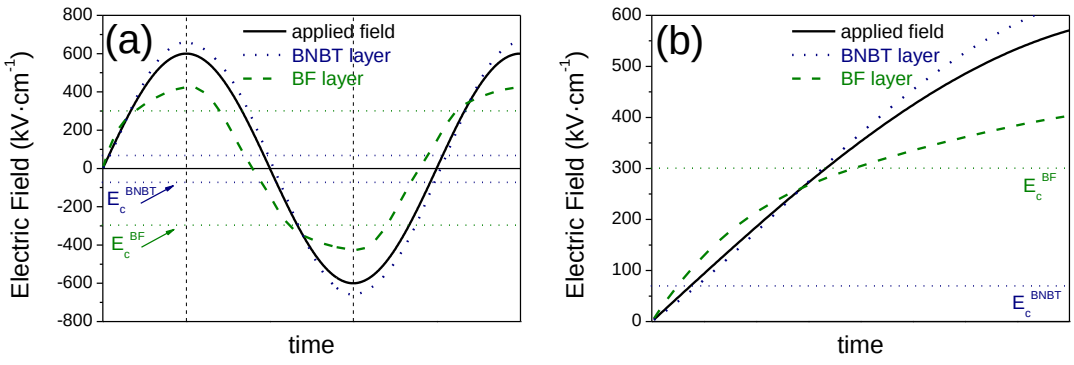

Figure 5.23: *a) Calculated distribution of the electric field in a BNBT/BF bilayer. b) Detail of the field evolution.*

The large difference in the maximum polarization values between the two layers leads to the inhomogeneous distribution of the electric fields already shown. This makes impossible reaching saturation in the BF layer. The lower polarization achieved in the BF layers not prevent the presence of the larger depolarization field in the BNBT layer

and the objective of obtaining large remnant polarization values may not be obtained. In fact, we have substituted the large P_s, BF layers for Ca modified BF layers in MLC2 films. This choice complies with the requirement of having close values of the saturation polarization for both constituent phases in the multilayer composite film.

Similarly to the analysis carried out for the MLC films, the results of the calculations for two layers with thickness: d_{BNBT} = 360 nm and d_{BF} = 120 nm are compared with the experimental results obtained for the MLC2 films (Figure 5.24). The input parameters for the calculations are summarized in Table 5.4. The calculated hysteresis loop is similar to that of MLC2-BNBT film, with the coercive field and saturation polarization values close. The main difference is here the remnant polarization values, which show that this film show better remanence than the calculations. They show a good agreement with the experimental values of MLC2-BF, although the experimental saturation polarization values are larger than the calculated.

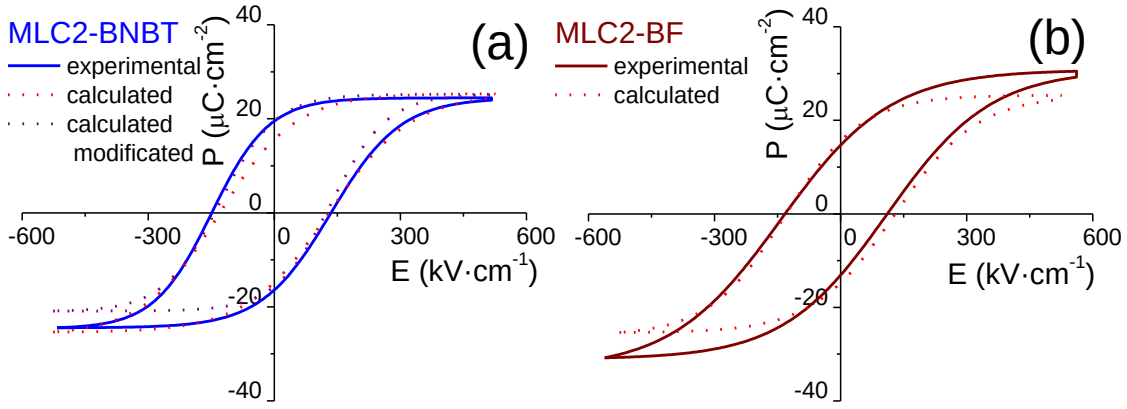

Figure 5.24: *Experimental and calculated P-E hysteresis loops for the multilayer composite films: a) MLC2-BNBT and b) MLC2-BF.*

***Table 5.4**. Parameters of the BNBT and BF layers used in the calculations of the effective ferroelectric properties of the MLC2 films.*

	Ps ($\mu C \cdot cm^{-2}$)	*Pr* ($\mu C \cdot cm^{-2}$)	*Ec* ($kV \cdot cm^{-1}$)	*K'*	σ(@1 kHz) ($1 \cdot \Omega^{-1} cm^{-1}$)
BCF layer(Chapter IV)	*22*	*20*	*300*	*500*	$1 \cdot 10^{-7}$
BNBT layer (Chapter III)	*28*	*12*	*68*	*700*	$1 \cdot 10^{-7}$
BNBT layer (improved remanence)	*25*	*18*	*100*	*700*	$1 \cdot 10^{-7}$

The BNBT layer achieves improved remanence in the MLC2-BNBT, as this layer is sandwiched between two BF layers. We can obtain a better fitting of the experimental hysteresis loop using the following values for the BNBT layer in the calculations: P_s = 25 $\mu C \cdot cm^{-2}$ and P_r = 18 $\mu C \cdot cm^{-2}$ (Figure 5.24a).

As we have discussed before, the efficiency of the creation of an internal field in the BNBT layer to reduce its fast depolarization is based on the actual distribution of the electric field in the layers of the multilayer composite film. The electric fields obtained in the calculations are shown in Figure 5.25.

Similarly to the results shown in Figure 5.23, the electric field in the BNBT layer, E^{BNBT}, follows closely the sinusoidal shape of the applied field, but now only achieves ~ 8 times the coercive field of this material (marked in the graph), which still ensures the full ferroelectric switching in this layer. In the case of the electric field in the BCF layers, E^{BCF}, the maximum electric field attained is ~2.4 times higher than the coercive field of BCF single phase (marked in the graph), which also ensures full polarization switching in this layer. This can be seen with more detail in Figure 5.25 b. The curve of the

electric field in the BCF layer follows the sinusoidal behavior of the applied field. This was not the case for the pure BF layers (Figure 5.23 b), which shows a change in the slope. This impedes reaching the saturation polarization and it has been attributed to large different in the P_s values between the BF and the BNBT layers. This difference is not present in the MLC2 films, and therefore, high values of the electric field are applied to the BCF layers, and allows the complete ferroelectric switching of this layer. This result indicates that the BCF layers are poled more efficiently, which results in more stable internal fields in the BNBT layers. This in turn induces more stable polarization with time, and MLC2 films show an improved retention behavior when compared to MLC films. This has been observed in Figure 5.18.

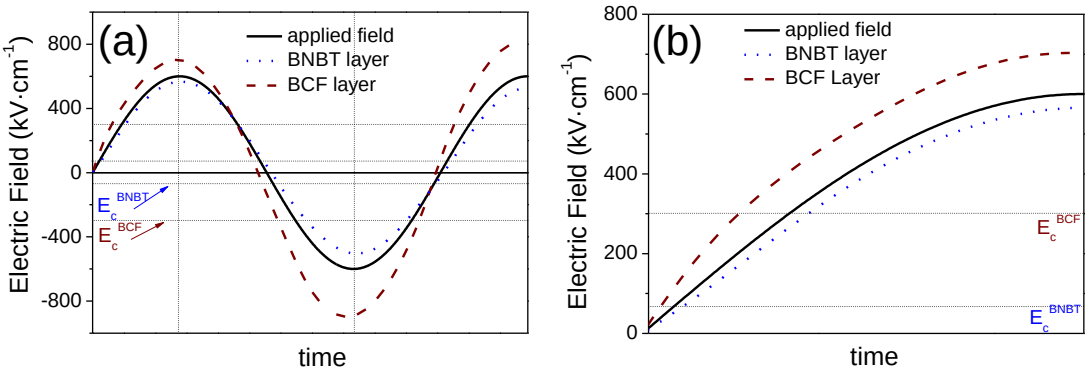

Figure 5.25: *a) Calculated distribution of the electric field in a BNBT/BCF bilayer. b) Detail of the field evolution.*

The comparison of the electric behavior of the BNBT-based multilayer composite films and that calculated for the simple combination of two layers, shows that the improvement on the remanence is achieved by the induction of an electric field in the BNBT layers by the surrounding BF-based layers. Due to the inhomogeneous distribution of the electric field in the layers, this mechanism is more effective the closer their saturation polarization values. The stability of the polarization achieved results in

an improved retention, which is an important characteristic searched for this multilayer composite films.

5.3 Piezoelectric properties.

Figure 5.26 shows the piezoelectric hysteresis loops of the MLC, MLC2 and the single phase BNBT films. We observe that the remnant value of the piezoelectric coefficient corresponding to the single phase BNBT film, d_{33r}= 11 pm·V^{-1}, is much lower than the saturation value, d_{33s}= 60 pm/V, as it corresponds to the low remanence of this thin film as explained in Chapter III. The remnant piezoelectric coefficients of the MLC (Figure 5.26 a) and MLC2 films (Figure 5.26 b) have values around the same value, d_{33r}=11 pm/V, but the saturation values go down to around d_{33s}=40 pm/V. It is remarkable the very low values of the coercive fields, between 15 and 30 kV·cm^{-1}.

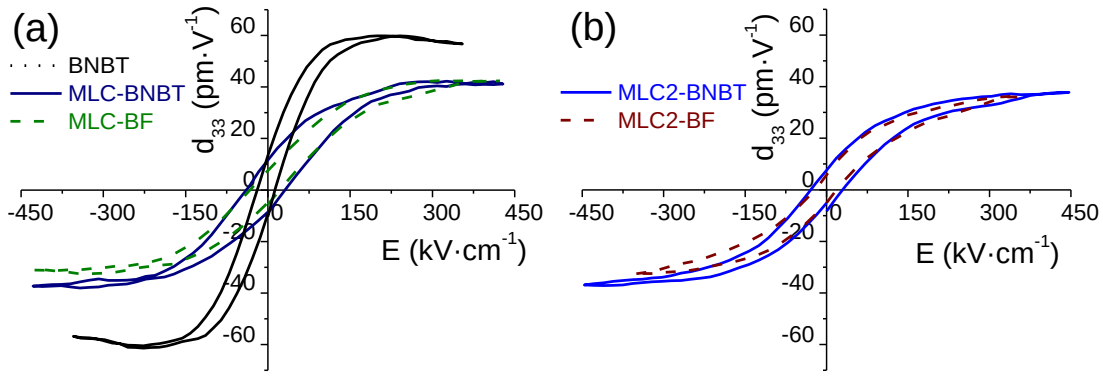

Figure 5.26: *Piezoelectric hysteresis loops of a) single phase BNBT and MLC films and b) MLC2 films.*

The measurement of the piezoelectric hysteresis loops is carried out at a very low frequency (~1 Hz). The coercive field of BNBT based films is very dependent on the measurement frequency, as we have discussed before (Figure 5.12). This effect caused by the relaxor ferroelectric character of BNBT, results in extremely low coercive fields for low frequency measurements. This also limits the maximum electric field to be

applied to the film before dielectric breakdown occurs. In this case we were not able to obtain piezoelectric loops using electric fields above 450 kV·cm^{-1}. We must take into account that the coercive fields for the BF and BCF layers in these multilayer composite films are around 300 kV·cm^{-1}, it is supposed that is independent of the measurement frequency due to the high T_c (Curie Temperature 1107 K) of this materials, and that saturated hysteresis loops are achieved for 600 kV·cm^{-1} (Figures 510. and 5.16). Therefore, in the range of the electric fields applied during the piezoelectric loops shown in Figure 5.25 the BF layers are not poled completely and they are not inducing any polarization in the BNBT layers. As a result, the piezoelectric loops of the multilayer composite films show the a lack of remanence close to that of the single phase BNBT film. Besides, the BF layers do not contribute to the neat piezoelectric coefficient, but act as constraint layers, lowering the maximum displacement achieved and thus the saturation piezoelectric coefficient, as it is observed in the piezoelectric loops of MLC and MLC2 films. We conclude that, unfortunately, the measurement procedure does not allow to show the enhancement of the remnant piezoelectric properties of the BNBT-based multilayer composite films studied here.

5.4 Magnetic behavior.

5.4.1. Bilayer composite films.

Figure 5.27 shows the M-H hysteresis loops of the bilayer composite films. It can be seen that both BNBT/BF and BF/BNBT films show clear ferromagnetic behavior with neat remanence and coercitivity at 4.2 K and at room temperature, as it is shown in the insets of the Figure 5.27a. BNBT/BF film shows a remnant magnetization M_r = 1.0 emu·g^{-1} at 42 K, which is reduced down to M_r = 0.2 emu·g^{-1} at room temperature. The

values obtain for BF/BNBT film are much lower (M_r = 0.4 emu·g^{-1} at 42 K and almost disappears at 300 K). The coercive magnetic field is also lower for the BF/BNBT film (H_c = 0.1 10^3 Oe at 4.5 K) than for BNBT/BF (H_c = 0.7·10^3 Oe at 4.5 K).

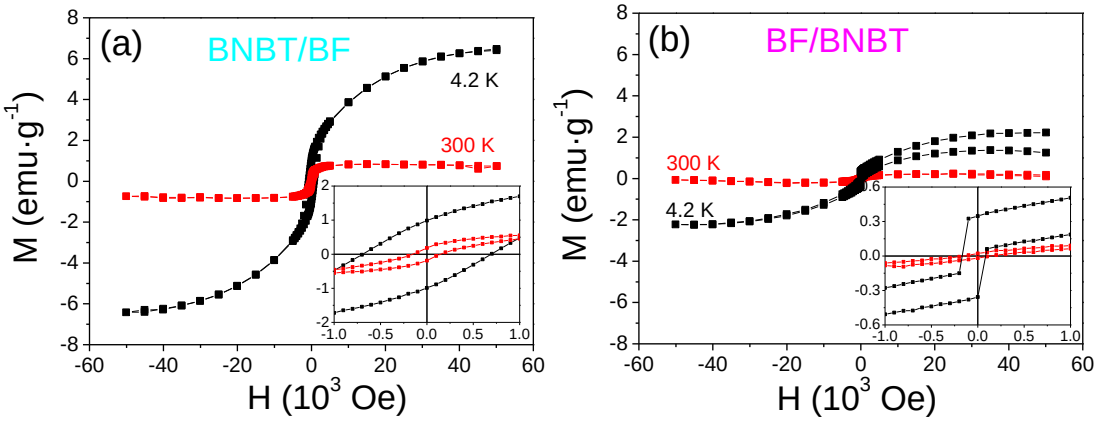

Figure 5.27: *M-H hysteresis loops at different temperatures of a) BNBT/BF and b) BF/BNBT films. The inset shows a magnified view of the central region of the loops.*

Other important aspect to that it is possible to observe in the bilayer BF/BNBT (Figure 5.27 b) is that the magnetization is different in the final part of the loop (open loop). This can be related with the stress rearrangement induced at high magnetic applied field, thus provoking changes in the magnetization with time due to the magnetostrictive effect inherent to the BF phase. In the other bilayer BNBT/BF this effect not appear because the in the BF layer the stress are higher and have less mobility.

5.4.2. Multilayer composite films (MLC).

Figure 5.28 shows the M-H hysteresis loops of MLC films, which also have neat remanence and coercitivity (insets of Figure 5.28). The MLC-BNBT film presents higher remnant magnetization (M_r = 1.0 emu·g^{-1}) than MLC-BF (M_r = 0.5 emu·g^{-1}). This almost disappears at room temperature for the MLC-BNBT film, while for MLC-BF film

a value of M_r = 0.3 emu·g^{-1} is kept. Regarding the coercitivity, both films have H_c values of 0.5·10^3 Oe.

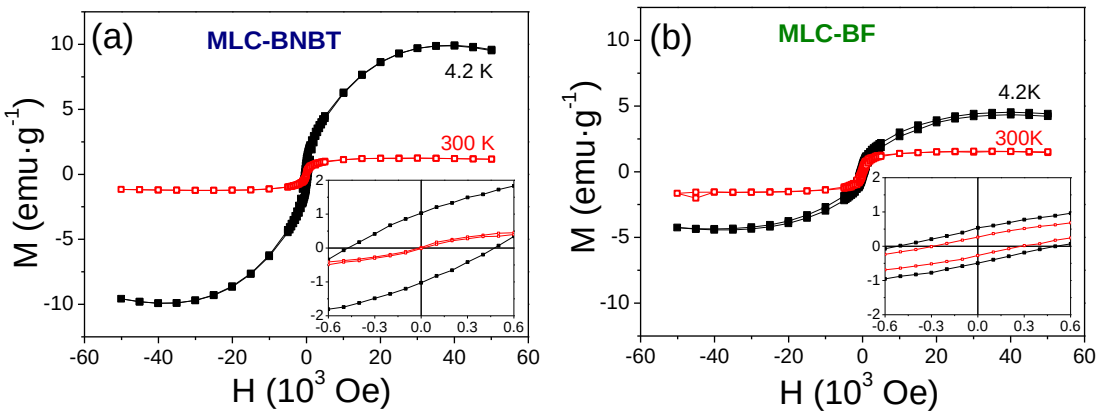

Figure 5.28: *M-H hysteresis loops at different temperatures of a) MLC-BNBT and b) MLC-BF films. The insets show a magnified view of the central region of the loops.*

5.4.3. Multilayer composite films with Ca doped BF layers (MLC2).

The use of Ca doped BF layers produces multilayer composite films with the highest remnant magnetization values of this study (Figure 5.29). MLC2-BNBT presents M_r=1.4 emu·g^{-1} and MLC2-BF M_r=1.9 emu·g^{-1}. Although MLC2-BNBT film loses most of this remnant magnetization at room temperature (M_r=0.1 emu·g^{-1}), MLC2-BF shows the highest value obtained at this temperature for the films analyzed (M_r=0.8 emu·g^{-1}). The coercive magnetic fields obtained are of the order of the ones obtained in the rest of the multilayer composite films: H_c = 0.8·10^3 Oe for MLC2-BNBT and H_c = 0.5·10^3 Oe for MLC2-BF.

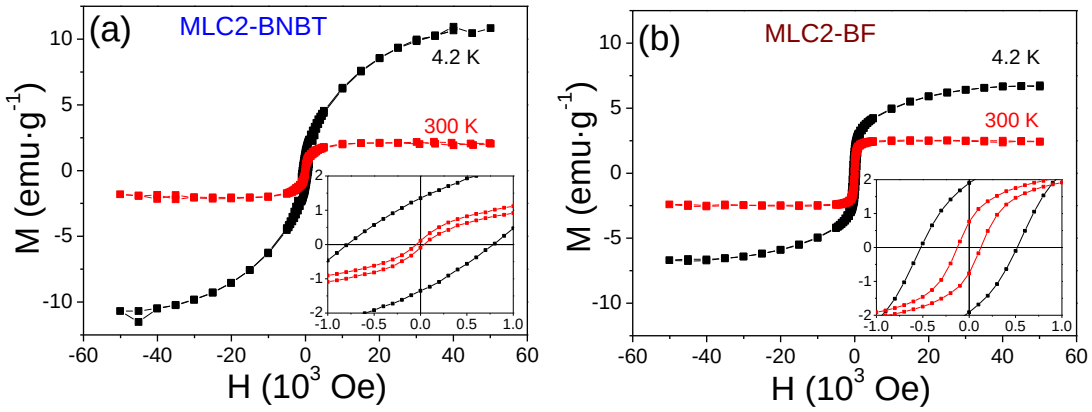

Figure 5.29: *M-H hysteresis loops at different temperatures of a) MLC2-BNBT and b) MLC2-BF films. The insets show a magnified view of the central region of the loops.*

5.4.4. Remnant magnetization in multilayer composite films.

The appearance of magnetic remanence and coercitivity is not the expected behavior for the $BiFeO_3$ thin films. It has been reported that the antiferromagnetic spin order of $BiFeO_3$ is not homogenous, but space modulated [13], as an incommensurate cycloid structure. The antiferromagnetic vector is normally locked within the cycloid, averaged to zero, but the effect of an epitaxial constraint in a film can release this latent magnetization [14]. Besides, the same effect has been observed for polycrystalline single phase BF films with columnar grain growth [3]. This is a similar situation for the polycrystalline BF layers in the multiferroic composite films studied here. We can argue that the origin of the enhanced magnetization in these films can be attributed to strain effects on the columnar grains, in analogy with the epitaxial films. In the case of the bilayer composite films, we clearly observe that the film with the BF layer deposited on the substrate (BNBT/BF) has a larger value of M_r than that of the BF/BNBT film with a BF top layer instead (Table 5.5). The gradient of residual stress due to the different thermal expansion coefficients of substrate and film affects strongly the layer closer to the substrate. Therefore, the bottom BF layer is subjected to a larger stress, and this

may be the origin of their larger magnetic remanence. The same trend is observed for the MLC films. The film with a bottom BF layer (MLC-BNBT), and thus more stressed, shows higher M_r than the film with the BF layer in the middle of the film (MLC-BF) (Table 5.5)

Another aspect to take into account in the improvement of the magnetic properties is grain size effects. The size of the crystals may play a role in the interruption of the continuity of the cycloidal arrangements. Doping with Ca^{2+} results in a decrease of the grain size of the BF layers (Chapter IV). If we observe the values of M_r of the MLC2 films in Table 5.6, we realize that, with the same layer configuration as MLC films, the values are higher. According to the microstructural studies of Chapter IV, the grain size goes from 107 nm of pure BF films down to 22 nm of Ca doped films. This small size is lower that the length of the cycloid (60 nm), and, therefore, grain size becomes in this film the most important factor of disruption. As a result the highest remnant magnetization values correspond to the MLC2 films.

Table 5.5. *Summary of the remnant magnetization and coercive magnetic fields at 4.2K for the multilayer composite films.*

Layer configuration	*FILM NAME*	M_r $(emu \cdot g^{-1})$	H_c $(10^3\ Oe)$
BNBT/BF	*BNBT/BF*	*1.0*	*0.7*
BF/BNBT	*BF/BNBT*	*0.4*	*0.1*
BF/BNBT/BF	*MLC-BNBT*	*1.0*	*0.5*
BNBT/BF/BNBT	*MLC-BF*	*0.5*	*0.5*
BCF/BNBT/BCF	*MLC2-BNBT*	*1.4*	*0.8*
BNBT/BCF/BNBT	*MLC2-BF*	*1.9*	*0.5*

We can conclude that the two factors that control the occurrence of ferromagnetism in the multilayer composite films are the stress state and grain size of the BF layers. The choice of the layer configuration and variations that affect the grain size (like layer thickness or doping) results in different values of the remnant magnetization.

5.5 Conclusions on the functionality of multilayer composite films with BNBT and BF layers.

The thorough characterization of the functional properties of lead free multilayer composite films constituted by BNBT and BF layers allows us to identify the configurations that lead to the best performance for their integration in devices.

Thin films with compositions close to the Morphotropic Phase Boundary of $(Bi_{0.5}Na_{0.5})_{1-x}Ba_xTiO_3$ suffer from a lack of remanence that can be partly solved in this work by placing a thin layer between two layers of pure or Ca modified $BiFeO_3$. Pure BF layers produce multilayer composite films with significant remanence. But if we use Ca doped BF layers instead, with a saturation polarization closer to BNBT, more stable polarization with time is achieved in the multilayer composite film.

The use of the magnetic properties of $BiFeO_3$ thin films for magnetoelectric applications requires firstly reducing the large conductivity of these films at room temperature. We have shown that combined with dielectric layers electric conduction can be controlled, allowing the effective application of an electric field and the switching of the polarization. Besides, the size reduction can be used to extract the latent magnetization in this composition, and thus, Ca doped BF layers, with the

smallest grains, produce films with significant remnant magnetization, even at room temperature.

5.6 References.

[1] I. Bretos, R. Jiménez, C. Gutiérrez-Lázaro, I. Montero, and M. L. Calzada, Appl. Phys. Lett. 104, 092905,(2014).

[2] D. Pérez-Mezcua, R. Sirera, I. Bretos, J. Ricote, R. Jiménez, L. Fuentes-Cobas, R. Escobar-Galindo, D. Chateigner, and M. L. Calzada, J. Am. Ceram. Soc. 97, 1269, (2014).

[3] C. Gutiérrez-Lázaro, I. Bretos, R. Jimenez, J. Ricote, H. El Hosiny, D.Pérez-Mezcua, R. J. Jiménez Rioboo, M. García-Hernández, and M. L. Calzada, J. Am. Ceram. Soc. 96, 3061, (2013).

[4] R. E. Newnham, Ann. Rev. Mater. Sci. 16,47 ,(1986).

[5] M. Dawber, P. Chandra, P.B. Littlewood, J.F. Scott. J. of Phys. C. 15, L393, (2003).

[6] Y.T. Or, C.K. Wong, B. Ploss, F.G. Shin. J. Appl. Phys. 93, 4112, (2003).

[7] S.L. Miller, R.D. Nasby, J.R. Schwank, M.S. Rodgers, P.V. Dressendorfer. J. Appl. Phys. 68, 6463 ,(1990).

[8] S.L. Miller, J.R. Schwank, R.D. Nasby, M.S. Rodgers. J. Appl. Phys. 70, 2849, (1991).

[9] R. Jiménez, C. Alemany, M.L. Calzada, A. González, J. Ricote, J. Mendiola, Appl. Phys. A 7, 607, (2002).

[10] H. Liu , Z. Liu , Q. Liu , K. Yao, Thin Solid Films 500, 105 – 109, (2006).

[11] C.-S. Woo, J. H. Lee, K. Chu, B.-K. Jang, Y.-B. Kim, T. Y. Koo, P. Yang, Y. Qi, Z. Chen, L. Chen, H. C. Choi, J. H. Shim, C.-H. Yang, Phy. Rev B. 86, 054417, (2012).

[12] X.J. Lou. J. Appl. Phys. 105. 094107, (2009).

[13] I. Sosnowska, T. Peterlin-Neumaier, E. Steichele. J. Phys. C 15, 4835, (1982).

[14] F. Bai, J. Wang, M. Wuttig, J.F. Li, N. Wang, A.P. Pyatakov, A.K. Zvezdin, L.E. Cross, D. Viehland. Appl. Phys. Lett. 86, 032511, (2005).

CAPÍTULO-VI

CONCLUSIONES

Y PERSPECTIVAS DE FUTURO.

6.1 Conclusiones generales.

En este trabajo se ha conseguido obtener composites multicapas de láminas delgadas libres de plomo con propiedades funcionales mejoradas con respecto a las láminas constituyentes. Se han estudiados diferentes configuraciones de estos composites demostrando cuales son las más eficaces para resolver los problemas presentes en la láminas de una sola fase, por ejemplo el problema de la baja polarización remanente de BNBT se mejora al poner estas capas entre dos capas polarizadas de BF. Y las capas de BNBT funcionan como barrera para disminuir las corrientes de fugas no lineales en las capas de BF que impedían la correcta polarización y así la integración de este material en dispositivos micro-electrónicos. Del estudio detallado de las láminas objeto de esta tesis se ha demostrado que:

1. *En las láminas delgas de BNBT los bajos valores de polarización remanente obtenidos se deben al carácter relaxor-ferroeléctrico de las mismas.*
2. *Los altos valores de conductividad observados en las capas de BF a campos eléctricos elevados, se deben a corrientes de fugas no lineales. Estas corrientes se pueden controlar variando la temperatura de cristalización, excesos de Bi, y el dopaje de estas láminas con Ca^{2+}.*
3. *Al combinar en forma de composites multicapa de láminas delgadas las composiciones estudiadas en esta tesis se obtuvieron mejoras en la polarización remanente de las láminas de BNBT, se disminuyeron las corrientes de fugas no lineales de las capas de BF y se obtuvo una mejorada magnetización remanente latente. Lo cual hace que estos materiales compuestos sean muy prometedores para su integración en nuevos micro-dispositivos.*

6.2 Perspectivas de futuro.

Después de haber estudiado en profundidad las propiedades funcionales de composites multicapa en forma de lámina delgada, y haber demostrado su potencialidad para integrarse en microdispositivos gracias a las mejoras conseguidas en su polarización y magnetización remanentes, se puede comenzar el proceso de optimización de estas láminas y la aplicación de los procesos de microfabricación necesarios para su integración en prototipos.

Por ejemplo, la incorporación de capas de BF dopadas con Ca^{2+} (BCF) en los composites multicapa merece una mayor atención, teniendo en cuenta los buenos resultados obtenidos con una polarización remanente estable en el tiempo y significativos valores de magnetización remanente. Si observamos la microestrucura de estas capas , estas presentan una significativa porosidad y tamaños de grano del orden de 22 nm, podemos concluir que hay margen de mejora en su preparación. Un estudio completo que establezca las condiciones óptimas de preparación de estas láminas, similar al realizado en las láminas de $BiFeO_3$ puro, proporcionará capas BCF con más densas y un tamaño de grano controlado que aumenten los valores de polarización y magnetización remanente de los composites multicapa estudiados en esta tesis.

En relación a la integración en microdispositivos de estos composites multicapa en forma de lámina delgada, ya se han realizado los primeros trabajos que han permitido establecer los problemas que deben resolverse durante la microfabricación. Se escogió con este fin fabricar uno de los dispositivos más estudiados por su simplicidad, las micropalancas (cantilevers) activas en las que su movimiento es controlado por una

lámina piezoelectrica. Estas micropalancas se pueden usar en microscopía de fuerzas atómicas o como sensores de masa.

El proceso de micro-fabricación se llevó a cabo durante una estancia breve realizada en la Universidad de Twente, laboratorio de nanotecnologías MESA+ del grupo de materiales inorgánicos. Para realizar dicha micro-fabricación en las láminas MLC de esta tesis se desarrolló un protocolo de trabajo formado por diferentes pasos de procesos físicos y químicos, como muestra la Figura 6.1, con el fin de obtener las palancas activas piezoeléctricas con un solo punto de apoyo (free-standing cantilever). El proceso consta de los siguientes pasos:

- *Figure 6.1 a, Selección de la muestra a micro-fabricar sobre sustratos de Si(100) y con electrodo inferior de PT.*
- *Figure 6.1 b, deposición de Au como electrodo superior por sputttering en toda la muestra.*
- *Figure 6.1c, depósito de una foto-resina protectora para fotolitografía, para crear el patrón de los electrodos superiores de oro, con las palancas.*
- *Figure 6.1d, dibujo del patrón de los electrodos superiores de Au y las palancas través de la eliminación de la parte no protegida de la capa de electrodo superior por ataque con iones reactivos (RIE, del inglés reactive ion etching).*
- *Figure 6.1 e, eliminación de la resina foto-resistente por un ataque químico, con una disolución que solo disuelve la resina.*
- *Figure 6.1f, depósito de la resina fotoresistente con una nueva forma, con el objetivo de proteger ahora los cantilever y la parte de la muestra que no se desea eliminar.*

- *Figure 6.1 g , ataque químico de las láminas ferroeléctricas con solución de ácido fluorhídrico (BHF, del inglés buffered hydrofluoric acid). El ataque con esta solución se realiza hasta detectar la capa de Pt del electrodo inferior.*
- *Figure 6.1 h, ataque por RIE de la capa de Pt y SiO_2.*
- *Figure 6.1 i, ataque químico anisotrópico con hidróxido de potasio (KOH) caliente (120 ^{0}C) para eliminar el Si (100) de la parte inferior de los cantievers y dejarlos con un único punto de sujeción (del inglés, free-standing cantilevers).*
- *Figure 6.1 j , eliminar la resina fotoresistente con un ataque químico.*

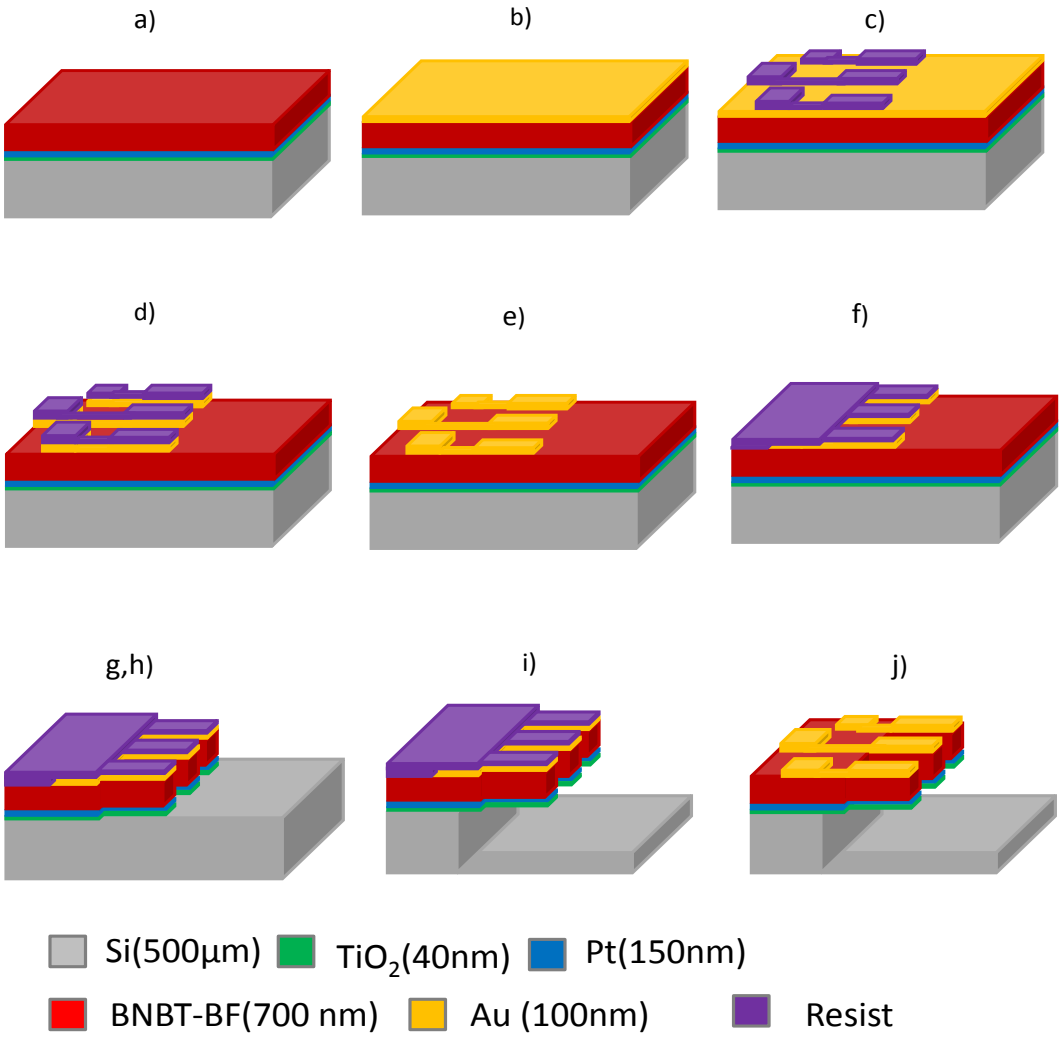

***Figure 6.1**: Esquema diseñado para la micro-fabricación de las micropalancas con un composite multicapa de BNBT y BF.*

El resultado de este proceso nos reveló diferentes cuestiones a mejorar para completar con éxito el proceso de micro-fabricación. Las imágenes de las micropalancas obtenidas recogidas en la Figura 6.2a demuestran que el proceso de micro-fabricación se realizó con éxito hasta alcanzar los pasos g y h, donde se les da la forma a los cantilevers por ataques químicos del material piezoeléctrico activo y, además se atacaron las capas del electrodo inferior de Pt y SiO_2. En el siguiente paso, en el que se elimina el Si del substrato para conseguir que la micropalanca quede libre con un solo punto de apoyo, apareció un problema que imposibilitó la culminación del proceso: el ataque químico selectivo con KOH en caliente que debe eliminar solo el Si cristalino, logró también despegar las micropalancas del Si del electrodo inferior (Figura 6.2 b). Esto es una evidencia de que los composites multicapa presentados en esta tesis tienen poca adherencia al electrodo inferior para soportar estos ataques químicos con disoluciones.

a) b)

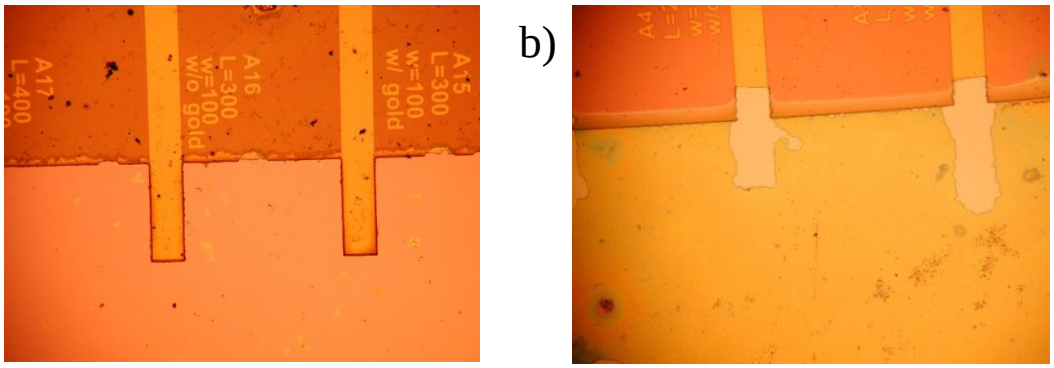

***Figure 6.2**: Imágenes de las micropalancas en pasos intermedios del proceso de microfabricación, a) forma de las micropalancas después de haber atacado el material piezoeléctrico y las capas de Pt y SiO_2,(pasos g, h) b) las micropalancas desaparecen, dejando un rastro del electrodo inferior tras el ataque con KOH durante el proceso de eliminación del Si.*

De los resultados de estos experimentos podemos concluir que la adhesión entre las láminas y el electrodo inferior debe mejorarse. Una primera solución es la elección de un electrodo que muestre mejor adhesión con las láminas depositadas sobre ella que el Pt. Una alternativa es la perovskita $SrRuO_3$. Pero quizás la mejor solución sería el uso de sustratos de silicio sobre aislante (SOI, del inglés silicon on insulator). Estos substratos tienen una capa de Si crecida sobre el óxido nativo (SiO_2) de una oblea de Si. Los ataques son detenidos por esta capa de óxido, que actúa como barrera. Por tanto, permiten hacer la micro-fabricación de las micropalancas por la parte inferior de las mismas, evitando que los ataques químicos afecten la intercara muestra/substrato, resultando un método menos agresivo de fabricación, y con el que los problemas de adhesión relacionados con el método de preparación de las láminas y el electrodo inferior de Pt usado no serían críticos. Para la preparación de estos composites multicapa en estos nuevos sustratos, es necesario realizar un estudio para optimizar el depósito, y que puede suponer parte del trabajo futuro que se realice a partir de los resultados de esta tesis.

PUBLICATIONS DERIVED FROM THIS THESIS.

Papers

- *Perez-Rivero, J. Ricote, I. Bretos, M.L. Calzada, J. Pérez de la Cruz, J.R.A. Fernandes, R. Jiménez."Morphotropic phase boundary in solution derived* $(Bi_{0.5}Na_{0.5})_{1-x}Ba_xTiO_3$ *thin films: Part II Functional properties and phase stability". Journal of the American Ceramic Society, 97 - 4, pp. 1276 - 1282. 2014.*
- *Armando Perez Rivero, Jesús Ricote, Iñigo Bretos, Mar García Hernández; M. Lourdes Calzada; Ricardo Jiménez. "Lead-free multilayer composite films based on ferroelectric* $(Bi_{0.5}Na_{0.5})_{0.45}Ba_{0.55}TiO_3$ *and multiferroic* $BiFeO_3$*". Journal of applied physics. 117, pp. 064105-1 - 064105-10. 2015.*
- *A. Perez-Rivero, M. Tomczyk, R. Jiménez, I. Bretos, J. Ricote, P. M. Vilarinho and M. L. Calzada. "Polarization switching at room temperature of undoped* $BiFeO_3$ *thin films crystallized at temperatures between* $400 \leq T \leq 500\ ^0C$*". Journal of Materials Science: Materials in Electronics, DOI 10.1007/s10854-015-3150-9, 2015.*
- *A. Perez-Rivero, J. Ricote, M. G. Hernández, M. L. Calzada, R. Jiménez. "Enhanced Ferroelectric and ferromagnetic properties in BNBT/ BF bi-layer composites". Journal of Applied Physics. (Sent to).*

Presentations in conferences

- *Pérez-Rivero, R. Jiménez, I. Bretos, M.L. Calzada and J. Ricote, "Enhancement of the functional properties of lead-free* $(Bi_{0.5}Na_{0.5})_{1-x}Ba_xTiO_3$ *thin films around*

the Morphotropic Phase Boundary". ISAF-ECAPD-PFM, Aveiro, Portugal. Julio 2012.

- *A. Pérez-Rivero, D. Mezcua, C. Gutiérrez-Lázaro, I. Bretos, J. Ricote, R. Jiménez, R. Sirera, M.L. Calzada , "Functional properties of nanostructured solution derived lead- free $(Bi_{0.5}Na_{0.5})_{1-x}Ba_xTiO_3$ thin films in the proximity of the Morphotropic Phase Boundary". Joint Conference COST MPO904 Action "Single-and multiphase ferroics and multiferroics with restricted geometries" & the 9th Edition IEEE-ROMSC 2012, Iasi, Rumania, September 2012.*
- *Armando Janier Perez Rivero, J. Ricote, I. Bretos, M.L. Calzada, J. Pérez de la Cruz, J.R.A. Fernandes and R. Jiménez. "Propiedades funcionales de láminas delgadas libres de plomo de $(Bi_{0.5}Na_{0.5})_{1-x}Ba_xTiO_3$ con composiciones cercanas a la MPB". Jornadas de Jóvenes Investigadores, Instituto de Cerámica y Vidrio (ICV-CSIC), Madrid, España, Junio 2013.*
- *A.Perez-Rivero, J. Ricote, I. Bretos, M.L. Calzada, J. Pérez de la Cruz, J.R.A. Fernandes and R. Jiménez. "Enhancement of the functional properties of films at the Morphotropic Phase boundary of lead-free $(Bi_{0.5}Na_{0.5})_{1-x}Ba_xTiO_3$". XI Reunión Nacional de Electrocerámicas, Zaragoza, España, Junio 2013.*
- *A. Pérez-Rivero, J. Ricote, I. Bretos, M.L. Calzada, R. Jiménez. "Functional properties and phase stability of morphotropic phase boundary $(Bi_{0.5}Na_{0.5})_{1-x}Ba_xTiO_3$ thin films". 13th International Meeting on Ferroelectricity, Kraków, Poland, Septiembre 2013.*
- *J. Ricote, R. Jiménez, A. Pérez-Rivero, I. Bretos, D. Pérez-Mezcua, M.L. Calzada, N. Salazar, A. Gil, R. Sirera "Recent advances in alternative lead free*

piezoelectric, solution derived $(Bi_{0.5}Na_{0.5})_{1-x}Ba_xTiO_3$ *thin films". 13th International Meeting on Ferroelectricity, Kraków, Poland, Septiembre 2013.*

- *M. Tomczyk , A. J. Pérez Rivero , R. Jiménez , J. Ricote , I. Bretos , M. L. Calzada and P. M. Vilarinho. "Low temperature fabrication of ferroic* $BiFeO_3$ *thin films by chemical solution deposition". 13th International Meeting on Ferroelectricity, Kraków, Poland, Septiembre 2013.*
- *R. Jiménez, A. Perez-Rivero, I. Bretos, J. Ricote, and M.L. Calzada. " Improved properties of multiferroic multilayer composite thin films based on ferroelectric* $(Bi_{0.5}Na_{0.5})_{1-x}Ba_xTiO_3$ *and* $BiFeO_3$*". EUROMAT 2013, Sevilla, España, Septiembre 2013.*
- *A. Perez-Rivero, I. Bretos, M.L. Calzada, J. Ricote and R. Jiménez. "Improved properties of the lead free solid solution* $(Bi_{0.5}Na_{0.5})_{1-x}Ba_xTiO_3$ *prepared as multilayer composite thin films with* $BiFeO_3$*". Conference for Young Scientists in Ceramics , The Tenth Students' Meeting SM-2013 and The Third ESR Workshop, COST MP0904. Serbia , November 2013.*
- *Mª Lourdes Calzada; Iñigo Bretos; Ricardo Jiménez; Jesús Ricote; Dulce Pérez Mezcua; Armando J. Perez Rivero; Norberto Salazar; Rafael Sirera. "Synthesis strategies in solution for the low-temperature processing of complex oxide ferroelectric thin films. Opportunities of ferroelectrics in flexible electronics". E-MRS 2014 Spring Meeting: European Materials Research Society. Lille, Francia, Mayo 2014.*
- *Armando J. Pérez Rivero; Ricardo Jiménez; Iñigo Bretos; Mar García Hernández; Mª Lourdes Calzada; Jesús Ricote. "Ferroelectric multilayer composite films based on the solid solution* $(Bi_{1/2}Na_{1/2})TiO_3$*-*$BaTiO_3$*". E-MRS*

2014 Spring Meeting: European Materials Research Society. Lille, Francia, Mayo 2014.

- *Mª Lourdes Calzada; Iñigo Bretos; Ricardo Jiménez; Jesús Ricote; Dulce Pérez Mezcua; Armando J. Perez Rivero; Norberto Salazar; Rafael Sirera; Monika Tomczyk; Aiying Wu; Paula M. Vilarinho; Christopher De Dobbelaere; An Hardy; Marlies K. Van Bael. "Solution methods for the low-temperature fabrication of functional oxide thin films. Ferroelectrics and multiferroics in microelectronics and flexible electronics". Electroceramics XIV: 14th Internacional Conference on Electroceramics & Their Applications. Bucharest, Rumanía , Junio 2014.*
- *Armando J. Perez Rivero; Jesús Ricote; Iñigo Bretos; Mar García Hernández; Mª Lourdes Calzada; Ricardo Jiménez. "Improved functional properties of lead-free multilayer composite films combining $(Bi_{0.5}Na_{0.5})_{1-x}Ba_xTiO_3$ and multiferroic $BiFeO_3$". Electroceramics XIV: 14th Internacional Conference on Electroceramics & Their Applications. Bucharest, Rumanía, Junio 2014.*
- *Mª Lourdes Calzada; Iñigo Bretos; Ricardo Jiménez; Dulce Pérez Mezcua; Armando Perez Rivero; Norberto Salazar; Rafael Sirera. "Ferroelectric oxide thin films from solution deposition methods for applications in micro and flexible electronics". Materials Science & Technology 2014 Conference & Exhibition. Pittsburgh (Pennsylvania), Estados Unidos de América, Octubre 2014.*
- *A. Perez-Rivero, J. Ricote, M.L. Calzada, R. Jiménez, R. Steenwelle, G. Rijnders. "Macroscopic piezoelectric properties of lead-free*

($Bi_{0.5}Na_{0.5})_{0.945}Ba_{0.055}TiO_3$-based multilayer composite films". 14th International Conference European Ceramic Society. Toledo, Madrid, Spain, June 2015.

- *Ricardo Jiménez, A. Pérez Rivero, I. Bretos, J. Ricote, M.L. Calzada, A. Torres-pardo, E. García González, J.M González-Calbet. "Size effect related Relaxor behaviour in $Na_{1-x}Sr_{x/2}NbO_3$ $0 \leq x \leq 0.4$ and $(Bi_{0.5}Na_{0.5})_{1-x}BaxTiO_3$ $0.05 \leq x \leq 0.15$ lead free solid solutions". EMF 2015. Porto, Portugal, June 2015.*